The Pennsylvania State University

The Graduate School

Department of Geosciences

ESTIMATING THE AGES OF GLACIAL LANDFORMS FROM THE STATISTICAL DISTRIBUTIONS OF COSMOGENIC EXPOSURE DATES

A Dissertation in

Geosciences

by

Patrick J. Applegate

Submitted in Partial Fulfillment
of the Requirements
for the Degree of

Doctor of Philosophy

December 2009

The dissertation of Patrick J. Applegate was reviewed and approved* by the following:

Richard B. Alley
Evan Pugh Professor of Geosciences
Dissertation Co-Advisor
Co-Chair of Committee

Michael E. Mann
Professor of Meteorology
Dissertation Co-Advisor
Co-Chair of Committee

David Pollard
Senior Scientist, Earth and Environmental Systems Institute

Andrew M. Carleton
Professor of Geography

Thomas V. Lowell
Professor of Geology, University of Cincinnati
Special Member

Katherine H. Freeman
Professor of Geosciences
Associate Department Head for Graduate Programs and Research

*Signatures are on file in the Graduate School

ABSTRACT

Glacial landforms, especially moraines, have long been used as indicators of decreased temperature or increased precipitation in the past. Cosmogenic exposure dating of moraine boulders provides a method for estimating moraine ages. However, geomorphic processes interfere with cosmogenic exposure dating. To improve the accuracy of the cosmogenic exposure dating method, quantitative methods for assessing the effects of geomorphic processes on cosmogenic exposure dating are needed.

To address this need, this dissertation describes models of two geomorphic processes and their effects on the cosmogenic exposure dating of moraines. These processes are moraine degradation and inheritance. Both models use Monte Carlo techniques to estimate the statistical distributions of exposure dates from moraine boulders, given specific assumptions about the histories of the boulders. The moraine degradation model is based on prior examples from the literature; the inheritance model is novel.

Some implications of this work for cosmogenic exposure dating of moraines follow.

Different geomorphic processes give rise to different statistical distributions of cosmogenic exposure dates. Moraine degradation produces distributions that are skewed toward the young tail of the distribution, whereas inheritance produces distributions that are skewed toward the old tail of the distribution.

Simple procedures for estimating moraine ages from cosmogenic exposure dates perform well in some cases and poorly in others, sometimes producing moraine age estimates that are incorrect by thousands of years. Simple estimators tested here include the mean, the mean after discarding outliers, the youngest date, and the oldest date.

Explicit inversion of the models against collections of cosmogenic exposure dates may represent an improvement over simple methods of estimating moraine ages. These inverse

methods yield estimates of the rates and magnitudes of geomorphic processes acting in glaciated basins, as well as the moraines' ages.

Field sampling criteria that preferentially choose pristine boulders may yield exposure dates that underestimate the ages of moraines by thousands of years. This statement assumes that the moraines lose several meters of material from their crests over their lifetimes, that the boulders erode at a constant rate after being exhumed, and that inherited nuclides are not present in the boulders.

TABLE OF CONTENTS

LIST OF FIGURES

LIST OF TABLES

ACKNOWLEDGEMENTS

I thank the following people for their contributions to my doctoral work.

Richard Alley, Mike Mann, Dave Pollard, Andrew Carleton, and Tom Lowell served on my doctoral committee. Klaus Keller served as an unofficial committee member. Richard Alley, Tom Lowell, Nathan Urban, Klaus Keller, Kris Peterson, Greg Balco, Dave Pollard, Mike Mann, Andrew Carleton, and Ben Laabs commented on various drafts of this dissertation.

Richard Alley's undergraduate course on climate change provided the foundation for Chapter 1. Chapter 2 grew out of a final project for the Mathematical Modeling in Geosciences course taught by Rudy Slingerland and Lee Kump. Nathan Urban suggested the inverse methods described in Chapter 3. Brent Goehring supplied recalculated exposure dates for Chapter 3. Tom Lowell encouraged me to write Appendix A. Dave Pollard's comments allowed me to write Appendix B.

Meredith Kelly, Tom Lowell, Aaron Putnam, Ed Evenson, Mike O'Neal, and Ben Laabs let me participate in field trips to the Quelccaya Ice Cap of Perú, the Wind River Range of Wyoming, and the Uinta Mountains of Utah. Jeff Over, Ben Laabs, Dori Farthing, Scott Giorgis, Richard Young, and Amy Sheldon invited me to teach for a semester at SUNY-Geneseo.

The geology faculty at the University of Cincinnati, especially Tom Lowell, David Nash, Attila Kilinc, and Kees DeJong, provided a base for my graduate education. At Purdue, Darryl Granger taught me how to apply cosmogenic nuclides and Monte Carlo methods, and how to write a thesis. At Penn State, Klaus Keller, Tim Bralower and Rudy Slingerland contributed to my professional development through their graduate courses.

Richard Alley's contributions to this work are too numerous to mention individually, but his advice improved all chapters of this dissertation. Richard set a good example for me at all times.

Tom Lowell oversaw my long education in Quaternary geology, beginning with the Ice Age exhibit in the Cincinnati Museum Center. Tom's attitude of healthy skepticism motivated this work.

Len Applegate and Kathy and Vince May gave me quiet places to write. Their contributions to this work are indirect, but major. Other indirect contributors include David Wilson, Kris Peterson, and Brett Carpenter.

This work was partly supported by the National Science Foundation (grants 0531211, 0539578, and 0424589), the Comer Science and Education Foundation, and the Geological Society of America (grant 8736-08). Additional support was provided by the Department of Geosciences through a Parizek Graduate Fellowship and an Ohmoto Graduate Fellowship, by the Earth and Environmental Sciences Institute through a research assistantship, and by the Pennsylvania State University through a University Graduate Fellowship and an Anne C. Wilson Research Award.

For a successful technology, reality must take precedence over public relations, for Nature cannot be fooled.

-- Richard Feynman, *The Pleasure of Finding Things Out* (Robbins, J., ed., 1999, Perseus, p. 169).

And for to pass the time this book shall be pleasant to read in, but for to give faith and belief that all is true that is contained herein, [you are] at your liberty.

-- William Caxton, preface, *Le Morte Darthur* (Strachey, E., ed., 1901, Macmillan, p. 2).

Chapter 1

Introduction

This dissertation describes new methods for assessing the influence of geomorphic processes on cosmogenic exposure dating of moraine boulders. This work is intended to explain observations that already exist in the literature. Therefore, this first chapter provides a context for these observations, and describes the paleoclimatic questions that these observations were intended to answer. Subsequent chapters describe the methods developed in this work and the results of applying those methods to observations.

This dissertation builds on the author's MS thesis (Applegate, 2005), which also discusses glacial geomorphology and geochronology. Interested readers are referred to that work for more discussion of glacial geomorphology, cosmogenic exposure dating, and climate questions related to glacier size changes.

Glacial geomorphology and glacial geochronology are young scientific fields (see historical review in Oldroyd, 1996). Scientific interest in the behavior and history of glaciers dates to 1840, when Agassiz published his *Études sur les glaciers* (*Studies on Glaciers*; Agassiz, 1967). The earliest efforts to determine absolute chronologies for pre-historic changes in glacier extents are even more recent. The oldest glacial chronology studies that are still relevant today are probably the laminated sediment records from Scandinavia and New England (de Geer, 1912; Antevs, 1922; see review in Petterson, 1996). These studies date to the latter half of the 19th century and the early part of the last century.

Glacier mass balance and the present distribution of glacier ice

A glacier is a body of ice that persists throughout the year. The ice in a glacier flows laterally under its own weight, much like a viscous fluid. In addition, the ice in true glaciers is mostly or entirely exposed to view. These characteristics differentiate glaciers from other, superficially similar, bodies of snow and ice. For example, snowfields and snow aprons do not last throughout the year and do not flow. The ice in permafrost lasts throughout the year, but is buried and does not flow. Rock glaciers are composed partly of flowing ice, but rock glacier ice is largely covered by debris.

Glaciers grow and shrink in response to changes in their mass balances. The mass balance of a glacier is the difference between the yearly rate of mass gain from snowfall and the yearly rate of mass loss from melting, sublimation, and calving. Sublimation is the direct transformation of solid ice to water vapor. Sublimation requires far more energy to remove a unit mass of ice than does melting, and it is especially important where the air near the upper surface of a glacier is extremely dry (Rupper and Roe, 2008). Calving is the breaking off of ice masses from the glacier; it usually occurs where glacier ice enters a body of water, such as an ice-marginal lake or the ocean (Alley et al., 2007). Calving sometimes also occurs where ice flows over a cliff.

In the modern world, glaciers occur at high latitudes and high altitudes. Near the poles, glaciers extend down to sea level. Closer to the equator, glaciers are found only on mountains thousands of meters above sea level. The ice sheets of Greenland, West Antarctica and East Antarctica contain well over 90% of the total present-day mass of continental ice (Lemke et al., 2007); mountain glaciers account for only a small percentage of this total mass.

The history of glaciation over the last several million years

During the last 3-5 million years, glaciers and ice sheets have sometimes been much larger and more extensive than they are presently. The most recent time when ice mass on the continents reached a peak was about 20 ka (20,000 years ago), during the so-called Last Glacial Maximum. At that time, the ice mass on the continents was about three times the present amount (compare Table 4.1 of Lemke et al., 2007, with Figure 6.8 of Jansen et al., 2007). In eastern North America, the Laurentide ice sheet extended from Labrador and northern Canada to Long Island (Dyke and Prest, 1987; Dyke, 2004). Ice extents in Europe and Asia were also much greater than at present (Boulton et al., 2001; Mangerud et al., 2004). Glaciers and ice sheets appeared in places where today they do not exist, such as the British Isles (Clark et al., 2004) and atop Mauna Kea volcano in Hawaii (Porter, 2004).

The marine isotopic record of continental glaciation

We know about the history of continental ice mass over the last several million years primarily from the oxygen isotopic compositions of the shells of planktonic organisms in deep sea sediments (Broecker, 2002, and references therein). Oxygen has three stable nuclides, ^{16}O, ^{17}O, and ^{18}O, of which ^{16}O is the most abundant. The natural abundance of ^{17}O is much less than that of the other two oxygen isotopes, so we can speak only of ^{16}O and ^{18}O. When ice sheets grow on the continents, the oceans become enriched in the heavier isotope of oxygen, ^{18}O. This phenomenon happens because water molecules containing the lighter isotope, ^{16}O, preferentially evaporate from the oceans and fall out as precipitation over the continents, where they are stored in the growing ice sheets. As the oceans become isotopically heavier, so do the shells of small organisms called foraminifera that live in the oceans. When these organisms die, their shells fall

to the sea floor. In a pile of these shells, the oldest shells are at the bottom and the youngest shells are at the top. A sediment core from the deep sea therefore contains a record of the oxygen isotopic composition of the sea surface water over time, which is related to the mass of ice on the continents. Water temperatures also influence the oxygen isotopic compositions of foraminifera shells, but fortunately this effect amplifies the continental ice mass signal. The ratios of magnesium and calcium concentrations in the foraminifera shells provide an independent estimate of water temperature, allowing us to isolate the continental ice mass signal.

The marine oxygen isotope record shows about 12 glacial cycles over the last million years (Raymo and Nisancioglu, 2003). During the last 800 ka, these cycles have a common structure. Each cycle begins with a long buildup of continental ice mass, followed by an abrupt disintegration of the ice sheets. The remainder of the cycle reflects a comparatively warm interglacial period. The overall glacial cycle, from interglacial to interglacial, lasts about 100 ka.

The causes of glacial/interglacial cycles

The glacial/interglacial cycle over the last 800 ka has been explained by variations in the earth's orbit (Hays et al., 1976), which affect the amount of sunlight reaching the high latitudes of the Northern Hemisphere during summer. Reduced insolation at high northern latitudes in summer produces cool summers, leading to ice buildup on the continents. Under this model, summer insolation in the north is more important than that in the south because there is more accommodation space for additional ice in the high northern latitudes.

The earth's orbit has three major modes of variability (Milankovitch cycles; Alley, 2001; Broecker, 2002). The longest-period mode, eccentricity, affects the shape of the earth's orbit around the sun. The earth's orbital path is an ellipse, with the sun at one focus of the ellipse. When eccentricity is at a minimum, the path becomes nearly circular; when eccentricity is larger,

the earth's orbit is more elliptical. A full eccentricity cycle lasts about 100 ka from peak to peak. The second mode, obliquity, describes the inclination of the earth's axis relative to a line drawn normal to the plane of the orbit. The obliquity mode has a period of about 41 ka. Last, the precession cycle influences whether the north pole is inclined toward or away from the sun at closest approach. This cycle has a period of about 20 ka. Mathematical descriptions of how these cycles affect solar insolation over time at different latitudes exist in the literature (Berger, 1978; Berger and Loutre, 1991).

Despite the close correspondence of insolation at high northern latitudes with the oxygen isotope record of continental ice mass, two major questions remain unanswered. First, the effect of the eccentricity cycle on insolation is weak, out of proportion to its apparent effect on the earth's climate (Hays et al., 1976). Several workers have suggested that the 100-ka glacial cycle arises due to an emergent property of the great ice sheets or the climate system, rather than the eccentricity cycle itself (e.g., Pollard, 1982; Paillard, 1998; cf. Weertman, 1976). That is, ice sheets become more prone to collapse after they grow to a particular size, and they attain that size every 100 ka on average. Alternatively, perhaps the ends of glacial cycles occur at the end of every second or third obliquity cycle (Huybers and Wunsch, 2005). Because the length of an obliquity cycle is about 40 ka, this variability would give rise to an average ice age cycle length of 100 ka. A second unsolved problem lies in the oxygen isotope record before about 800 ka, when glacial cycles had smaller amplitudes and a period of about 41 ka. No totally satisfactory explanation exists for this "41 ka world" or for the abrupt lengthening in the period of glacial cycles that occurred at 800 ka (Raymo and Nisancioglu, 2003; cf. Huybers, 2006).

Glacial expansions not driven by orbital cycles: the Younger Dryas example

Although the largest changes in continental ice mass appear to be driven by orbital cycles, we know of geographically widespread changes in glacier and ice sheet size that were not caused by variations in high-latitude insolation. For example, the Younger Dryas cold event (12.9-11.6 ka; Barrows et al., 2007, and references therein) was associated with glacier expansions in New England, Great Britain, mainland Europe, and possibly the western United States and New Zealand (e.g., Borns et al., 2004; Clark et al., 2004; Ivy-Ochs et al., 2006, 2007; Gosse et al., 1995a; Denton and Hendy, 1994; Ivy-Ochs et al., 1999). The Younger Dryas interrupted the warming at the end of the last glaciation, abruptly returning parts of the world to near-glacial conditions. The traditional explanation for this cold event involves a sudden flood of glacial meltwater entering the northern Atlantic (Broecker et al., 1989). This pulse of fresh water floated on the salty water of the northern Atlantic, interrupting the density-driven sinking of ocean water near the southern tip of Greenland and causing the poleward transport of heat by currents in the Atlantic to stop. Support for this traditional explanation of the Younger Dryas cold event has declined recently, because evidence for the passage of floodwaters through the possible drainageways at the appropriate time is lacking (Lowell et al., 2005; Fisher and Lowell, 2006). However, no insolation-based alternative hypothesis is under consideration.

Our best record of the Younger Dryas cold event comes from ice cores drilled through the Greenland ice cap (see review in Alley, 2000). As snow accumulates on a glacier or ice sheet, it records the net thickness of the snow that falls in each year. The water molecules in the ice contain oxygen isotopes that are sensitive to the local air temperature (Dansgaard, 1964, as discussed in Broecker, 2002; cf. Pierrehumbert, 1999). Moreover, the ice in an ice sheet has a "memory" of surface temperatures, because the rate of snowfall in the center of an ice sheet is usually greater than the speed at which past large temperature changes diffuse out of the ice

(Paterson, 1994). These climate indicators reflect the magnitude and abruptness of the onset of the Younger Dryas in central Greenland. The net accumulation rate of new snow dropped by one-third to two-thirds, and temperatures declined by 10-15 °C, over about a century (Cuffey and Clow, 1997; also see Severinghaus et al., 1998). Recent work suggests that this temperature change was seasonal; that is, Younger Dryas summers were only a few degrees C cooler than at present, but the winters were much colder than modern winters (Denton et al., 2005; Chiang and Bitz, 2005; Broecker, 2006; Kelly et al., 2008).

The terrestrial record of glaciation

A complete picture of the history of continental glaciation requires knowledge of the geographic distribution of ice at different times in the past. Neither the marine oxygen isotope record nor the Greenland ice cores provide this information. For example, the marine oxygen isotope record indicates that there was more ice on the continents during the Last Glacial Maximum than there is at present, but this record alone tells us nothing about where this extra ice was stored.

Fortunately, glacier processes produce landscape elements that record the past distribution of continental ice. These landscape elements include moraines, polished bedrock, and outwash terraces. Moraines are ridges of debris that indicate the former margins of glaciers and ice sheets. Outwash terraces contain river gravels deposited by streams fed by glacial meltwater. Polished bedrock sometimes crops out on the walls and floors of glacial valleys, especially where these surfaces are steep.

These landscape elements are produced by the transport of sediment by glaciers and their meltwater streams. Glaciers transport sediment both on their upper surfaces and at the interface between the ice and the underlying bedrock. At the glacier's bed, the ice drags sediment and

pieces of rock over the underlying bedrock, which becomes polished. Near the glacier's margin, sediment falls off the upper surface of the glacier, melts out of subglacial ice, or is stacked in frozen sheets from the lower surface of the glacier, producing moraines (Lawson, 1979; Kruger, 1996; Benn and Evans, 1998). Moreover, glacier meltwater picks up sediment and transports it away from the glacier margin, forming outwash terraces.

Of these landscape elements, moraines are perhaps the most useful in reconstructing past ice extents. Frontal moraines, those that are roughly perpendicular to the overall direction of ice flow, are thought to be isochronous. That is, the upper surfaces of frontal moraines are believed to be the same age everywhere (cf. Gosse et al., 1995b; Vacco et al., 2009). Under this assumption, frontal moraines indicate the areal extent of ice at the time of deposition of the moraines. Polished bedrock indicates that the point where the bedrock is found was covered by ice at some time in the past. Outwash terraces indicate that there was glacier ice upstream from the terrace at the time of terrace deposition. Thus, polished bedrock and outwash terraces yield less information on past glacial extents than do moraines. However, outwash terraces often survive long after the moraines of the same age have been removed by subsequent glacier advances. Thus, outwash terraces provide our only record of old glaciations in many places (e.g., Sharp et al., 2003).

However, the moraine record of past ice extents is incomplete. As glaciers advance, they remobilize sediments deposited during earlier glacial episodes, including older moraines (Gibbons et al., 1984). Thus, the moraine record is self-censored. Moreover, subaerial erosion eventually removes those moraines that are not overlapped by subsequent advances (Kirkbride and Brazier, 1998). These problems in the record misled early glacial geomorphologists into believing that there had been only four great glaciations in recent geologic time (Oldroyd, 1996, and references therein). This idea was disproven when the marine oxygen isotope record became available.

Climate questions and moraines

Thus, glaciers grow and shrink in response to climate changes, and they deposit moraines that indicate the glaciers' past extents. If we could determine the ages of moraines, we would obtain a partial record of climate changes over time (Lowell, 2000; cf. Jones and Mann, 2004). This record might reflect geographic patterns that are not captured by marine sediments or ice cores.

Accurate, precise dating of moraines could provide answers to the following questions. This list is not exhaustive.

1. When were there cold periods during recent geologic time? Moraines outside of present-day glacial limits formed when the local climate was favorable to glacier growth. Glaciers grow when the climate becomes either colder or snowier (Plummer and Phillips, 2003; Laabs, 2006; Anderson and Mackintosh, 2006), but temperature effects dominate precipitation in most cases (Oerlemans, 2005; Denton et al., 2005). Dating moraines therefore yields the times of cold periods in the recent past.

2. Were major climate changes globally synchronous? In a set of moraines deposited during a single glaciation, the outermost moraine is the oldest; the inset moraines become progressively younger with distance upvalley. The outermost moraine was deposited immediately after the glacier stopped advancing and just before it began to retreat. Therefore, dating the outermost moraine in a set indicates when the climate changed from a regime favoring glacier growth to one favoring glacier retreat (Lowell, 1999). For example, precise dating of prominent moraines from the last glaciation could be used to determine whether the last deglaciation began at the same time everywhere (Lowell et al., 1995; Licciardi et al., 2004; Applegate, 2005; Schaefer et al., 2006; Laabs et al., 2009).

3. How geographically widespread were abrupt climate changes? For climate changes with short onset times, the geographic distribution of moraines that date to the time of the climate change indicates what parts of the globe were affected. For example, it was long thought that the Younger Dryas cooling was caused by a slowdown of the ocean circulation (Broecker, 2003; see above). Modeling studies show that such a slowdown would cause a pronounced cooling around the North Atlantic basin, but not elsewhere (e.g., Vellinga and Wood, 2002). Indeed, field workers have published moraine chronologies that show glacier advances during Younger Dryas time from eastern North America and western Europe (Lowell et al., 1999; Borns et al., 2004; Clark et al., 2004; Ivy-Ochs et al., 2006, 2007). However, other workers have identified Younger Dryas-age glacier advances at other sites far from the North Atlantic (e.g., Denton and Hendy, 1994; Gosse et al., 1995; Ivy-Ochs et al., 1999). Because both the proposed mechanism for the Younger Dryas cooling and the ages of the extra-North Atlantic moraines are under debate at present (Lowell et al., 2005; Barrows et al., 2007), this question remains open for the Younger Dryas.

Answering these questions requires careful dating of moraines in multiple glaciated drainages in each field area. Individual glaciers may behave very differently from others in the same mountain range, due to local influences on mass balance such as debris cover or windblown snow (Gillespie and Molnar, 1995). Over short time scales, even glaciers that drain the same icefield may advance and retreat at different times (Luckman, 2000). Thus, it is necessary to date moraines in several valleys to establish a representative chronology for each field area.

Glacial geochronologic methods

The methods that are most commonly used to determine the ages of moraines are radiocarbon dating, cosmogenic exposure dating, and optically stimulated luminescence dating.

Reviews of these methods are available elsewhere (Taylor, 2000; Cerling and Craig, 1994; Gosse and Phillips, 2001; Fabel and Harbor, 1999; Aitken, 1997; also see Applegate, 2005). Therefore, only brief descriptions are presented here.

Radiocarbon dating estimates how long ago an organism died. The atmosphere contains a certain amount of the radioactive isotope of carbon, ^{14}C, in carbon dioxide molecules. Living things have a concentration of radiocarbon that is in equilibrium with the atmospheric concentration; plants incorporate the radiocarbon from atmospheric carbon dioxide in their tissues, and animals eat the plants. When these organisms die, they stop exchanging carbon with the atmosphere, and so the radiocarbon concentration in the remains declines over time. Thus, the radiocarbon concentration of animal or plant remains in glacial sediments suggests how long ago the sediments were deposited, provided the time lag between the death of the organism and the age of the sediments can be estimated. The method does require calibration, because the radiocarbon concentration of the atmosphere varies over time.

Cosmogenic exposure dating helps determine how long rocks have been at the earth's surface. Primary cosmic rays strike atoms in the upper atmosphere, producing particle cascades that include high-energy protons and neutrons, plus muons (Gosse and Phillips, 2001). These secondary cosmic rays break atomic nuclei in rocks into smaller fragments. Because the nuclear fragments contain fewer protons than the original nuclei, they become atoms of other elements with smaller atomic numbers. The concentrations of these nuclei in rock surfaces increase with exposure time. Therefore, the concentrations of cosmogenic nuclides in boulders on the crests of a moraine should be directly related to the age of the moraine. However, the method makes several important assumptions. First, the boulders must have arrived at the moraine with no preexisting concentration of cosmogenic nuclides. Second, the sampled points must not have been covered by snow, sediment, or rock at any time since deposition of the moraine. If the first assumption is violated, the exposure dates will be too old; if the second assumption is violated,

the exposure dates will be too young. Geomorphic processes are often responsible for these problems (see review in Ivy-Ochs et al., 2007). As with radiocarbon dating, the method must be calibrated (Balco et al., 2008, and references therein), because the production rates of cosmogenic nuclides vary with altitude, latitude, and time.

Optically stimulated luminescence dating estimates the burial time of sediment, especially fine quartz sand deposited by running water. Buried sediment is bombarded by radiation produced by the decay of radioactive elements in the surrounding sediment. The radiation displaces electrons into "traps" in the crystal lattices of the sand grains. When exposed to light or heat, the trapped electrons "fall" back to their usual places, releasing photons. The number of photons released is proportional to the burial time. Where stream sediments are buried by a moraine, optically stimulated luminescence dates provide a maximum limiting estimate of the moraine's age. As with cosmogenic exposure dating, the method assumes that the sediment had no stored signal at the time of burial. This condition is most often fulfilled by fluvial sediments, which are exposed to light during transport. Further uncertainties are introduced by the water content of the sediment, because water shields sand grains from radiation. In addition, the radioactivity of the sediment is often hard to measure, and the sensitivity of different grains to radiation can vary strongly within the same sample.

Of these three methods, cosmogenic exposure dating is perhaps the most widely used. Under ideal circumstances, exposure dating estimates the ages of moraines directly. In contrast, there is typically a time lag between the death of an organism, or the laying down of fine sand, and the construction of an associated moraine. The only circumstance in which radiocarbon dates directly estimate the time of moraine construction is that in which an advancing glacier buries living plants (e.g., Lowell, 1990). In addition, sampling opportunities for exposure dating are much more common than for radiocarbon dating or optically stimulated luminescence dating.

Most moraines have bouldery surfaces; exposures in moraines that provide opportunities for radiocarbon dating or optically stimulated luminescence dating are comparatively rare.

Nuclides used in cosmogenic exposure dating

Cosmic rays produce a variety of nuclides in surface rocks, but only some of these species are useful in exposure dating. The useful nuclides are those that have half-lives of a few thousand years or more, are rare in earth surface rocks except where produced by cosmic rays, have production rates of at least a few atoms per gram of rock per year, and do not escape from rocks over time. The nuclides that meet these criteria include beryllium-10, chlorine-36, aluminum-26, helium-3, carbon-14, and neon-21 (Gosse and Phillips, 2001; Muzikar et al., 2003).

This dissertation discusses just one of these nuclides, beryllium-10 (^{10}Be). Opportunities for applying beryllium-10 in cosmogenic exposure dating studies are widespread, because beryllium-10 is produced in the common mineral quartz. The cosmogenic nuclides aluminum-26 and carbon-14 also are produced in quartz, but their concentrations are more difficult to measure precisely than those of beryllium-10. Helium-3 and neon-21 occur in olivine, which is much rarer than quartz in moraine boulders (see Licciardi et al., 2001, for a rare counterexample). Last, the production systematics of beryllium-10 are easier to model than those of chlorine-36 (Gosse and Phillips, 2001). For these reasons, the majority of cosmogenic exposure dating studies use beryllium-10.

Problems in cosmogenic exposure dating

Despite the obvious potential of beryllium-10 exposure dating for determining the ages of moraines, problems in applying the method remain.

First, the scatter among exposure dates from single moraines is often unexpectedly large. The 1σ measurement uncertainty of beryllium-10 exposure dates generated using modern analytical methods is small, about 3-5% of the central estimate (e.g., Kelly et al., 2008). Moraine surfaces are thought to be about the same age everywhere, and measurement errors tend to be normally distributed. Therefore, we expect that exposure dates from a single moraine crest should obey a normal distribution, and this distribution should have a standard deviation consistent with the measurement uncertainty. In practice, these criteria are rarely fulfilled; the observed scatter is, on average, about 40% of the oldest exposure date, after old outliers are discarded (Putkonen and Swanson, 2003).

Second, there is little agreement between studies in terms of how to estimate the ages of moraines from highly scattered collections of exposure dates. Proposed estimators include measures of a data set's central tendency (e.g., the mean of the exposure dates, the mean weighted by the inverse square of the measurement uncertainty, and the mode), as well as extreme estimators (the oldest date and the youngest date). Often, some of the exposure dates are discarded before one or another of these estimators is applied.

This variety of interpretive methods produces an unacceptably large uncertainty in the estimated ages of moraines. For last-glacial moraines, about 20 ka old, the range of exposure dates can be several thousand years (e.g., Laabs et al., 2009). If any age estimate between the youngest date and the oldest date is permissible, then the uncertainty in moraine age estimates is at least as great as this range. This uncertainty is too large to provide useful answers to the paleoclimate questions listed above.

Outline of this dissertation

Given these problems, this dissertation asks two questions. First, why are cosmogenic exposure dates from single moraines so widely distributed? Second, given this degree of scatter, how can we best determine the ages of moraines from collections of cosmogenic exposure dates?

This work addresses these problems from a modeling perspective. The models presented here use Monte Carlo methods (Bevington and Robinson, 2003) to estimate the probability distributions of exposure dates under particular sets of geomorphic assumptions. The models are then compared against observed data sets by adjusting the model input parameter values until the models reproduce the distributions of the observations.

The remaining chapters are arranged as follows. Chapter 2 describes two numerical models that explain the variability in exposure dates from moraines. Chapter 3 gives methods for inverting these models against collections of exposure dates. Last, Chapter 4 describes other problems that are addressed by this work, and suggests potential solutions.

Appendix A is a technical comment that was published in *Science* (Applegate et al., 2008). This comment describes early versions of the numerical models described in Chapter 2. Appendix B describes the production of cosmogenic nuclides in spherical solid bodies; a more developed version of this work will be submitted as a technical note in the future.

Authorship statement

Chapters 2-4 and Appendix B are intended for eventual submission as journal articles; Appendix A has already been published. Although these chapters and appendices have multiple contributors, I (Patrick J. Applegate) am the primary author for all parts of this dissertation. The

model code and simulations are exclusively my work, and the bulk of the interpretations are mine.

Chapter 2

Modeling the statistical distributions of cosmogenic exposure dates from moraines

Cosmogenic exposure dating provides a method for estimating the ages of glacial moraines deposited in the last ~100,000 years. Cosmic rays break atoms in surface rocks at predictable rates. Thus, the ages of moraines are directly related to the concentrations of cosmic ray-produced nuclides in rocks on the moraine surfaces, under ideal circumstances. However, many geomorphic processes may interfere with cosmogenic exposure dating. Because of these processes, boulders sometimes arrive at the moraines with preexisting concentrations of cosmogenic nuclides, or else the boulders are partly shielded from cosmic rays following deposition. Many methods for estimating moraine ages from cosmogenic exposure dates exist in the literature, but we cannot assess the appropriateness of these methods without knowing the parent distribution from which the dates were drawn on each moraine. Here, we make two contributions. First, we describe numerical models of two geomorphic processes, moraine degradation and inheritance. Second, we assess the robustness of several methods for estimating the ages of moraines from collections of cosmogenic exposure dates. Our models estimate the probability distributions of cosmogenic exposure dates that we would obtain from moraine boulders with specified geomorphic histories, using Monte Carlo methods. We expand on pioneering modeling efforts to address this problem by placing these models into a common framework. We also evaluate the sensitivity of the models to changes in their input parameters. The sensitivity tests show that moraine degradation consistently produces left-skewed distributions of exposure dates; that is, the distributions have long tails toward the young end of the distribution. In contrast, inheritance produces right-skewed distributions that have long tails toward the old side of the distribution. Given representative distributions from these two models, we can determine which methods of estimating moraine ages are most successful in recovering the correct age for test cases where this value is known. The mean is a poor estimator of moraine age for data sets drawn from skewed parent distributions, and excluding outliers before calculating the mean does not improve this mismatch. The extreme estimators (youngest date and oldest date) perform well under specific circumstances, but fail in other cases. We suggest a simple estimator that uses the skewnesses of individual data sets to determine whether the youngest date, mean, or oldest date will provide the best estimate of moraine age. Although this method is perhaps the most globally robust of the estimators we tested, it sometimes fails spectacularly. The failure of simple methods to provide accurate estimates of moraine age points toward a need for more sophisticated statistical treatments.

Cosmogenic exposure dating is an important technique for learning about glacier size changes during the last ~10^5 yr of geologic time (Gosse and Phillips, 2001). Glaciers and ice sheets grow and shrink in response to climate change (Dyurgerov and Meier, 2000; Oerlemans, 2005; Jansen et al., 2007). Therefore, reconstructions of past glacier sizes over time yield information on past climates and rates of sea level rise. As glaciers advance and retreat, they mark their former margins with ridges of debris, called moraines (Gibbons et al., 1984). In cosmogenic exposure dating, field geomorphologists collect samples from boulders on the crests of moraines, and the concentrations of certain rare chemical species (cosmogenic nuclides) are measured in the samples. These cosmogenic nuclides are produced at predictable rates in surface materials by cosmic rays (Lal, 1991; Gosse and Phillips, 2001). Under ideal conditions, the ages of the moraines can be calculated directly from the nuclide concentrations (e.g., Gosse et al., 1995a).

Unfortunately, geomorphic processes bias cosmogenic exposure dates (see review in Ivy-Ochs et al., 2007). If the boulders contain some preexisting concentration of cosmogenic nuclides when they are deposited on the moraine, then the exposure dates will tend to overestimate the moraine's age. Most other processes tend to reduce the apparent exposure times of the boulders. For example, cover by snow or sediment reduces the flux of cosmic rays through the upper surfaces of the boulders. The exposure dates from these shielded boulders will underestimate the true age of the moraine on which they rest. Similarly, erosion of boulders removes the most nuclide-rich part of the rocks (Lal, 1991); therefore, eroded boulders also yield exposure dates that underestimate the age of their host moraine.

The effects of these processes on the distributions of exposure dates from moraines are not known *a priori*, and this lack of knowledge complicates efforts to estimate the ages of moraines from cosmogenic exposure dates. This uncertainty is reflected in the variety of procedures for estimating the ages of moraines that are described in the literature. Many workers

prefer to use some measure of the central tendency of a data set; such estimators include the arithmetic average, the mean weighted by the inverse variance, and the mode (e.g., Kaplan et al., 2005; Licciardi et al., 2004; Kelly et al., 2008). Other investigators prefer extreme estimators, including both the youngest and the oldest dates (e.g., Benson et al., 2005; Briner et al., 2005). For data sets with large ranges, the choice of estimator has a profound effect on the estimated ages of the moraines (for example, compare Chevalier et al., 2005, with Brown et al., 2005). The choice of estimator is typically informed by geomorphic observations. However, without knowledge of the underlying parent distribution from which the dates are drawn, we cannot evaluate the effectiveness of these different procedures.

We might evaluate the effects of geomorphic processes on cosmogenic exposure dating by performing a positive control experiment. In such an experiment, we would identify a moraine whose age was known independently, perhaps from bracketing radiocarbon dates (e.g., Kowalski et al., in prep.). We would then collect many samples from this moraine for cosmogenic exposure dating, and compare a histogram of the exposure dates to the independently known age of the moraine. The distribution of the exposure dates about the true age of the moraine would tell us the effects of geomorphology on the exposure dates from that moraine, other factors being equal.

Unfortunately, such a positive control experiment is impractical. To achieve robust results, we would need many exposure dating samples from one moraine. The exact number of samples required is poorly defined, but it seems likely that 50 samples are insufficient (see Murphy, 1964, his Fig. 6). Because cosmogenic exposure dates are expensive, the necessary number of samples is probably not achievable. In addition, the geomorphic processes that affect exposure dating are likely to be highly variable between field sites. Thus, we would need to repeat the experiment on a large sample of moraines, multiplying the cost many times. Moreover, there are few sites where the ages of moraines are known independently, and these sites are

already included in the nuclide production rate calibration database (Balco et al., 2008). Last, there are potential confounding effects. The difference between the independently determined age of a moraine and any individual exposure date is influenced by errors in estimating both the age of the moraine and the local production rates of cosmogenic nuclides, as well as geomorphic processes. Thus, a positive control experiment to isolate the effects of geomorphic processes on exposure dating is prohibitively expensive, probably cannot be done for a representative sample of moraines, and is subject to strong confounding effects from uncertainties in moraine age estimates and nuclide production rates.

Monte Carlo-based numerical models offer a means of assessing the effects of geomorphic processes on cosmogenic exposure dating that avoids the disadvantages of positive control experiments. Although these models can never replace field observations, they provide a test bed for understanding existing exposure dates. Such models can generate thousands of synthetic exposure dates in a few minutes on desktop computers. Thus, these models do not have the large costs associated with collecting a representative number of samples from individual moraines. In these models, the user prescribes the age of the moraine and the nuclide production rate. Therefore, there are no confounding effects in the model experiments from errors in estimating these values.

In this chapter, we present Monte Carlo models of two geomorphic processes that introduce biases into exposure dating. These processes are moraine degradation and inheritance, which we describe below. Our models are based on earlier work (e.g., Zreda et al., 1994; Hallet and Putkonen, 1994; Putkonen and Swanson, 2003; Benson et al., 2005; see also Muzikar, 2009). We expand on these groundbreaking studies in several ways. First, we provide explicit descriptions of the mathematical formulations of the models, pointing out the simplifying assumptions that are inherent in these formulations. We test the models' sensitivity to changes in

their input parameters. Last, we provide code for these models that is written in MATLAB, an easily understood, high-level programming language.

In Chapter 3, we describe methods for making explicit comparisons between the output of our models and individual data sets. This comparison can indicate which of the two processes we treat here is dominant on a particular moraine. More importantly, this inverse modeling procedure yields explicit estimates of moraine age, as well as other model parameters.

Methods

Numerical models

We describe models of two geomorphic processes that influence cosmogenic exposure dates from moraine boulders. These processes are moraine degradation and inheritance. In this section, we describe how our models treat these two processes, and we present preliminary results from these models.

These models are deliberately simplified. In theory, we could build a comprehensive model of moraine geomorphology that would incorporate all of the processes that influence exposure dates on moraines. However, we wish to invert these models against observations, to allow direct estimation of moraine ages from collections of cosmogenic exposure dates (Chapter 3). In a model inversion, the maximum number of model parameters that can be estimated from a data set is typically smaller than the number of observations. Our models have three to five parameters each, and most collections of cosmogenic exposure dates from moraines contain about five observations (Putkonen and Swanson, 2003). Therefore, our models are already at the complexity limit imposed by the sizes of most available data sets.

In any case, the usefulness of our models should be evaluated by confronting them with data (Box and Draper, 1987; Hilborn and Mangel, 1997). We describe this confrontation between our models and exposure dates from the literature in Chapter 3. If our models produce good representations of observed data sets, then perhaps we have identified the most important processes that influence exposure dates on moraines.

The moraine degradation model

In moraine degradation (Fig. 2.1), slope processes remove material from the crests of moraines and redeposit this material at the bases of the moraine slopes. The theoretical basis for understanding the redistribution of sediment on moraine slopes comes from observations made on fault scarps, wave-cut bluffs, and other landforms composed of unconsolidated sediment. These landforms become less steeply inclined and more rounded over time, suggesting that hillslope evolution can be modeled as a diffusive process (Nash, 1986; Hanks, 2000; Pelletier et al., 2006; Pelletier, 2008). That is, material moves downhill at a rate that is proportional to the local gradient. This observation implies that a sharp-crested moraine will become shorter (less tall) over its lifetime, as material moves from the moraine's crest to the toe of its slope (Anderson and Humphrey, 1989; Hallet and Putkonen, 1994; O'Neal, 2006; Putkonen et al., 2007; Pelletier, 2008).

Moraine degradation imparts a bias to cosmogenic exposure dates because it exposes boulders at the moraine crest that have been buried in sediment for some part of the moraine's history (Fig. 2.1). Moraines typically contain large rocks distributed throughout a fine-grained matrix (Dreimanis, 1988; Benn and Evans, 1998). Because slope processes preferentially move fine-grained material, the boulders become concentrated on the crest of the moraine. Some of these boulders have been partly shielded from cosmic rays by the overlying sediment; they

therefore contain smaller concentrations of cosmogenic nuclides than the boulders that have rested on the moraine crests since deposition of the moraine. The exhumed boulders yield cosmogenic exposure dates that underestimate the age of the moraine.

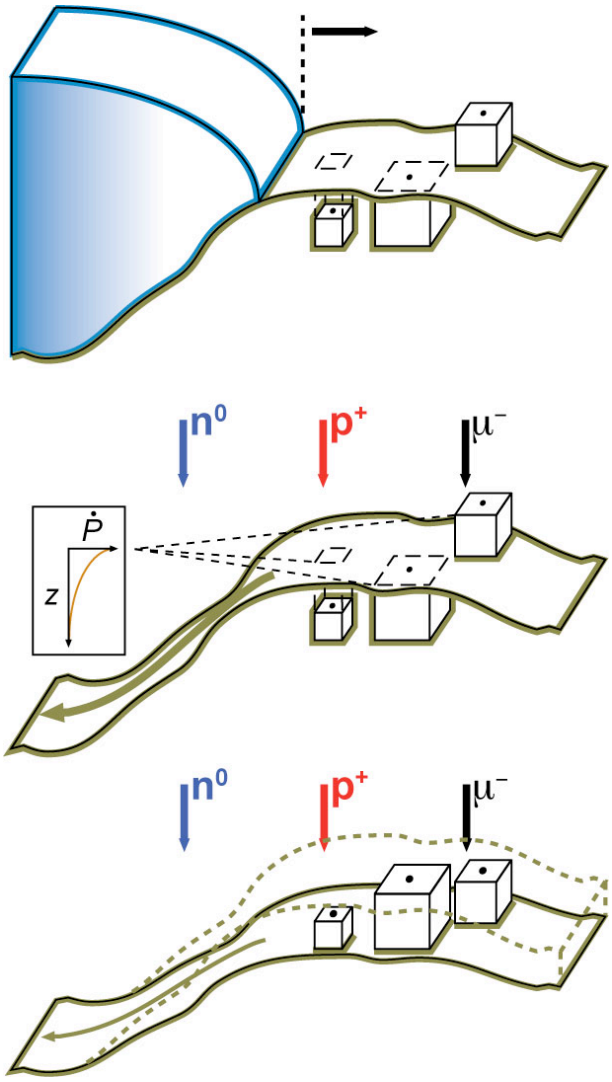

Figure 2.1: Conceptual model of moraine degradation.
Top: An advancing glacier margin constructs a new moraine. Some boulders, shown as cubes, are buried, whereas other boulders rest on the surface of the moraine.
Middle: The glacier margin retreats, abandoning the moraine. Several processes begin. The boulders begin to accumulate cosmogenic nuclides as they are bombarded by cosmic rays, shown as arrows. The cosmic ray flux is made up of neutrons (n^0), protons (p^+), and negative muons (μ^-). The production rate in each boulder depends on its burial depth; boulders at the surface accumulate nuclides most rapidly, and the production rate falls off exponentially with depth, as shown in the inset panel. At the same time that the boulders accumulate nuclides, loose sediment moves downhill.
Bottom: After some period of time, many boulders are on the moraine surface, including a large number that were originally buried. The moraine slope has diminished, and so has the downhill flux of sediment. The original surface of the moraine is shown as a dashed line. Eventually, the boulders are sampled, yielding a wide range of exposure dates.

The model framework that we describe here builds on earlier studies. The use of slope evolution models to study moraines was first considered by Anderson and Humphrey (1989); Zreda et al. (1994) developed a model for the production of nuclides in boulders buried in an eroding surface. The first model of cosmogenic nuclide production on a diffusively evolving

moraine was presented by Hallet and Putkonen (1994). This model was later developed further by Putkonen and Swanson (2003). Our model is closest to that of Putkonen and Swanson (2003).

To model the effects of slope processes on the height of moraines over time, we assume that moraines have an initial cross-section that is triangular, with an initial height h_0 and an initial slope S_0, which is the (dimensionless) tangent of the slope in degrees. This profile evolves over time according to the one-dimensional diffusion equation,

$$\frac{\partial z}{\partial t} = k\frac{\partial^2 z}{\partial x^2}$$

(Hanks, 2000), where $z(x, t)$ is the height of the moraine as a function of horizontal distance from the moraine crest x and time t; k is the topographic diffusivity (m^2/ yr). This rule assumes that k is constant over t and x (Pelletier et al., 2006; cf. Hallet and Putkonen, 1994; Roering et al., 2001). Solving this differential equation with our "sawtooth" initial moraine profile yields

$$z(x,t) = \frac{h_0}{2L}\left[\left(\frac{2\sqrt{kt}}{\sqrt{\pi}}\right)z_1 + z_2\right], \qquad \text{(eqn. 2.1)}$$

where

$$L = \frac{h_0}{S_0},$$

$$z_1 = \exp\left[\frac{-(L+x)^2}{4kt}\right] - 2\exp\left(\frac{-x^2}{4kt}\right) + \exp\left[\frac{-(L-x)^2}{4kt}\right], \text{ and}$$

$$z_2 = (L+x)\,\mathrm{erf}\left(\frac{L+x}{2\sqrt{kt}}\right) - 2x\,\mathrm{erf}\left(\frac{x}{2\sqrt{kt}}\right) + (L-x)\,\mathrm{erf}\left(\frac{L-x}{2\sqrt{kt}}\right)$$

(cf. Pelletier, 2008, his eqn. 2.45). Equation 2.1 agrees well with a Crank-Nicolson solution to equation 4 of Hallet and Putkonen (1994) if their $\beta = 0$; compare equation 4 of Hallet and Putkonen (1994) to equations 9.56 and 9.67 of Fletcher (1991). This analytical solution can be evaluated very quickly.

Setting $x = 0$ in equation 2.1 yields an expression for the height of the moraine's crest as a function of time,

$$h(t) = \frac{h_0}{L}\left\{\left(\frac{2\sqrt{kt}}{\sqrt{\pi}}\right)\left[\exp\left(\frac{-L^2}{4kt}\right) - 1\right] + L\,\mathrm{erf}\left(\frac{L}{2\sqrt{kt}}\right)\right\}. \qquad \text{(eqn. 2.2)}$$

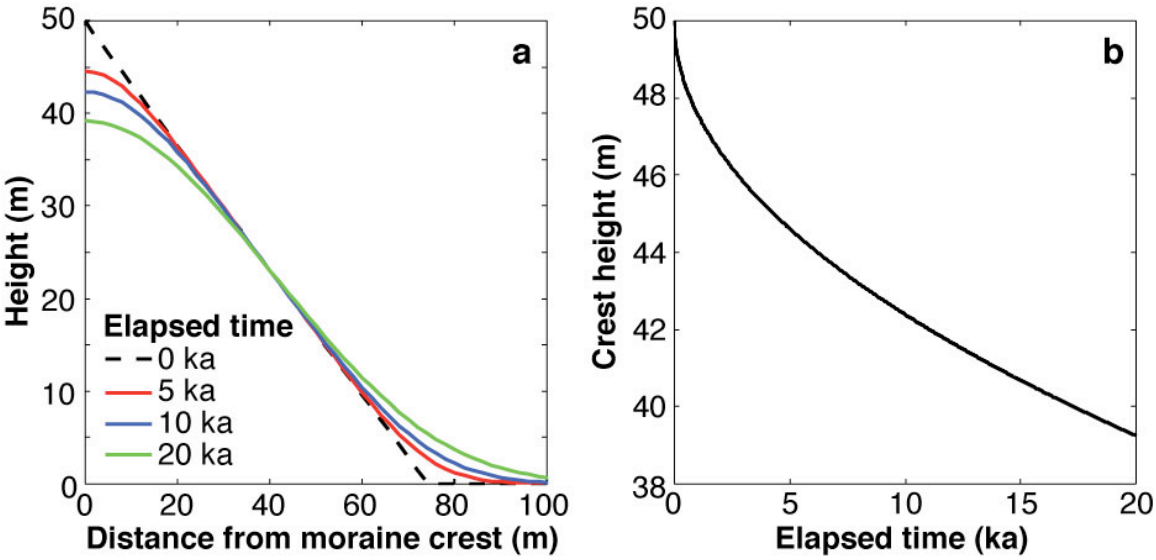

Figure 2.2: Evolution of moraine profile with time (a) and change in height of moraine with time (b) for a representative case. As time goes on, the moraine's profile changes most at the crest and at the toe of the slope, becoming generally more rounded. As material is transported from the crest to the toe of the slope, the moraine becomes shorter. The moraine loses height rapidly at first, then more slowly. In (a), only one-half of the moraine's profile is shown; the modeled moraine is symmetrical about the *y*-axis. Note that the moraine loses more than 10 m of its initial height over 20 ka. Compare (a) to Figure 1 of Hallet and Putkonen (1994); compare (b) to Figure 1 of Putkonen and Swanson (2003). In this figure, the moraine's initial height is 50 m, its initial slope is 34°, and its topographic diffusivity is 10^{-2} m^2/ yr.

Figure 2.2 shows solutions to equations 2.1 and 2.2 for selected parameter values. The left panel (Fig. 2.2a) shows the moraine half-profile for elapsed time values of 5 ka, 10 ka, and 20 ka. The moraine starts with a triangular profile, but becomes more rounded and shorter over time. The right panel (Fig. 2.2b) shows the height of the moraine as a function of time. The rate of crest lowering is rapid at first, then slows. In both panels, the initial moraine height is 50 m, the initial moraine slope is 34° (Putkonen and Swanson, 2003), and the topographic diffusivity is

10^{-2} m^2/ yr (Hanks, 2000; Putkonen et al., 2007). These values seem reasonable for the large, last-glacial moraines of the western United States.

Given equation 2.2, we can calculate the nuclide concentration in a boulder buried to some specified depth d_0 below the moraine's surface at the time of deposition. For purposes of calculating nuclide production rates, the depth of a boulder $d(t)$ is given by

$d(t) = h(t) - (h_0 - d_0)$ for $h(t) \geq h_0 - d_0$, and

$d(t) = 0$ for $h(t) < h_0 - d_0$.

Note that d_0 and d here refer to the depth of the top of the boulder, which is the point that will be sampled for cosmogenic nuclide measurements.

Values of d_0 that exceed h_0- h_f are not meaningful, because these boulders will still be buried in the moraine at the time of sampling. By h_f, we mean the final height of the moraine, achieved when t reaches the moraine's age. In addition, field geomorphologists typically do not sample boulders that stand less than some minimum height h_b above the moraine crest (~1 m; e.g., Gosse et al., 1995b). Thus, all the boulders that are sampled have values of d_0 that satisfy the criterion

$0 \leq d_0 \leq \max(d_0)$;

$\max(d_0) = h_0 - h_f - h_b$.

The production rate of most cosmogenic nuclides declines exponentially as a function of depth below material surfaces (Lal, 1991; see Zreda et al., 1994, for an important exception). That is,

$$P(d) = P_0 \exp\left(\frac{-d}{\Lambda}\right), \qquad \text{(eqn. 2.3)}$$

where P_0 is the production rate of the nuclide at the surface (atoms/ g rock/ yr), and Λ is the attenuation length of cosmic rays in the material (~160 g/ cm^2, divided by the material's density).

We use the Lal/Stone production rates from the CRONUS online calculator (Balco et al., 2008) to estimate P_0.

Equation 2.3 is a good approximation only at shallow depths, where nucleon production dominates; at greater values of $d(t)$, muon production becomes important (Gosse and Phillips, 2001). To account for muon production, we use the parameterization of Granger and Muzikar (2001, their eqns. 1-3). This scheme represents production at a given depth as the sum of four exponential terms, each with its own P_0 and Λ. That is,

$$P(d) = \sum_{i=1}^{4} P_i \exp\left(\frac{-d}{\Lambda_i}\right). \qquad \text{(eqn. 2.4)}$$

We scale these terms relative to their values at sea level and high latitude, again using the CRONUS online calculator (Balco et al., 2008). This expression is a parameterization; Heisinger et al. (2002a, 2002b) present alternative expressions that resolve the underlying physics. We use the relationship presented in equation 2.4 because it can be evaluated very quickly as a vector calculation in MATLAB. The speed of evaluation is important because this calculation must be performed approximately 10^7 times for each forward run of this model (see below).

Figure 2.3a shows the production rate of the cosmogenic nuclide beryllium-10 as a function of depth. Nucleon production dwarfs muon production at the surface, but muon production becomes increasingly important at greater depths (Fig. 2.3b).

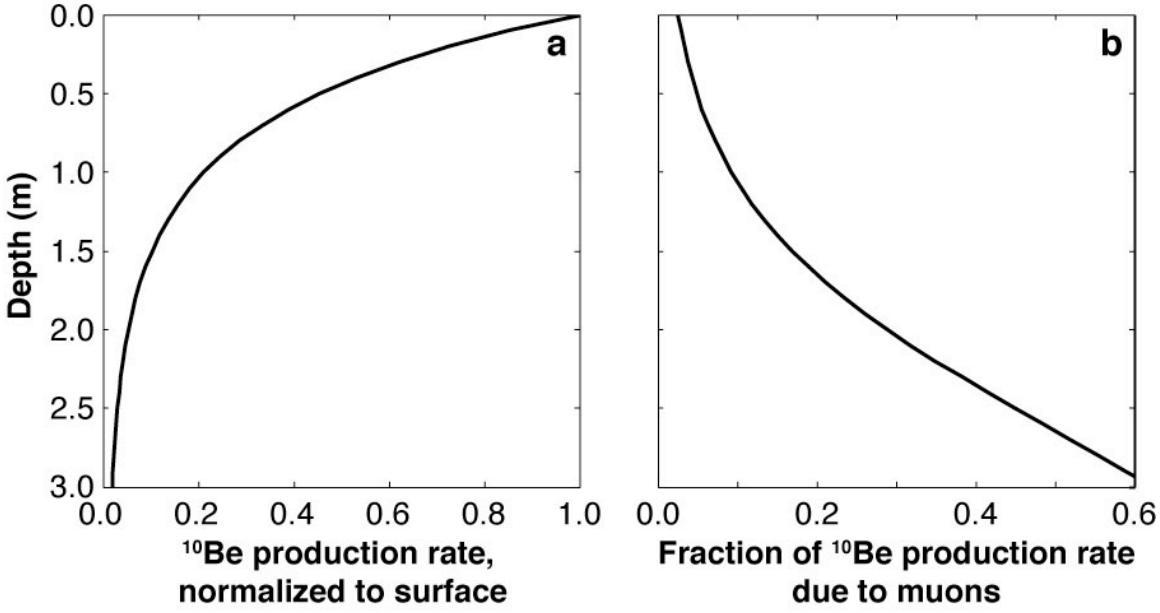

Figure 2.3: Production rate of beryllium-10 with depth (a) and fraction of beryllium-10 production due to muons as a function of depth (b) in quartzite, following Granger and Muzikar (2001). The total production rate of beryllium-10 is roughly exponential as a function of depth; production is greatest at the surface, and falls off below the surface with an *e*-folding length of a few tens of centimeters (Lal, 1991). Most production near the surface is caused by high-energy protons and neutrons, which produce beryllium-10 by splitting atoms of oxygen and silicon in quartz (Gosse and Phillips, 2001). At greater depths, most production is due to muons, which do not interact with target atoms in the rock as easily as high-energy protons and neutrons. Compare this figure to Figure 2a of Gosse and Phillips (2001). This figure assumes surface beryllium-10 production rates corresponding to sea level and high latitude and a rock density of 2.65 g/ cm^3.

Given equations 2.2 and 2.4, we can calculate the final concentration of cosmogenic nuclides in a moraine boulder. This calculation depends only on the moraine's initial geometry (h_0, S_0), its age, its topographic diffusivity k, and the boulder's initial depth d_0. However, the production rate in a given boulder is a piecewise function of time, because the production rate stops changing when the boulder breaks the surface of the moraine (that is, when d becomes 0; Fig. 2.4b). Therefore, we break the lifetime of the moraine into n time steps, each having a duration Δt. We then evaluate the change in concentration during each of these time steps. The final concentration C_f in any single boulder is the sum of the changes in concentration during the individual time steps, or

$$C_f = \sum_{i=1}^{n} \left\{ P(t)\Delta t - C_{i-1}\left[1 - \exp(-\lambda \Delta t)\right] \right\} \qquad \text{(eqn. 2.5)}$$

(Lal, 1991, his eqn. 6; cf. eqn. 2.6, below). The second term in brackets represents the progressive decay of unstable cosmogenic nuclides; λ is the decay constant of the appropriate nuclide (yr^{-1}; Gosse and Phillips, 2001; Balco et al., 2008). The difference between this approximation and an exact solution can be made arbitrarily small by reducing Δt. For the model runs shown in this dissertation, we used values of Δt ranging from 25 yr to 100 yr. Note that the initial concentration C_0 is taken to be zero here; we treat inheritance in the next section.

Figure 2.4a shows the depths of four boulders within the moraine as a function of time, assuming the same model parameters as in Figure 2.2. At the beginning of the simulation, one boulder is at the surface (d_0 = 0 m), another boulder is buried to a depth of 9 m (d_0 = 9 m), and the other two boulders are evenly spaced between these depths. As the moraine becomes shorter over time, the boulders approach the surface and are eventually exposed at the surface. Compare this figure to Figure 2.2b.

Figure 2.4b shows the concentrations of beryllium-10 as a function of time in each of the boulders whose depth trajectories are shown in Figure 2.4a. Again, the model parameters used to generate this figure are the same as those in Figure 2.2. The concentrations in the boulders increase slowly while the boulders are still buried in the moraine; after they reach the surface, the concentration increases roughly in proportion to surface residence time. Although the curves that describe nuclide concentration in the boulders as a function of time appear to be linear after the boulders reach the surface, they are slightly sublinear because of nuclear decay (eqn. 2.5). Note that the bulk of the final nuclide concentration in each boulder is acquired only after the boulder reaches the surface, even for the boulder that is buried most deeply in the moraine at the beginning of the simulation. This figure assumes that the beryllium-10 concentrations in all the boulders are zero when the simulation begins.

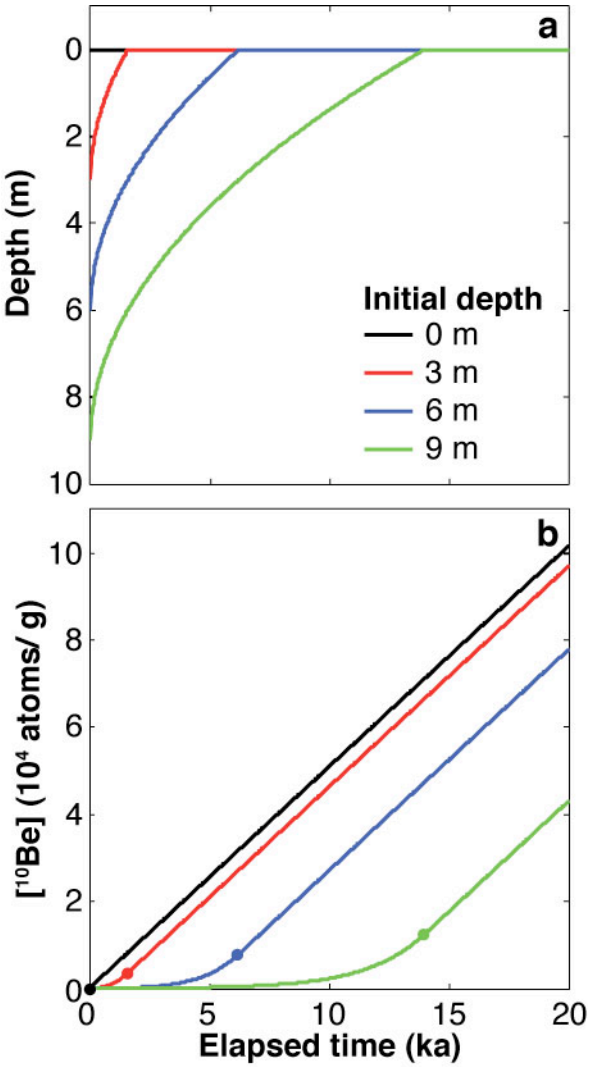

Figure 2.4: Depths of boulders in a degrading moraine over time (a) and beryllium-10 concentrations in the same boulders as a function of time (b). If boulders are uniformly distributed throughout the till, then some boulders will be at the surface when the moraine is deposited, whereas other boulders will be present in the till at greater depths. As time goes forward, the moraine becomes shorter (Fig. 2.2), and the boulders approach the surface. At the same time, cosmogenic nuclides are produced in the boulders (Fig. 2.3). For buried boulders, production rates increase slowly as the surface lowers, then become constant after the boulders are exposed at the surface. Note that the majority of the cosmogenic nuclides in each boulder are produced after the boulder reaches the surface, even for the most deeply buried boulder. In (b), the dots indicate the time when each boulder reaches the surface. As in Figure 2.2, the moraine's initial height is 50 m, its initial slope is 34°, and its topographic diffusivity is 10^{-2} m^2/ yr. The final heights of all the boulders are 1 m.

Although we do not emphasize boulder erosion in this chapter, the model treats erosion by the progressive removal of thin shells of material from boulder surfaces after they are exhumed from the till. In contrast to Hallet and Putkonen (1994), we do not allow boulders to shrink below the observed boulder height h_b (see Zreda et al., 1994). Instead, we determine the amount of time that each boulder will be exposed to surface weathering from equation 2.2, then specify initial sizes for the boulders that will result in the boulders having the observed height.

This model assumes that exhumed boulders do not topple or rotate as the crest of the moraine deflates. It also neglects the effects of cryoturbation (Lal and Chen, 2005). Toppling or rotation of boulders on a degrading moraine would produce a larger range of exposure dates than degradation alone, because these processes effectively reduce the measured nuclide concentrations in sampled boulders (Ivy-Ochs et al., 2007; Schaefer et al., 2008). Conversely, cryoturbation might bring boulders to the moraine surface sooner than would be predicted by diffusive removal of the moraine crest, thereby reducing the range of exposure dates from the moraine. In this chapter, we assume that these processes are not dominant.

Some moraines have geomorphic characteristics that are inconsistent with the assumptions used in constructing the moraine degradation model. For example, it would be inappropriate to apply our model of moraine degradation to the large Pinedale terminal moraines near Pinedale, Wyoming (Richmond, 1973; Gosse et al., 1995), particularly in the Halls Lake (Mud Lake) drainage. These moraines have broad, flat crests, where the local slope is close to zero. Consequently, the downhill flux of material at the crests of these moraines should be small. We expect that these moraines have lost little material from their crests over time. Moreover, limited exposures in roadcuts at Fremont Lake show that there are few or no boulders in the subsurface till (E. Evenson, personal communication). This observation invalidates the assumption that the boulders are uniformly distributed throughout the outermost Pinedale-age moraine at Fremont Lake.

The inheritance model

Boulders that are deposited on a moraine with nonzero concentrations of cosmogenic nuclides are said to have inheritance. The inherited nuclides were produced in each boulder during one or several periods of "pre-exposure" (Ivy-Ochs et al., 2007). That is, the boulders

were incompletely shielded from cosmic rays before being deposited on the moraine. These boulders contain larger concentrations of cosmogenic nuclides than boulders that were completely shielded from cosmic rays at all times before being incorporated into the moraine. Exposure dates from boulders with inherited nuclides tend to overestimate the age of the moraine.

There are at least two potential sources of pre-exposed boulders in glaciated landscapes (Ivy-Ochs et al., 2007). First, boulders may topple onto the glacier surface from cirque headwalls or adjacent, oversteepened valley walls (Seong et al., 2009). These boulders then ride the glacier's surface to the terminus, where they fall onto the moraine. Second, glaciers may re-entrain boulders deposited in the valley bottom during an earlier advance, or pluck boulders from bedrock outcrops at the glacier bed. These boulders are then transported subglacially to the glacier terminus, where they may be emplaced at the moraine surface by thrusting (e.g., Kruger, 1996) or other ice-marginal processes.

The mathematical descriptions of these two situations are nearly identical. In both cases, the concentration measured in each boulder is the sum of the inherited component acquired during pre-exposure, and the post-depositional component that reflects the exposure history of the boulder after moraine construction.

The model that we describe here is based on an earlier model presented by Benson et al. (2005), which treated inheritance in boulders derived from cirque headwalls. Our model uses a mathematical formulation that is similar to the one used by Benson et al. (2005), but treats a larger set of geomorphic situations. In addition, our model of inheritance is similar to the model of nuclide concentrations in sediment over time used in cosmogenic burial dating (Granger et al., 2001; Granger and Muzikar, 2001). Following this pioneering work, we assume that the sampled clasts had two distinct periods of residence in the landscape, and that the rate of change of nuclide concentrations in the clasts was different during these two periods.

For simplicity, we begin by describing the model treatment of inheritance in reworked boulders (Fig. 2.5). We then point out a slight change in the model formulation that allows it to treat inheritance in boulders derived from cirque headwalls and valley walls.

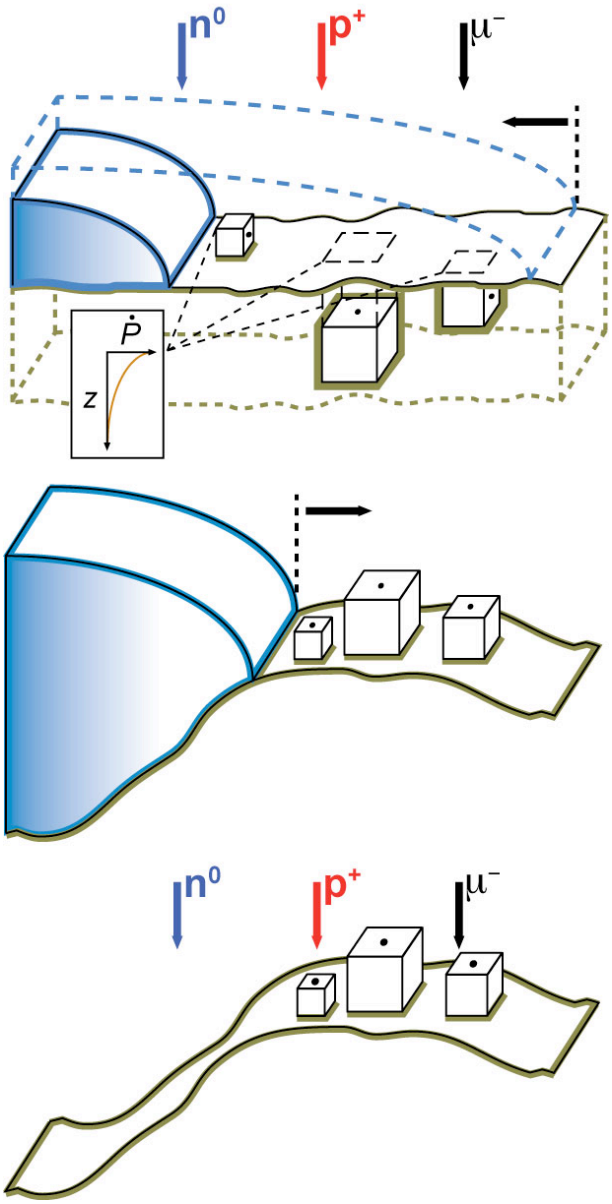

Figure 2.5: Conceptual model of inheritance, as caused by boulder reworking.
Top: A retreating glacier margin deposits a till carpet on its former bed. The till carpet is outlined in dashed, brown lines. Some boulders, shown as cubes, are distributed throughout the till carpet. The boulders contain different concentrations of cosmogenic nuclides, depending on their depth in the till carpet and the length of time since the margin of the ice sheet uncovered the overlying till surface. The dot on each boulder represents the point that will eventually be sampled for cosmogenic nuclides.
Middle: The glacier readvances, eroding to some depth within the till carpet and incorporating the boulders into a new moraine. Glacial transport rotates the boulders to their final orientations.
Bottom: The glacier margin abandons the new moraine, and the boulders accumulate more cosmogenic nuclides. Eventually, the boulders are sampled, yielding a wide range of exposure dates.

For reworked boulders, the inherited concentration in each boulder depends on the time between deposition of the boulder by the retreating ice and entrainment of the boulder by the readvancing glacier t_{pre}, and on how deeply the boulder was buried during this time d_{pre}. Both

these parameters are unknown for any individual boulder, but it is reasonable to say that they must range from zero to some maximum.

$0 \le t_{\text{pre}} \le \max\left(t_{\text{pre}}\right)$, and

$0 \le d_{\text{pre}} \le \max\left(d_{pre}\right)$.

The maximum time $\max(t_{\text{pre}})$ represents the time between the beginning of the penultimate glacial retreat and the time of moraine deposition; the maximum depth $\max(d_{\text{pre}})$ is the maximum thickness of material eroded by the glacier during its readvance.

Note that d_{pre} refers to the depth of the point on each boulder that is eventually sampled, not the top of the boulder, during the predepositional exposure time. Field geomorphologists typically sample the upper surfaces of boulders, because those surfaces receive the maximum flux of cosmic rays. However, glacial transport rotates boulders, and so the sample point is not necessarily the same as the apex of the boulder during the predepositional exposure time. Sampling of the sides of moraine boulders yields a range of nuclide concentrations (Schaefer et al., 2008), consistent with theoretical predictions of the distribution of nuclide production in solids (Masarik and Wieler, 2003; Lal and Chen, 2005).

For a boulder buried in a till sheet, equation 2.4 gives the production rate in the point that is eventually sampled. Given this production rate, the inherited concentration C_{pre} is

$$C_{pre} = \frac{P\left(d_{\text{pre}}\right)}{\lambda}\left[1 - \exp\left(-\lambda t_{\text{pre}}\right)\right]$$

(Lal, 1991, his eqn. 6), and the final concentration C_{f}, achieved after the boulder has rested on the moraine for a time t, is

$$C_f = C_{\text{pre}} \exp\left(-\lambda t\right) + \frac{P_0}{\lambda + \varepsilon\Lambda^{-1}}\left[1 - \exp\left(-\lambda t\right)\right] \qquad \text{(eqn. 2.6)}$$

(Lal, 1991, his eqn. 6). Here, ε is the erosion rate of the boulders after they are delivered to the moraine (cm/ yr; assumed negligible), and Λ is the attenuation length of the nucleonic component

of cosmogenic nuclide production (~160 g/ cm^2, divided by the material's density; Lal, 1991; Gosse and Phillips, 2001).

Our model is readily adapted to treat inheritance in boulders derived from cirque headwalls and valley walls, as in Benson et al. (2005). From a nuclide production perspective, the angle of the overlying surface is the critical difference between a boulder buried in a till sheet and one that is still in a cirque headwall; for a till sheet, the overlying surface should be nearly horizontal, whereas cirque headwalls are quite steep. To model nuclide production as a function of depth below inclined surfaces, we use the parameterization of Dunne et al. (1999, their eqn. 18). This parameterization gives results within 3% of estimates from a more explicit model (Dunne et al., 1999), even for the steep slopes representative of cirque headwalls (~30°; Benson et al., 2005).

This inheritance model relies on many assumptions. First, we assume that there are no nuclides inherited from any periods of residence in the landscape preceding the last glacial cycle. Because many cosmogenic nuclides have half-lives that are long compared to glacial cycles (Gosse and Phillips, 2001; Shackleton, 2000), this assumption requires that glaciers sweep out most of the easily eroded material from their valleys during each advance. Second, we assume that surface production rates were the same during the predepositional exposure time as they are in the boulders' observed positions. Because some boulders are undoubtedly coming from higher elevations than the present-day moraine crests, this assumption tends to underestimate surface production rates during the predepositional exposure time. Future versions of this model will need to incorporate information on the elevation distribution of glaciated basins (e.g., Bierman et al., 2005). Third, we assume that the density contrast between the boulders and the surrounding material is small; otherwise, the production rate in the sample point would differ, depending on the orientation of the boulder during its predepositional exposure time. For boulders that travel to the moraine atop glacial ice, some cosmogenic nuclide atoms are produced during the transport

time (Seong et al., 2009), and our model neglects this production. Moreover, glaciers do erode boulders during subglacial transport, and this model does not include that process. We tolerate these problems for the sake of developing this preliminary model.

Monte Carlo simulation

As we indicated in the introduction, our objective is to use the statistical distributions of real exposure dates to estimate the ages of moraines and gain information on the geomorphic processes acting on the moraines. We present our methods for comparing models to data in Chapter 3. In the remainder of this section, we show the distributions of exposure dates produced by the models under assumptions that are reasonable for a variety of field situations.

To determine a statistical distribution of apparent exposure dates from our models, we use Monte Carlo methods (Hilborn and Mangel, 1997; Bevington and Robinson, 2003). In Monte Carlo simulation, the values of highly variable model parameters are chosen randomly from predefined probability distributions. The model is then run for these parameter values, and the output is saved. This process is repeated many times; depending on the speed of the model and the desired precision, Monte Carlo model evaluations may include thousands to millions of individual model runs. The model output is then plotted as a histogram, which is a graphical representation of the probability distribution.

In our models, there are several free parameters that will be different for each boulder on a moraine. We have no way of determining, for example, how deeply buried any individual boulder was at the time of moraine deposition. The moraine degradation model has only one highly variable parameter, the initial depth d_0; the inheritance model has two highly variable parameters, the predepositional exposure time t_{pre} and the depth during the predepositional exposure time d_{pre}.

Because all these free parameters range from zero to some maximum, we choose random values for these parameters from continuous uniform distributions. In a continuous uniform distribution, all real numbers that lie between the minimum and maximum ends of the distribution are equally probable (Hilborn and Mangel, 1997; Bevington and Robinson, 2003). For our models, the minimum ends of these distributions are always 0; the maximum ends are specified by max(d_0), max(t_{pre}), and max(d_{pre}).

For each draw of these randomly chosen parameter values, we calculate the final concentration C_f (eqns. 2.5 and 2.6, above) and the apparent exposure time t_{app}, according to

$$t_{app} = \frac{-1}{\lambda}\ln\left(1 - \frac{C_f \lambda}{P_0}\right) \qquad \text{(eqn. 2.7)}$$

(Lal, 1991, his eqn. 6). This expression reflects the "naïve" estimate (Wolkowinsky and Granger, 2004) of moraine age from a single boulder sample, neglecting boulder erosion and all other geomorphic processes.

Note that we differentiate between moraine-level parameters and boulder-level parameters. Moraine-level parameters in the degradation model include the moraine age, topographic diffusivity, initial height, and initial slope; in the inheritance model, the moraine-level parameters are the moraine age, the maximum predepositional exposure time, and the maximum predepositional burial depth. The boulder-level parameters are the initial depth of boulders below the moraine surface in the degradation model, and the predepositional exposure time and burial depth in the inheritance model. In estimating the probability distribution of cosmogenic exposure dates from a single moraine, we vary the boulder-level parameters, but the moraine-level parameters remain constant.

Plotting non-normal distributions

Most common methods of plotting collections of exposure dates from moraines implicitly assume that the dates are drawn from a normal distribution. This assumption is unjustified for the distributions produced by our models, which are clearly not normal. Therefore, we represent the statistical distributions of exposure dates using histograms, cumulative density functions, and box plots (Chambers et al., 1983; Croarkin and Tobias, 2006). These plotting methods are robust, even for statistical distributions that vary considerably from the normal distribution.

Histograms are probably the most familiar method of representing distributed data, but the choice of bin size exerts a strong control on the shape of the histogram. In a histogram, the synthetic observations are sorted into bins. The heights of the bars on the histogram are proportional to the number of observations in each bin.

Unlike histograms, plots of cumulative density functions do not require arbitrary choices about how to group the data. On a plot of a cumulative density function, the *y*-axis represents the probability that any individual observation is equal to or less than a particular value on the *x*-axis (Press et al., 1992, their ch. 14; Hilborn and Mangel, 1997; Croarkin and Tobias, 2006). The *x*-axis therefore ranges from the minimum to the maximum of the observations; the *y*-axis ranges from 0 to 1.0.

Box plots provide a compact way of representing distributed data; placing several box plots next to one another allows quick comparison of distributions. In a box plot, the position and width of the box indicates where the middle 50% of the observations lie. That is, the box represents the interquartile range of the data (Chambers et al., 1983; Croarkin and Tobias, 2006). The line in the box is the median, or the value that separates the lower half of the observations from the upper half. In this dissertation, the ends of the whiskers indicate the positions of the

largest and smallest observations. Often, box plots indicate outliers as dots or small crosses outside the whiskers (Chambers et al., 1983), but we do not follow this practice.

Results

Model output for representative parameter values

The output from the moraine degradation model is shown in Figure 2.6. All these figures assume the same parameter values used in Figures 2.2 and 2.4; as before, the initial height of the moraine is 50 m, the initial slope of the moraine is 34° (Putkonen and Swanson, 2003), the topographic diffusivity is 10^{-2} m^2/ yr (Hanks et al., 2000; Putkonen et al., 2007), and the age of the moraine is 20 ka. In addition, we specify that the tops of all sampled boulders must be at least 1 m above the crest of the moraine at the time of sampling.

Figure 2.6a illustrates the relationship between the initial depth of a given boulder and the apparent exposure time yielded by that boulder. As expected, the more deeply buried samples yield younger apparent exposure times.

Figures 2.6b and 2.6c show the statistical distribution of the exposure dates produced by the degradation model for these parameter values. The distribution is strongly left-skewed; that is, more of the probability mass falls to the left of the distribution's peak than would be the case if the distribution were normal. The corresponding cumulative density function rises slowly, then more rapidly as it approaches the true age of the moraine (20 ka). The box portion of the box plot, which represents the position of the bulk of the data, falls on the right-hand side of the plot.

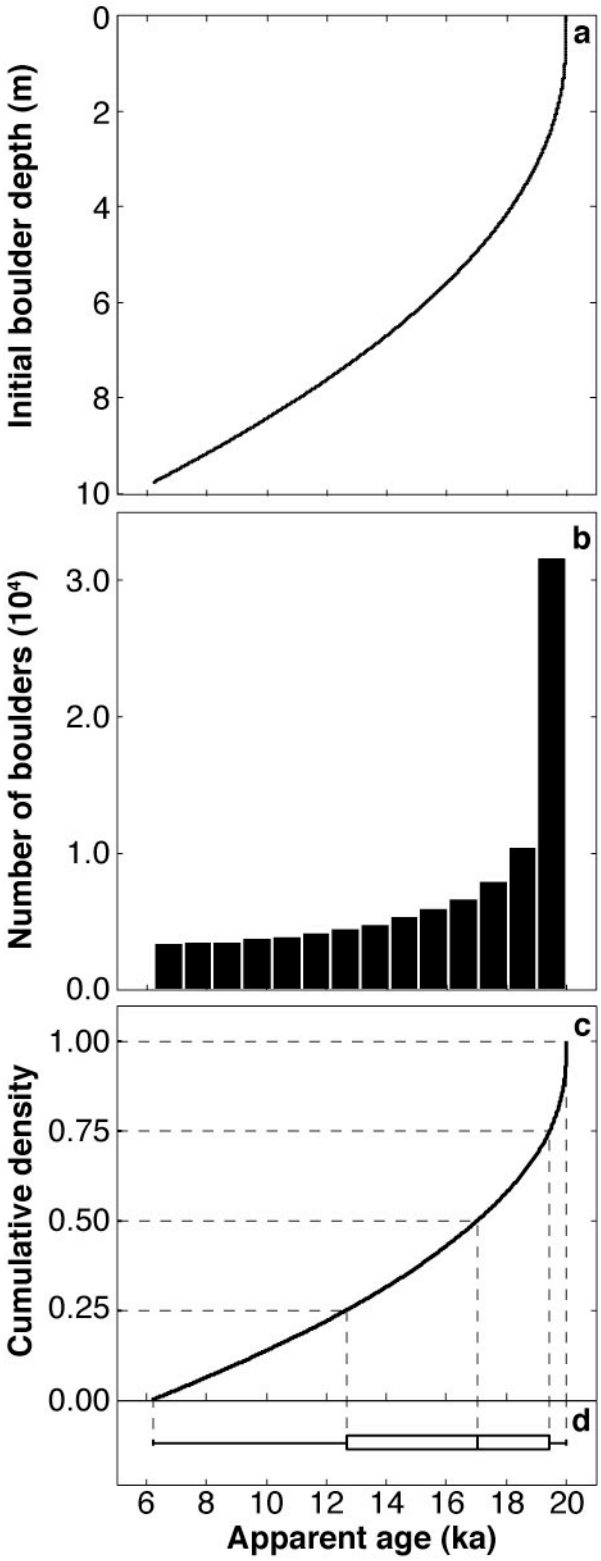

Figure 2.6: Distribution of cosmogenic exposure dates produced by the moraine degradation model for a representative case. Panel (a) shows the exposure dates yielded by boulders as a function of their initial burial depth in the moraine (compare Fig. 2.4b). Panel (b) shows a histogram of these apparent ages. Most of the exposure dates cluster around the true age of the moraine (20 ka), but there is a long, heavy tail to the left. That is, the distribution of exposure dates produced by the moraine degradation model is left-skewed. The total number of observations shown in this histogram is 10^5. Panels (c) and (d) show the cumulative density function and box plot of the 10^5 observations shown in the histogram. Dashed lines in (c) and (d) show the relationship of the box plot to the cumulative density function; breaks in the box plot represent the quartiles of the distribution (Chambers et al., 1983). As in Figures 2.2 and 2.4, the moraine's initial height is 50 m, its initial slope is 34°, and its topographic diffusivity is 10^{-2} m^2/ yr. The final heights of all the boulders are 1 m.

The output from the inheritance model is shown in Figures 2.7a-2.7c. These plots assume a moraine age of 20 ka, a maximum predepositional exposure time of 100 ka, a maximum depth during the predepositional exposure period of 2 m, an overburden density of 2.0 g/ cm^3, and a flat surface geometry during the predepositional exposure period. Again, the total number of synthetic observations in each of these plots is 10^5.

Figure 2.7a shows contours of the apparent exposure time produced by the inheritance model as a function of the model's free parameters, predepositional exposure time and predepositional exposure depth. As expected, the samples that yield the greatest apparent exposure times are those that had the greatest length of time to acquire inherited nuclides and were near the surface during that time. That is, the samples that appear oldest have the longest predepositional exposure times and the smallest predepositional exposure depths.

Figures 2.7b and 2.7c show the statistical distributions of exposure dates expected from the inheritance model for these parameter values. The distribution is right-skewed; it contains a mode close to the true age of the moraine (20 ka), and a long, heavy tail to the old side, as shown in the histogram (Fig. 2.7b). These features of the distribution are reflected in the cumulative density function (Fig. 2.7c), which rises rapidly, then levels off. The box portion of the box plot falls near the left end of the plot.

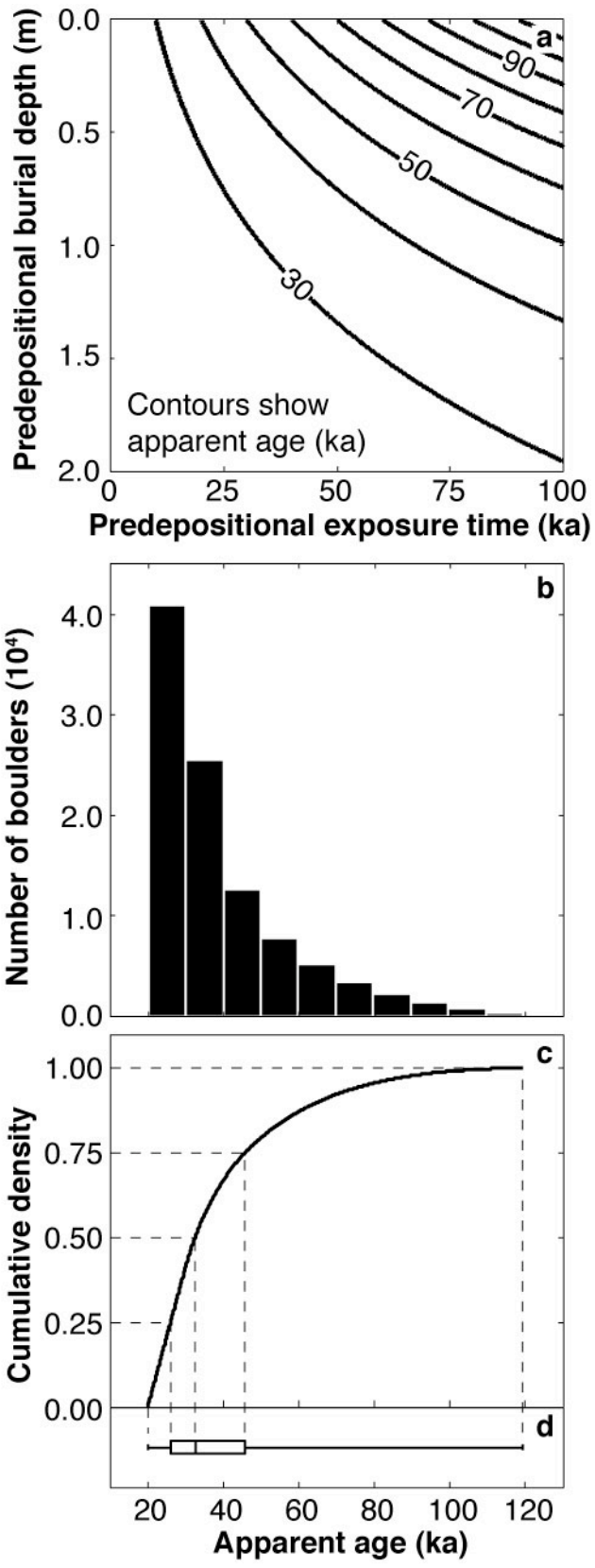

Figure 2.7: Distribution of cosmogenic exposure dates produced by the inheritance model for a representative case. Panel (a) shows contours of the apparent ages yielded by boulders as a function of the length of time that they were exposed to cosmic rays and the depth to which they were buried during that time. Panel (b) shows a histogram of exposure dates produced by random sampling of 10^5 synthetic observations from the contour plot in (a). In contrast to the distribution produced by the moraine degradation model (Fig. 2.6), the inheritance model produces right-skewed distributions. The bulk of the exposure dates fall near the true age of the moraine (20 ka), but there is a long, heavy tail to the right. Panels (c) and (d) show the cumulative density function and box plot of the 10^5 observations shown in the histogram. The true age of the moraine is 20 ka, the maximum predepositional exposure time is 100 ka, and the maximum predepositional burial depth is 2.0 m.

Sensitivity of modeled distributions to input parameter choices

Some of the parameters used in our models are either highly uncertain, or else vary considerably between moraines. In this section, we show how the modeled distributions of exposure dates change as individual parameters vary. Figures 2.8 and 2.9 illustrate the sensitivity of the two models using box plots (Chambers et al., 1983).

In both models, the moraine age controls the position of the box plot along the time axis. In the inheritance model, the spread of the exposure dates is independent of moraine age; the distance between the ends of the whiskers is the same for all values of moraine age. In contrast, the moraine age does affect the spread of exposure dates yielded by the degradation model; that is, younger moraines show less spread than older moraines (Fig. 2.8; Putkonen and Swanson, 2003). The increase in spread among exposure dates with age for degrading moraines happens because older moraines have more time to lose material from their crests (Fig. 2.2), and this process exposes more boulders that have spent progressively less time exposed to the full surface flux of cosmic rays (Fig. 2.4).

In the degradation model, the spread of dates is most strongly controlled by the topographic diffusivity, although the initial slope and initial height of the moraine also have some influence on the scatter (Fig. 2.8). Small diffusivities cause the moraine's height to change only slightly over its lifetime, and so few new boulders are exhumed at the crest of the moraine. Very large diffusivities flatten the moraine in a few thousand years after its construction; the reduced spread in exposure dates produced by the model for a diffusivity of 1 m^2/ yr happens because such a high diffusivity exposes most of the buried boulders within a few thousand years after the deposition of the moraine. Such large diffusivities cause the moraine to disappear almost totally over 20 ka, so they are inconsistent with the observed persistence in the landscape of topographically distinct moraines (see Hanks, 2000; Putkonen et al., 2007). The modeled

distributions of exposure dates from tall moraines are wider than distributions from shorter moraines of the same age (Putkonen and Swanson, 2003), although the width of the distribution stops increasing as the initial height of the moraine is made greater than ~35 m. The range of modeled exposure dates increases monotonically with the initial slope of the moraine.

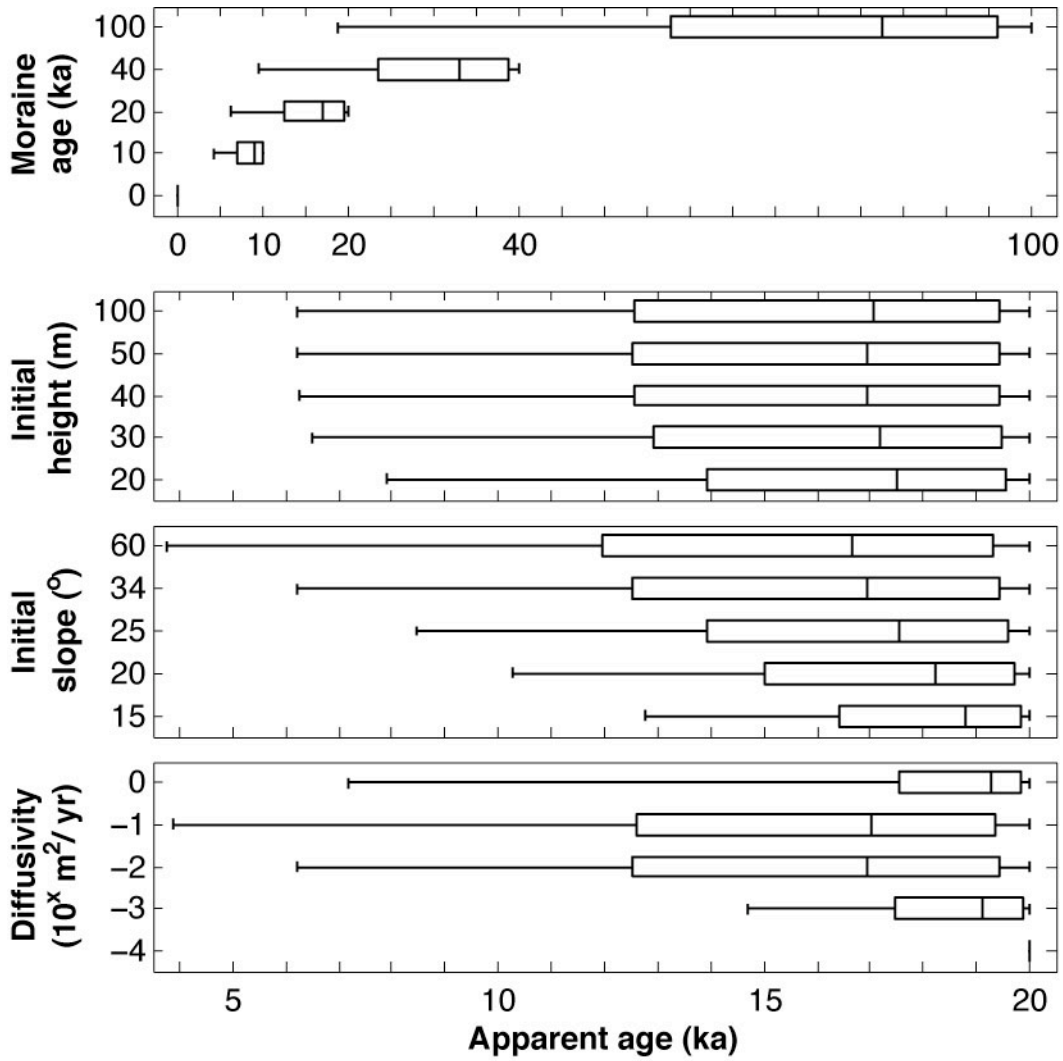

Figure 2.8: Sensitivity of the moraine degradation model to changes in its input parameters. See text for discussion. In each panel, one of the model parameters is varied between the values shown on the *y*-axis, whereas the other model parameters are held constant at the base values. As in Figures 2.2, 2.4, and 2.6, the base values for the input parameters specify that the moraine's initial height is 50 m, its initial slope is 34°, and its topographic diffusivity is 10^{-2} m^2/ yr.

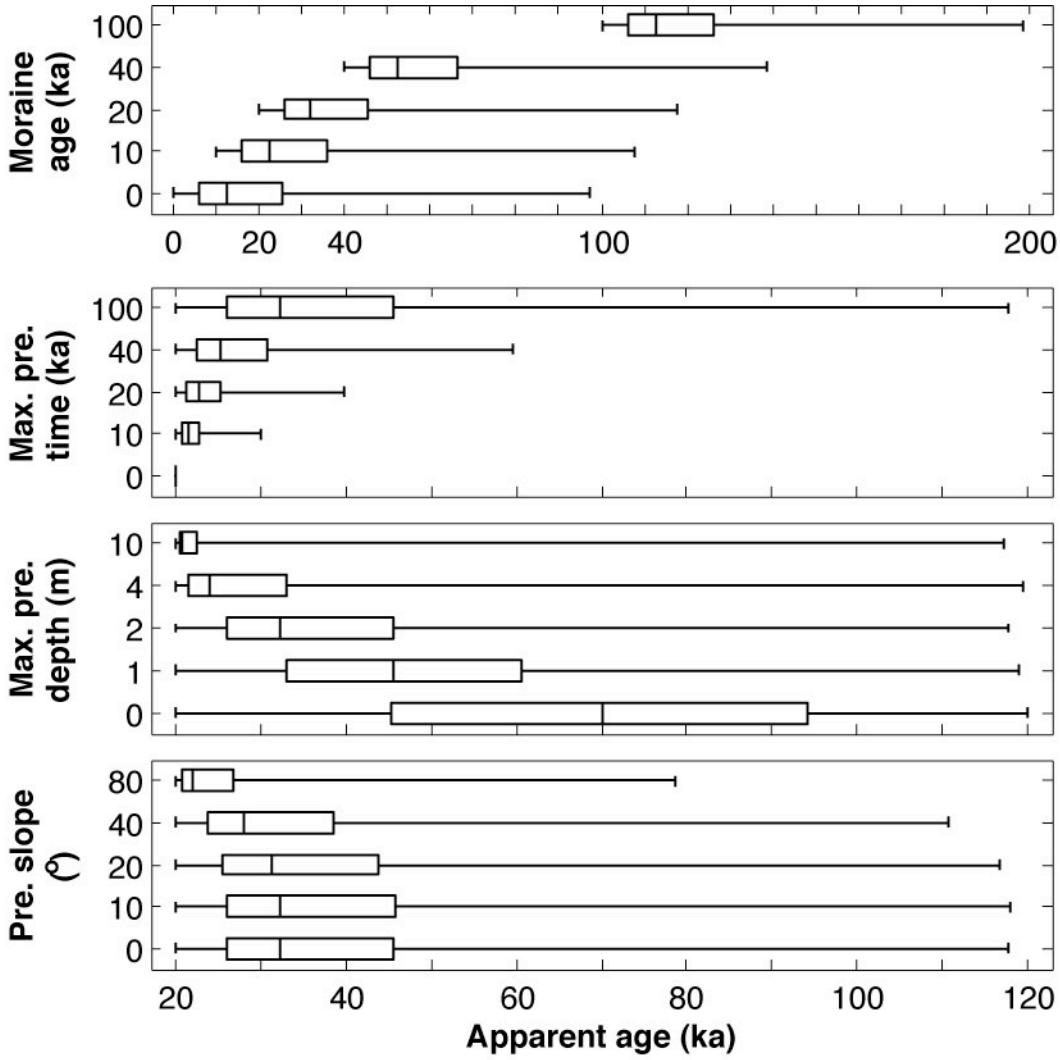

Figure 2.9: Sensitivity of the inheritance model to changes in its input parameters. See text for discussion. In each panel, one of the model parameters is varied between the values shown on the *y*-axis, whereas the other model parameters are held constant at the base values. As in Figure 2.7, the base values for the input parameters specify that the true age of the moraine is 20 ka, the maximum predepositional exposure time is 100 ka, and the maximum predepositional burial depth is 2.0 m.

In the inheritance model, the maximum predepositional exposure time controls the width of the distribution, and the maximum predepositional exposure depth controls where the bulk of the data falls between the extreme ends of the distribution (Fig. 2.9). A large value for the maximum predepositional exposure time causes a wide range of exposure dates; a small value

produces a narrow range. Large values of the maximum predepositional exposure time concentrate most of the observations near the young end of the range, whereas smaller values place more of the observations into the tail of the distribution.

Increasing the surface slope has only a small effect on the distributions of exposure dates produced by the inheritance model (Fig. 2.9). There is little difference between the distributions of modeled exposure dates for boulders derived from flat surfaces and those for boulders derived from sloped surfaces with inclinations of 30° or less, because the depth dependence of nuclide production changes only slightly over this range of slopes (Dunne, 1999). A 30° slope is representative of cirque headwalls (Benson et al., 2005), a likely source for supraglacial boulders. The model sensitivity to surface slope is not extreme, even for larger slope values.

Discussion

There is no plausible combination of parameters that can cause the output from the moraine degradation model to resemble the output from the inheritance model (compare Fig. 2.6b with Fig. 2.7b, Fig. 2.6c with Fig. 2.7c, and Fig. 2.8 with Fig. 2.9), except in the special case where neither process is active. The statistical distributions of exposure dates produced by the moraine degradation model are always left-skewed (Fig. 2.6b); conversely, the distributions of exposure dates produced by the inheritance model are always right-skewed (Fig. 2.7b). That is, the cumulative density functions from the degradation model are always concave-up (Fig. 2.6c), and the cumulative density functions from the inheritance model are always concave-down (Fig. 2.7c). On the box plots, the box occurs near the right-hand end of the distribution in the degradation model (Fig. 2.8), and near the left-hand side of the plot for the inheritance model (Fig. 2.9).

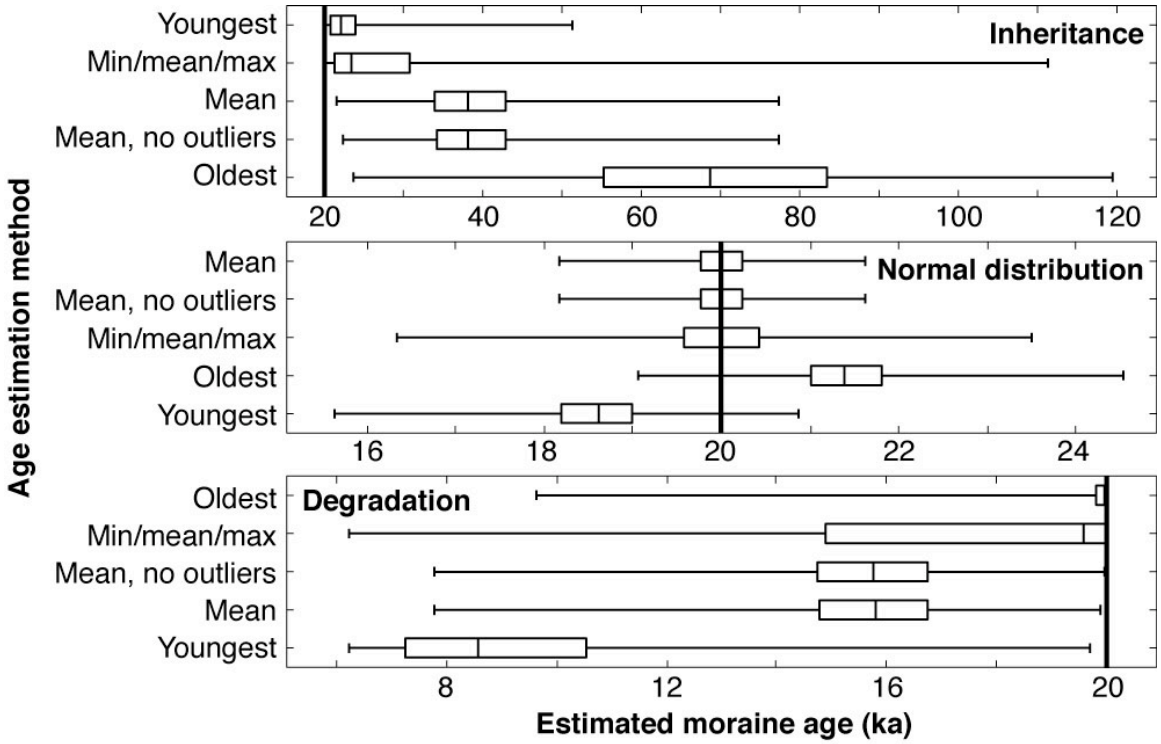

Figure 2.10: The reliability of different interpretive methods in estimating moraine ages from collections of cosmogenic exposure dates. Each box plot represents age estimates from 10^6 randomly selected data sets containing eight synthetic cosmogenic exposure dates each. The heavy, vertical black line in each panel represents the true age of the moraine, which is 20 ka in each case. In each panel, the methods listed on the *y*-axis are listed according to how close the median age estimate falls to the true moraine age; the method listed at the top is the best for the indicated parent distribution, and the method listed at the bottom is the worst. This ordering is insensitive to the number of samples in each data set for reasonable data set sizes ($3 \leq n \leq 21$). The parent distribution in the middle panel is a normal distribution with a mean of 20 ka and a standard deviation of 1 ka, corresponding to a case where all of the scatter between the exposure dates is due to measurement error. The parent distributions in the other two panels are those shown in Figures 2.6 and 2.7.

We can now examine how successful different methods for estimating moraine ages will be, given the statistical distributions of exposure dates yielded by our models (Fig. 2.10). Common methods include the mean, the mean after discarding outliers, the oldest date, and the youngest date. In this case, we define outliers as those observations that are more than twice the standard deviation away from the mean of the exposure dates in a data set.

To this list of methods, we add the min/mean/max technique, which was suggested by our modeling results. If a data set has a skewness greater than 0.5, we infer that the dates are biased by inheritance, so we take the youngest date. If the skewness is less than -0.5, we assume moraine degradation, and take the oldest date. If the skewness is between -0.5 and 0.5, we take the mean.

Of these methods, min/mean/max appears to be the most widely applicable; however, none of these methods is universally successful in recovering the known ages of moraines for our modeled distributions (Fig. 2.10). The median of the min/max/mean age estimates always lies within a few thousand years of the true age for the parent distributions we examine here. This statement is not true of any other method that we have tested. However, the min/max/mean estimate of moraine age sometimes overestimates or underestimates moraine ages by tens of thousands of years.

The min/mean/max method fails because the skewness of a small data set ($n < \sim 50$) is a poor guide to the form of the parent distribution (Fig. 2.11). For a moraine where geomorphic processes do not affect exposure dating, we would expect the exposure dates to be normally distributed (Balco, in press), and to have a standard deviation equal to the measurement uncertainty of the dates. By definition, this parent distribution will have a skewness of zero. However, the skewness of a small number of exposure dates drawn randomly from this parent distribution has a poor chance of approximating the true skewness of the parent distribution. Most randomly selected data sets containing a small number of observations will give either a positive or negative skewness. Under the min/mean/max framework, we would wrongly conclude that we should take the oldest or the youngest date from these data sets, whereas the average is the maximum likelihood estimator of the moraine's age (Bevington and Robinson, 2003). This problem is most pronounced for the smallest data sets ($n = 3$), for which the distribution of skewnesses is U-shaped.

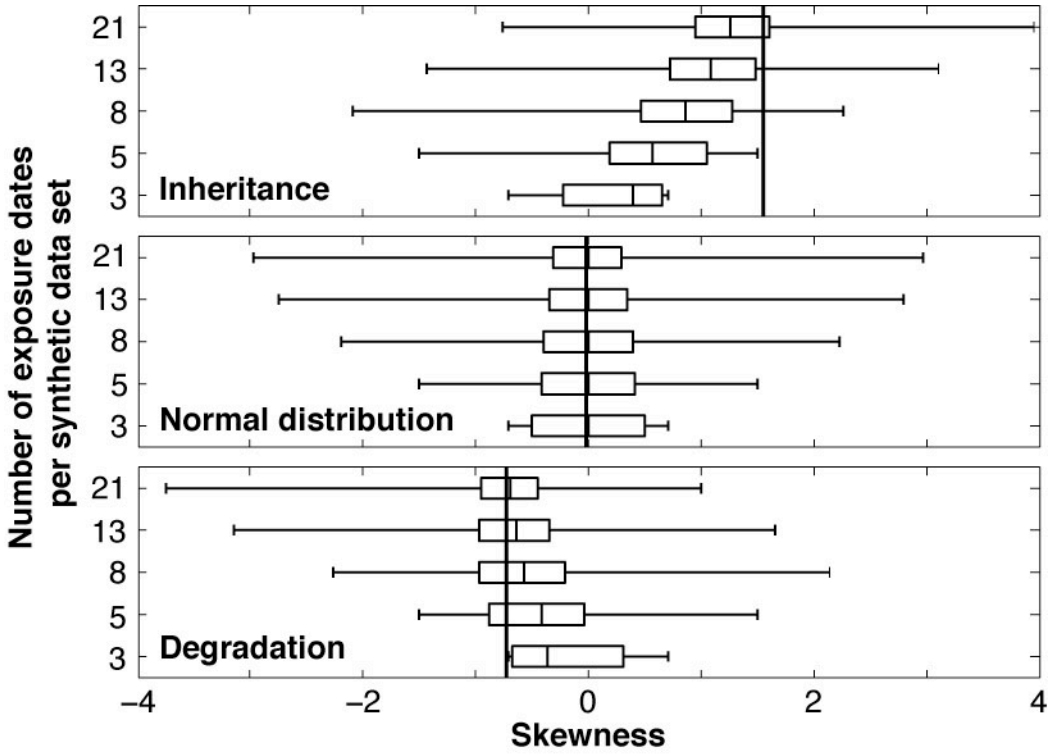

Figure 2.11: Skewnesses of randomly chosen data sets, compared to the skewnesses of the underlying parent distributions. Each box plot indicates the skewnesses of 10^6 randomly selected data sets that contain a number of exposure dates indicated by the corresponding value on the *y*-axis. The skewnesses of the underlying parent distributions are indicated by the heavy, black, vertical line in each panel. Even large data sets ($n = 21$) can provide a misleading estimate of the skewness of the parent distribution. In particular, randomly chosen data sets will often yield skewnesses that do not have the same sign as the underlying parent distribution. The parent distribution in the top panel is the same as that shown in Figure 2.7b; the parent distribution in the bottom panel is shown in Figure 2.6b. The parent distribution in the middle panel is a normal distribution with a mean of 20 ka and a standard deviation of 1 ka.

These problems persist for data sets drawn from distributions generated by the inheritance model and the degradation model. For highly skewed parent distributions like those produced by the inheritance model, the interquartile range of sample skewnesses does not even overlap the skewness of the parent distribution until the number of observations in each data set is about 15. To our knowledge, there is no moraine with more than 15 independent, published cosmogenic exposure dates.

Taking the mean after discarding outliers fails to correctly estimate the ages of moraines for skewed parent distributions (Fig. 2.10) because the bias imparted by geomorphic processes is continuous, rather than binary. Discarding outliers before taking the mean implicitly assumes that bias is either present or absent in each exposure date. Our model results suggest, instead, that the majority of exposure dates from moraines that are affected by geomorphic processes have some degree of bias, even though small biases are more common than large ones (Figs. 2.6, 2.7; Benson et al., 2005). These small biases lead the mean away from the correct answer, if that answer lies at one end of the distribution.

The extreme estimators work well in very specific circumstances (Fig. 2.10), but we cannot reliably determine when to apply these estimators (Fig. 2.11). The extreme estimators involve choosing the youngest date or the oldest date from a data set. If we believe correctly that the parent distribution from which a set of exposure dates is drawn is skewed in one direction or the other, then the corresponding extreme estimator is the best choice for determining the moraine's age (Fig. 2.10). However, an incorrect guess about the form of the parent distribution will likely cause a large error in estimating the age of a moraine using an extreme estimator. Because our skill in determining the form of parent distributions from small data sets is limited (Fig. 2.11), the extreme estimators should be used with caution.

The failure of simple methods to correctly estimate the ages of moraines in our test cases indicates that more sophisticated methods are necessary. Direct inversion of our models against data may allow more accurate estimation of moraine ages from collections of cosmogenic exposure dates. We present methods for this inversion in the next chapter.

Chapter 3

Extracting moraine ages and geomorphic process information from the statistical distributions of cosmogenic exposure dates

New statistical methods allow estimation of both moraine ages and rates and magnitudes of geomorphic processes from collections of cosmogenic exposure dates. Cosmogenic exposure dating holds considerable promise for estimating the ages of glacial landforms, because exposure dates record the ages of geomorphic surfaces directly if confounding factors are absent. However, exposure dates from single moraines are sometimes spread over thousands of years, and the best way to choose the age of the landform from a widely scattered set of exposure dates is often unclear. As a first step toward addressing this problem, we have developed methods for fitting models of two potential confounding processes to the statistical distributions of exposure dates from moraines. These processes are moraine degradation, which causes exposure dates to underestimate the ages of moraines, and inheritance, which causes exposure dates to overestimate the ages of moraines. We present fits of these models to collections of exposure dates from Gurreholm Dal in eastern Greenland and from the Uinta Mountains of Utah. The resulting fits yield information on both the ages of the moraines and other parameters of geomorphic interest, such as the depth of glacial erosion and the topographic diffusivity.

Cosmogenic exposure dating is a powerful method for estimating the ages of glacial landforms, but geomorphic processes complicate the interpretation of the dates. Cosmic rays split atoms in surface rocks at predictable rates, producing measurable concentrations of isotopes that are otherwise rare in surface rocks (Gosse and Phillips, 2001; Muzikar et al., 2003). The concentrations of these cosmogenic nuclides in moraine boulders are directly related to the ages of the host moraines (Lal, 1991), assuming that the boulders had no preexisting concentration of cosmogenic nuclides when deposited on the moraine, and that the sampled surfaces of the boulders were exposed to the full surface flux of cosmic rays for the entire post-depositional history of the moraines. These assumptions are sometimes violated by geomorphic processes, which affect different boulders on the same moraine to varying degrees (Ivy-Ochs et al., 2007). Thus, the spread among exposure dates from a single moraine is often greater than we would

expect from the analytical uncertainty of the method (Putkonen and Swanson, 2003). Various methods exist for estimating moraine ages from exposure dates, and these methods give very different results when applied to highly scattered data sets (compare Chevalier et al., 2005, with Brown et al., 2005). This interpretive uncertainty confounds efforts to determine the timing of rapid climate changes from exposure dates.

Here, we suggest a new method for estimating moraine ages from cosmogenic exposure dates. This method matches the statistical distributions of exposure dates generated by geomorphic process models to the distributions of observed exposure dates from single moraines. The models' input parameters include moraine age, topographic diffusivity, and the depth of glacial erosion. The matching method yields estimates of these quantities.

This study improves on past work in several ways. Our method honors all the exposure dates within a data set; outlier deletion is not required, at least for the data sets that we examine here. Thus, the method reduces the interpretive uncertainties in exposure dating. Second, the method gives estimates of the rates and magnitudes of geomorphic processes. Because many hundreds of exposure dates already exist in the literature, our method provides a means to learn about geomorphic processes in a large sample of glaciated drainages. Last, our method allows us to draw inferences about individual moraines; most prior modeling studies in this area treat aggregate data sets representing many moraines (see Zreda et al., 1994, for an exception).

Methods

In Chapter 2, we described numerical models that predict the effects of two geomorphic processes on the statistical distributions of exposure dates from moraines. These processes, moraine degradation and inheritance, are thought to be pervasive influences on the exposure dating of moraines (Putkonen and Swanson, 2003; Benson et al., 2005; Putkonen and O'Neal,

2006); other processes may be important at some sites. In moraine degradation, slope processes remove material from the crest of a moraine and transfer it to the toe of the slope (Anderson and Humphrey, 1989; Pelletier, 2008). This process exposes boulders at the moraine crest that have been partly shielded from cosmic rays during some part of the moraine's postdepositional history. In inheritance, boulders acquire concentrations of cosmogenic nuclides in cirque headwalls, valley walls, or valley floors before being transported by the glacier to its terminus (Seong et al., 2009). Our models build on prior efforts, most notably those of Hallet and Putkonen (1994) and Benson et al. (2005).

Here, we invert these models against five data sets from the literature (see below). Given a collection of exposure dates from a single moraine and a process model, we run the model repeatedly, adjusting the input parameters each time. We search over reasonable parameter ranges to find the set of parameter values that produces the best match between the modeled and observed distributions of exposure dates. To find this best match, we use a genetic algorithm to minimize the Kolmogorov-Smirnov test statistic, which measures the mismatch between two statistical distributions (Appendix D). The method is able to recover the correct parameter values for simple test cases.

Moraine age is a parameter in both models. The output of the moraine degradation model also depends on the moraine's initial height, initial slope, and topographic diffusivity. The inheritance model requires the maximum exposure time and maximum burial depth for boulders during the predepositional exposure time, as well as the slope of the surface from which the boulders are derived. For boulders derived from subglacial material, the maximum burial depth corresponds to the maximum depth of glacial erosion; for boulders that are transported supraglacially, this parameter is related to the depth of landsliding onto the glacier surface. Each model has three important parameters. Sensitivity tests of the degradation model show that initial height is comparatively unimportant for tall moraines. Likewise, the slope of the surface from

which boulders with inherited nuclides are derived has a minor effect on the distributions produced by the inheritance model.

Selected data sets

To illustrate the application of our geomorphic models, we have chosen five data sets from the recent literature. Three of these data sets come from moraines in the Gurreholm valley in Scoresby Sund, eastern Greenland (Kelly et al., 2008); the others come from moraines in the Uinta Mountains of Utah (Munroe et al., 2006; Laabs et al., 2009).

In Gurreholm Dal, eastern Greenland, three groups of moraines lie between the Little Ice Age-equivalent moraines and where the valley empties into the fjord (Kelly et al., 2008). In order from youngest to oldest, these groups are the G-II, G-III, and G-IV moraines. The G-II and G-III moraine groups are thought to correspond to the inner and outer Milne Land stade moraines of Funder (1978). Each group contains moraines corresponding to 2-4 distinct positions of the glacier margin. The distance between the innermost and outermost moraines in any moraine group (~1 km) is small compared to the length of the valley, which is about 20 km from the outermost Little Ice Age moraine to the edge of the seawater filling the fjord. The stratigraphic positions of these moraine groups imply that all three groups must be older than the culmination of the Little Ice Age in Greenland and younger than the Last Glacial Maximum (Hakansson et al., 2007; Kelly et al., 2008).

On the southern slope of the Uinta Mountains of Utah, the river valleys contain prominent moraines of the Smiths Fork glaciation (Pinedale-equivalent; Atwood, 1909; Munroe et al., 2006, Laabs et al., 2009). The Lake Fork and Yellowstone drainages contain the two best-preserved moraine complexes of this age in the Uinta Mountains. In both of these drainages, the outermost Smiths Fork-age lateral moraines are well-defined and continuous. These moraines

may be several thousand years younger than the time of the Last Glacial Maximum in the western United States, because the glaciers that deposited the moraines were likely sustained by moisture from pluvial Lake Bonneville (Laabs et al, 2006; Munroe et al., 2006).

We have recalculated the exposure dates from our chosen sites using several presently accepted scaling methods (Balco et al., 2008; Appendix D). In the text and figures, we show the dates as calculated using the Lal/Stone scaling method (Lal, 1991; Stone, 2000). However, the choice of scaling method has little influence on the scatter among exposure dates for the moraines in our selected data sets (Appendix D).

The exposure dates in all five of our chosen data sets are likely influenced by geomorphic processes (Fig. 3.1). If measurement error is the only cause of the scatter among the exposure dates from a single moraine, the dates will be normally distributed, and the scatter of the dates will be consistent with the measurement uncertainties of the dates. Of the five data sets treated here, four are not normally distributed, as shown by their histograms and normal probability plots (Appendix D). The number of observations in each data set limits our ability to determine the forms of the parent distributions from which the dates are drawn. However, we are confident that all of the data sets have more scatter than can be explained by the measurement uncertainties of the dates, as shown by their reduced chi-squared scores (Appendix D; Fig. 3.1).

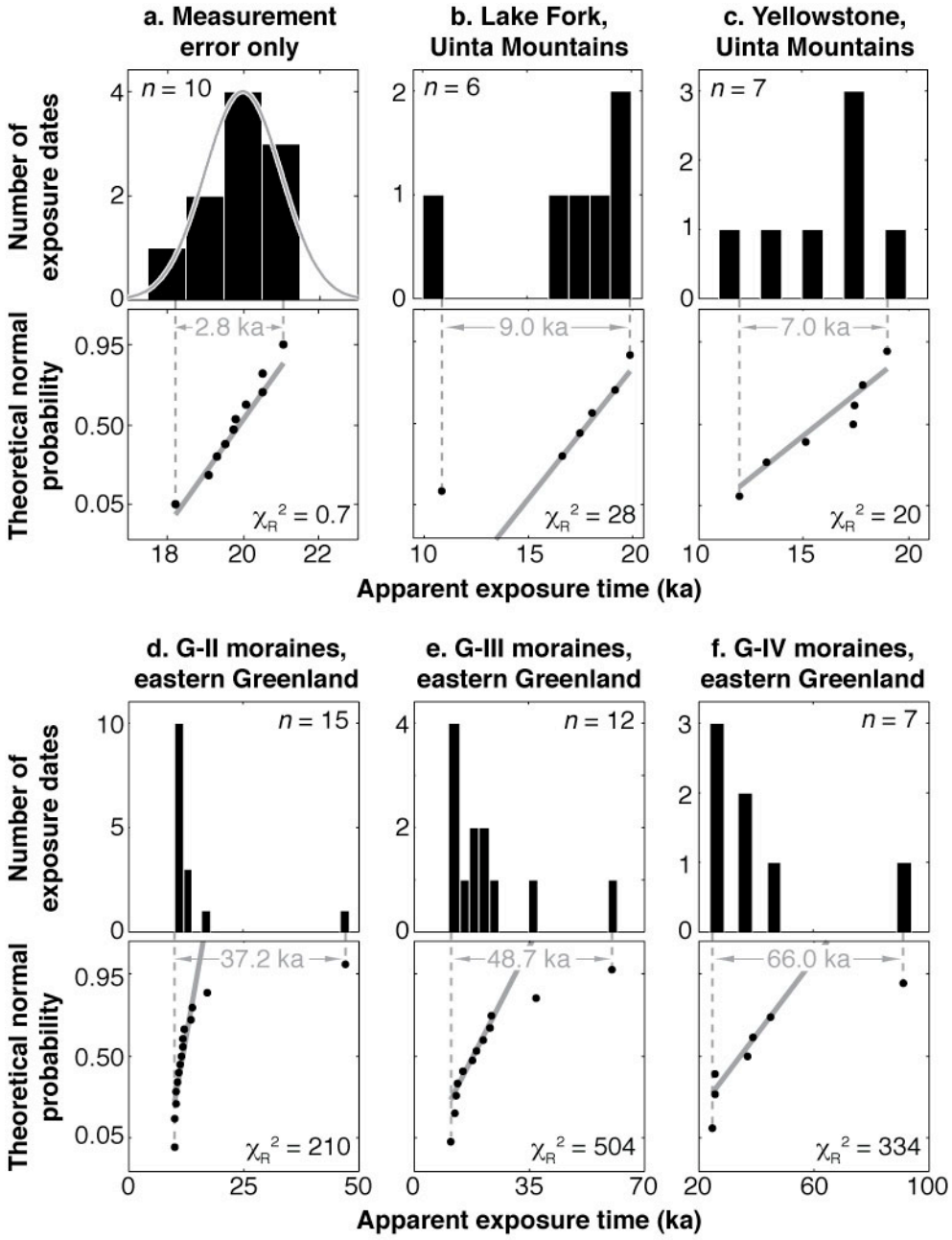

Figure 3.1: (Caption on following page.)

Figure 3.1: Comparison of a synthetic data set in which all the scatter is due to measurement error (a) to the data sets treated in this study (b-f; Kelly et al., 2008; Laabs et al., 2009). If all the scatter among a group of exposure dates from a single moraine is due to measurement error, the exposure dates will be normally distributed and will have a degree of scatter consistent with the measurement uncertainties of the dates. In each figure part (a-f), the top panel is a histogram of the exposure dates, and the bottom panel is a normal probability plot (Appendix). A normal probability plot provides a qualitative test for normality; if the dates (black dots) fall near the solid gray line, they are probably drawn from a normal distribution. The gray curve in the top panel of part a shows the expected distribution of exposure dates for a moraine that is 20 ka old, assuming a 1σ measurement uncertainty of 5% and an arbitrarily large number of exposure dates. This theoretical distribution has the familiar bell shape of the normal distribution. For a more reasonable number of exposure dates (n = 10), we might obtain a distribution like that shown by the histogram in the top panel of part a. When displayed on a normal probability plot, these dates fall in a line, confirming that they are drawn from a normal distribution. The dates in this hypothetical example have a reduced chi-squared statistic χ_R^2 of 0.7 (close to 1.0), indicating that their scatter is consistent with the measurement errors of the dates (Bevington and Robinson, 2003; Appendix D). In contrast, the exposure dates in our selected data sets (parts b-f) do not fall in a line on normal probability plots, and their χ_R^2 scores range from 20 to 504 (>> 1.0). These non-normal, highly scattered data sets are likely influenced by geomorphic processes. Note that, although the Yellowstone data set (part c) appears to be normally distributed, its χ_R^2 score is much larger than 1.0.

Results

We present the best-fit model curves for each data set in Figure 3.2. The model parameters that give rise to these best fits are shown in Table 3.1.

In general, these parameter estimates appear reasonable. The fits of the moraine degradation model to the data sets from the Uinta Mountains yield estimates of moraine age, initial slope, and topographic diffusivity that lie within reasonable ranges (Licciardi and Pierce, 2008; Putkonen and O'Neal, 2006; Hanks, 2000). Likewise, the estimated glacial erosion depths are generally consistent with past estimates (Briner and Swanson, 1998; Fabel and Harbor, 1999; James et al., 2002; Fabel et al., 2004).

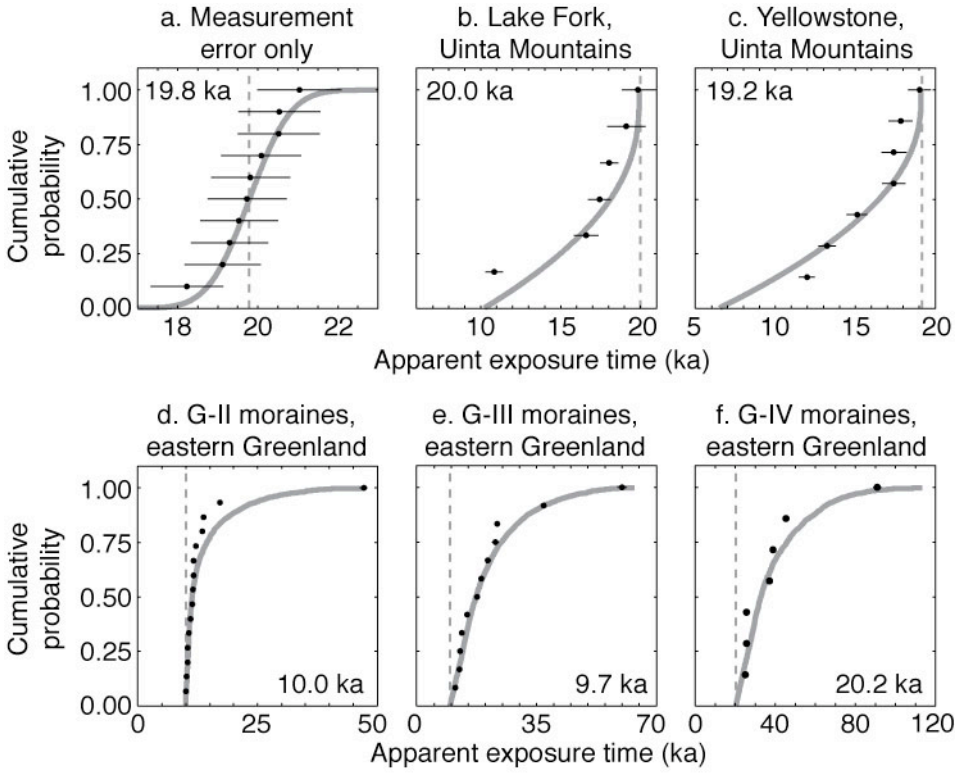

Figure 3.2: Fits of models to observations. The black dots with error bars represent the exposure dates and their 1σ measurement uncertainties, plotted in cumulative probability density space (Appendix D). The solid gray curves are the modeled distributions that provide the best fit to the observations, and the dashed vertical gray lines are the corresponding moraine age estimates; the values in each panel represent our best estimates of moraine age for these data sets. For a data set that is normally distributed and has a reduced chi-squared χ_R^2 score close to 1.0 (part a), the most appropriate model assumes a normal distribution, which has an *S*-shape on a cumulative probability density plot. The best estimate of moraine age is then just the mean of the exposure dates. Note that, because our randomly chosen exposure dates sample the young tail of the distribution more than the old tail (Fig. 3.1a), we do not recover the known age of the moraine (20 ka) in this synthetic example. In contrast, the moraine degradation model provides a better fit to our chosen data sets that are widely scattered and have most of the dates arranged to the young side of the mode (Lake Fork and Yellowstone; parts b and c). Further, our sample data sets that are widely scattered and have most of the dates on the old side of the mode are well fitted by the inheritance model (G-II, G-III, and G-IV; parts d, e, and f). On cumulative density plots, the moraine degradation model produces distributions that rise slowly, then more quickly; the inheritance model's distributions rise quickly, then level off.

Table 3.1: Best fits of the models to the eastern Greenland and Uinta Mountains data sets (Kelly et al., 2008; Laabs et al., 2009).

Degradation model

Data set	Moraine age (ka)	Initial slope (°)	Diffusivity (m^2/yr)	KS statistic
Lake Fork	19.98	39.45	$1.982 * 10^{-3}$	0.1977
Yellowstone	19.18	33.78	$8.761 * 10^{-3}$	0.2286

Inheritance model

Data set	Moraine age (ka)	Max. pre. exposure time (ka)	Max. pre. burial depth (m)	KS statistic
G-II	9.967	38.12	4.371	0.1333
G-III	9.740	55.56	1.919	0.1093
G-IV	20.21	96.28	1.978	0.1979

max. pre., maximum predepositional.
KS, Kolmogorov-Smirnov (see Appendix D).
The parameter estimates here are probably good to two or three significant figures. Four figures are reported to allow checking of the model fits.

However, the age estimates for the Greenland data sets deserve comment. First, the best-fit ages for the G-II and G-III moraine groups produce a stratigraphic inversion; given the relative positions of these moraine groups, the G-III moraines cannot be younger than the G-II moraines, contrary to the values presented in Table 3.1. This result probably indicates that the G-II and G-III moraines are very close in age, consistent with the original interpretations of Kelly et al. (2008). This outcome also points out a need for methods to determine the uncertainties of our parameter estimates (see Discussion, below). Moreover, the inferred age of the G-IV moraines is about 20 ka, corresponding to the height of the Last Glacial Maximum. It is generally thought that glacial ice in eastern Greenland was much more extensive than the margin position indicated by the G-IV moraines at this time (Hakansson et al., 2007). Without taking a position on this question, we note that our inferred age for these moraines is dominated by the youngest sample in the set. Further sampling on these moraines might yield younger exposure dates that would cause us to revise our inferred age.

Also, the maximum predepositional burial depth inferred for the G-II moraine boulders is much larger than that inferred for the G-III and G-IV moraine groups (Table 1). The significance of this result depends on whether these boulders were subglacially or supraglacially derived. If the boulders were derived from subglacial till or bedrock, this result seems contrary to our expectations. The G-II moraines were deposited by a thinner and less extensive ice cap than were the G-III and G-IV moraines (Kelly et al., 2008). In general, thick ice exerts a greater shear stress on its bed than does thin ice (Paterson, 1994), so we might expect thick ice to be more erosive than thin ice for the same subglacial conditions. On the other hand, perhaps the boulders fell onto the glacier from the adjacent bedrock slopes. In that case, the greater maximum predepositional burial depth for the G-II moraine boulders may reflect the abrupt exposure of destabilized bedrock slopes by downwasting ice, allowing deeper-seated landslides to fall onto the glacier surface. In any case, this result is only weakly significant; the large inferred predepositional burial depth for the G-II moraines is produced entirely by the oldest sample in the data set.

Discussion

This work suggests that widely scattered collections of cosmogenic exposure dates from moraines have a coherent structure that can be understood through modeling. The process of identifying this structure yields estimates of moraine ages and the rates and magnitudes of geomorphic processes acting in glaciated drainages.

This conclusion is subject to severe limitations. In particular, we present fits to only a few data sets, which we have selected because we are able to reproduce them with our models. There is some nonzero chance that any given data set will agree with one of our models, even if the model is not appropriate for the geomorphic situation. Thus, we cannot exclude the possibility that our model fits are due to chance, rather than to a real agreement between our models and the

geomorphic contexts of our chosen data sets. There are many data sets that we cannot fit well, such as the exposure dates from the outermost Pinedale moraine at Fremont Lake, Wyoming (Gosse et al., 1995b). Our inability to fit particular data sets may arise from the small numbers of exposure dates available from many moraines, or from the incompleteness of our models. Our modeling work to date treats inheritance and moraine degradation separately, but there must be sites where both processes are important. Moreover, some data sets probably reflect one or more geomorphic processes not treated by our models, such as boulder toppling, boulder erosion, or snow cover (Ivy-Ochs et al., 2007).

Still, we believe that our methods represent a promising avenue for future investigation. Any final answer to the problem of how to interpret cosmogenic exposure dates from moraines will have to explicitly account for the statistical distributions of these dates from individual moraines. We believe that our work is a step toward this eventual solution.

The statistical methods presented here do not provide uncertainties for their estimates of moraine age or geomorphic parameters. In the future, we will use resampling techniques, such as the bootstrap, to estimate these uncertainties. Because this chapter represents a proof of concept, rather than a final solution, formal uncertainty estimation is beyond the scope of this work. We expect that the geomorphic uncertainties associated with exposure dating will prove to be larger than the measurement uncertainty of the method.

We did not attempt to invert a combined model of moraine degradation and inheritance against our data sets, for two reasons. First, the data sets we treat here appear to be well described by one process each (Fig. 3.2). Second, the combined model would have too many parameters to estimate confidently, given the numbers of observations in our chosen data sets.

In fitting our models to data, one might be tempted to combine the data from moraines of the same morphostratigraphic age, to overcome the limitations imposed by small data sets. This temptation should be resisted. For example, the Yellowstone and Lake Fork moraines are in

similar geomorphic contexts, are about the same height, and are probably the same age (Laabs, 2009). Combining the exposure dates from these two moraines would bring the number of independent observations up to 13 from six or seven. However, this approach is inappropriate because the moraines may have had different post-depositional histories, and these varying histories may cause substantial differences in the distributions of exposure dates yielded by the moraines.

If the results presented here prove to be robust, our work has several implications for the practice of exposure dating on glacial landforms. First, neither moraine degradation nor inheritance necessarily affects cosmogenic exposure dating in all field areas. Our model fits suggest that the excess scatter among exposure dates from the Lake Fork and Yellowstone lateral moraines is caused exclusively by moraine degradation, whereas the exposure dates from Gurreholm Dal are influenced only by inheritance. Second, our model fits to the Gurreholm Dal data sets are inconsistent with past suggestions that the amount of inheritance in moraine boulders should be consistent between moraines deposited by the same glacier (Brown et al., 2005). The inferred maximum predepositional exposure time for these moraines increases with their stratigraphic age.

Chapter 4

Challenges in the use of cosmogenic exposure dating of moraine boulders to trace the geographic extents of abrupt climate changes

Cosmogenic exposure dating has sometimes been used to identify moraines associated with very short-lived climatic events, such as the Younger Dryas. Here, we point out some remaining challenges in using exposure dating of moraines to resolve abrupt climate changes. These challenges include identifying an optimal strategy for choosing boulders to sample for exposure dating, and potential errors in estimating production rates of cosmogenic nuclides caused by geomorphic processes. We fit a geomorphic process model that treats both moraine degradation and boulder erosion to collections of exposure dates from two moraines that date to around the time of the Younger Dryas. Subsampling of the modeled distributions shows that choosing boulders for exposure dating based on boulder height is a good strategy, whereas choosing boulders based on surface freshness is a poor strategy. Moreover, one of our fitted data sets is part of the global nuclide production rate database. Our fit of the moraine degradation model to this data set suggests that nuclide production rates at that site are several percent higher than previously thought. Potential errors associated with poor sampling strategies and production rate estimation are large enough to interfere with exposure dating of moraines, especially when the moraines are associated with abrupt climate changes. We suggest sampling strategies that may help reduce the effects of these problems.

Cosmogenic exposure dating of moraines is an attractive method for tracing the geographic extents of former abrupt climate changes. Glaciers grow and shrink in response to climate changes (Lowell, 2000; Oerlemans, 2005; Denton et al., 2005), and they deposit ridges called moraines at their margins (Gibbons et al., 1984). Thus, for abrupt climate changes that propagated over long distances quickly, we expect to find moraines of about the same age in mountain ranges within the area affected by the change. The crests of moraines are often studded with large boulders that can be sampled for cosmogenic exposure dating (e.g., Phillips et al., 1990; Gosse et al., 1995). In principle, cosmogenic exposure dating yields direct estimates of moraine ages; other Quaternary dating methods give only maximum or minimum age estimates, except in rare cases.

The Younger Dryas is an example of an abrupt climate change whose geographic extent has been traced partly with cosmogenic exposure dating of moraines. The Younger Dryas was an abrupt return to near-glacial conditions at the end of the last glaciation (12.9-11.7 ka; Barrows et al., 2007; Walker et al., 2009) that was first noted in pollen records from Europe (Mangerud et al., 1974). The subsequent elucidation of a Younger Dryas signal in the Greenland ice cores (Alley et al., 1993) precipitated a search for other records showing the same signal. At about the same time, the first successful exposure dating studies of moraines were undertaken (Phillips et al., 1990; Gosse et al., 1995). Thus, glacial geomorphologists used this new tool, exposure dating, to look for the Younger Dryas signal. Moraines that yielded exposure dates within the correct range were identified in the Alps (Ivy-Ochs et al., 1999, 2006, 2007; cf. Kelly et al., 2004), but also far from the European type areas of the Younger Dryas (Gosse et al., 1995; Ivy-Ochs et al., 1999). The Younger Dryas age assignments for these additional sites were later called into question by modeling studies (e.g., Vellinga and Wood, 2002) that showed that the Younger Dryas cooling was strong only around the North Atlantic basin, and weaker elsewhere in the Northern Hemisphere (though cf. Chiang and Bitz, 2005; Lowell et al., 2005; Broecker et al., 2006). In fact, the Southern Hemisphere likely warmed during the Younger Dryas (Broecker, 1989).

The analytical precision of cosmogenic exposure dating with beryllium-10 is high, suggesting that the method can identify moraines associated with abrupt climate changes such as the Younger Dryas. Confident identification of Younger Dryas moraines probably requires an uncertainty of 10% of the event's duration, or about 100 yr. Repeated sampling appears able to yield the desired precision. Measurements of beryllium-10 concentrations often have uncertainties of ~3% (e.g., Gosse et al., 1995; Owen et al., 2003; Kelly et al., 2008). Thus, the 1σ analytical uncertainties of beryllium-10 exposure dates from Younger Dryas moraines should be about 360 yr (3% of 12.0 ka). If measurement error were the only source of uncertainty in

exposure dating, we would need about 13 samples to reduce this 360-yr uncertainty to 100 yr (Bevington and Robinson, 2003, their eqn. 4-19; Fig. 4.1). Many published studies include 13 or more exposure dates, suggesting that this number of samples is achievable. Note that the uncertainty of the weighted mean is an appropriate characterization of the uncertainty in our age estimate of a moraine only where the dates are normally distributed and have a scatter consistent with the measurement uncertainties of the dates.

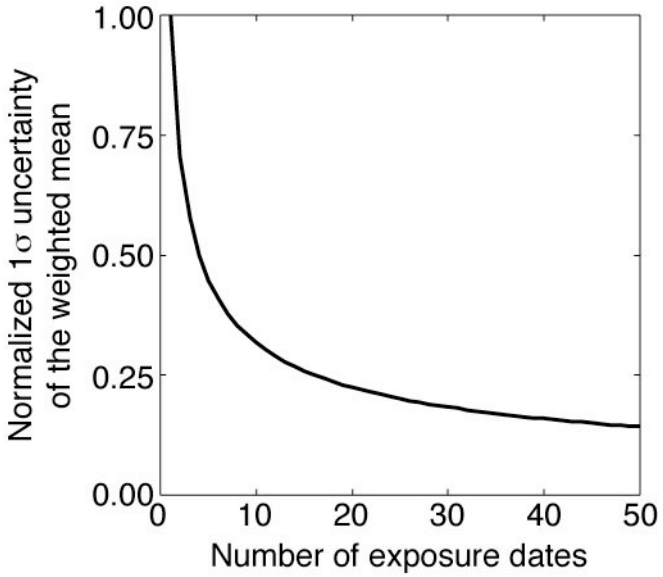

Figure 4.1: Uncertainty of the weighted mean as a function of the number of exposure dates available from a single moraine (Bevington and Robinson, 2003, their eqn. 4-19), normalized by the measurement uncertainty of one exposure date. This function provides a guide to the minimum number of samples that should be taken from a moraine in order to achieve a desired precision. Because geomorphic processes also contribute to the scatter among exposure dates on most moraines (Putkonen and Swanson, 2003; Balco and Schaefer, 2006; Ivy-Ochs et al., 2007), more samples will generally be needed.

However, the measurement of nuclide concentrations is only one step in the overall procedure of dating a moraine with cosmogenic nuclides. These steps are as follows.

1) collecting the samples (Gosse and Phillips, 2001; Briner, 2009),

2) processing the samples (Kohl and Nishiizumi, 1992; Bierman, 1994),

3) measuring the nuclide concentrations in the processed samples (Muzikar et al., 2003),

4) calculating the apparent exposure times of the samples from the nuclide concentrations (Lal, 1991; Gosse and Phillips, 2001; Balco et al., 2008), and

5) estimating the age of the moraine from the exposure dates.

All these steps contribute to the total uncertainty of cosmogenic exposure dating.

In this chapter, we indicate potential problems in the selection of samples for exposure dating and the calculation of exposure dates from nuclide concentrations (steps 1 and 4, above). Briefly, geomorphic process modeling suggests that sampling boulders with minimal surface weathering will yield too-young exposure dates on moraines that have lost material from their crests over time. Moreover, geomorphic processes likely introduce errors into the calibration of nuclide production rates. These problems limit our ability to confidently identify moraines associated with abrupt climate changes.

Practitioners of the exposure dating method are undoubtedly aware of these issues, but we have not seen them discussed in print. Here, we attempt to quantify the effects that these issues may have on exposure dating.

Prior work

This work builds on other contributions by us that treat methods for estimating the ages of moraines from exposure dates (step 5, above). We have developed models of two processes, moraine degradation and inheritance, that likely increase the scatter among exposure dates from moraines and cause the statistical distributions of these dates to be non-normal (Chapters 2 and 3; see also Zreda et al., 1994; Hallet and Putkonen, 1994; Putkonen and Swanson, 2003; Benson et al., 2005). Our work suggests that the statistical distributions of exposure dates from moraines should be left-skewed where moraine degradation is predominantly responsible for the scatter among exposure dates, and should be right-skewed where inheritance is the dominant process.

Our past work suggests that 1) the best method of estimating moraine ages varies between moraines, and 2) it is difficult to determine which method to apply to a given data set. The maximum exposure date in a data set is the best estimator of moraine age where moraine degradation is the dominant process, and the minimum exposure date provides the best estimate of moraine age where inheritance is responsible for most of the scatter (Phillips et al., 1990; Briner et al., 2005; Benson et al., 2005). Where measurement error dominates geomorphic biases, the mean is the best estimator of moraine age. Thus, one might choose which method to apply to any given data set based on the skewness of the dates. This method tends to yield results that are close to the correct answer for the parent distributions we have tested, but it sometimes fails spectacularly; the numbers of samples that are typically collected from moraines (20 or fewer per moraine) do not allow us to confidently determine the skewness of the parent distribution. Thus, we sometimes choose the wrong method for estimating moraine ages using the skewness criterion, leading to errors of thousands of years.

We have also developed methods for inverting our process models against observations (Chapter 3). Besides yielding explicit estimates of moraine age, our inverse methods also give estimates of the rates and magnitudes of the geomorphic processes described by the forward models. These inversions require a fairly large number of observations ($n \approx 10$ or greater) to achieve a good fit.

Selected data sets

We have attempted to identify moraines that were deposited at about the time of the Younger Dryas and have a sufficient number of published, independent beryllium-10 exposure dates that we can have reasonable confidence in our age assignments (Fig. 4.1).

Such moraines are rare. The Egesen stade moraines in the Alps seem firmly tied to the Younger Dryas (Ivy-Ochs et al., 2006; cf. Kelly et al., 2004), but we know of no Egesen moraine with more than four independent, published beryllium-10 exposure dates. Because the Egesen I and II moraines are geomorphically distinct in many Alpine valleys (Ivy-Ochs et al., 2006), the age difference between different moraine crests within the Egesen stade is likely to be substantial. This conclusion is supported by the exposure dates from Julier Pass, Switzerland, where the difference in the mean of the ^{10}Be exposure dates from the outer and inner Egesen moraines is about 860 yr (Ivy-Ochs et al., 2007, their Fig. 4). Hence, we do not combine exposure dates from the Egesen I and II moraines to increase the number of exposure dates.

Thus, we have chosen to use the beryllium-10 exposure dates (Fig. 4.2) from the inner Titcomb Lakes moraine (Wind River Range, Wyoming; Gosse et al., 1995a) and from the Waiho Loop moraine in New Zealand (Barrows et al., 2007; Applegate et al., 2008). Each of these moraines has some independent age control. The inner Titcomb Lakes moraine is correlated to the Temple Lake moraine of Zielinski and Davis (1987), elsewhere in the Wind River Range. The Temple Lake moraine is bracketed by radiocarbon dates that indicate an age of about 12.0 calendar ka (Balco et al., 2008; cf. Zielinski and Davis, 1987; Gosse et al., 1996). The Waiho Loop moraine has a large collection of radiocarbon dates that provide a minimum age estimate (Denton and Hendy, 1994), although the significance of these dates is debated (Broecker, 2003; Barrows et al., 2007; Turney et al., 2007).

For our purposes, it is unimportant whether or not these moraines belong to the Younger Dryas. It is sufficient that they are late glacial or early Holocene in age (10-15 ka), and have a comparatively large number of beryllium-10 exposure dates (n = 10 for the inner Titcomb Lakes moraine; n = 8 for the Waiho Loop). Both of these moraines also have exposure dates determined with other cosmogenic nuclides (Barrows et al., 2007; Balco et al., 2008), but we

neglect these other measurements here; our model is most appropriate for evaluating the distributions of beryllium-10 exposure dates.

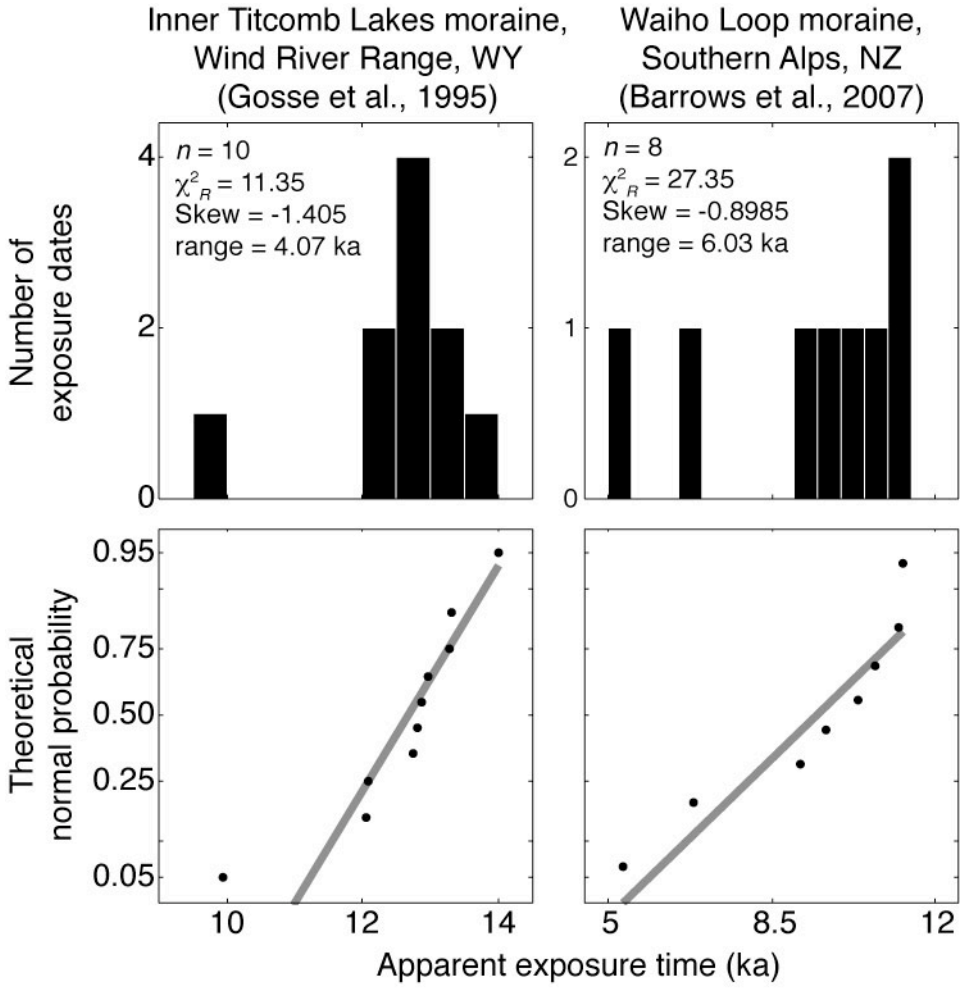

Figure 4.2: Beryllium-10 exposure dates from the inner Titcomb Lakes moraine (Gosse et al., 1995) and the Waiho Loop moraine (Barrows et al., 2007). The dates from these moraines fall fairly close to a line when displayed on normal probability plots (bottom panels; Chambers et al., 1983). Thus, we cannot rule out the hypothesis that these data sets are drawn from normal distributions. However, the scatter in these data sets is much larger than we would predict from the measurement uncertainties of the individual dates; their reduced chi-squared (χ^2_R; Bevington and Robinson, 2003) scores are much larger than 1. Thus, both these data sets are likely influenced by geomorphic processes.

For consistency, we have recalculated the exposure dates from the inner Titcomb Lakes moraine following Barrows et al. (2007; Appendix E). We also recalculated the Waiho Loop

beryllium-10 exposure dates; our recalculated dates agree with those reported by Barrows et al. (2007) to within 0.6%, suggesting that our calculation method is consistent with theirs. We did not use the CRONUS online calculator (Balco et al., 2008) because the calibration of the online calculator depends in part on the concentration measurements from the inner Titcomb Lakes moraine (see below). Thus, using the online calculator would introduce circularity into our results. In any case, the choice of scaling model has little influence on the scatter among exposure dates from individual moraines (Chapter 3), even at midlatitude sites where the effects of geomagnetic field changes are greatest.

Both these data sets are likely influenced by geomorphic processes. The reduced chi-squared scores of these data sets are much greater than 1 (Fig. 4.2), indicating that the data sets contain more scatter than can be explained by measurement error alone. We cannot rule out the possibility that these data sets are drawn from normal distributions, because the points representing the observations fall reasonably close to a line on normal probability plots (Fig. 4.2). However, both data sets have skewnesses less than -0.5, and these skewness values are more consistent with moraine degradation than either measurement error alone or inheritance (Chapter 2).

Explicit fitting of the degradation model to these data sets also suggests that moraine degradation is responsible for most of the scatter in each data set (Fig. 4.3, top; Table 4.1), although the model fit to the inner Titcomb Lakes data set is poor. For the purposes of these fits, we prescribed the initial height of each moraine and the erosion rate of the exposed boulders (1.0 mm/ka; Gosse et al., 1995a, b). We then used the Differential Evolution genetic algorithm to search for the minimum value of the Kolmogorov-Smirnov test statistic. The model evaluation with the minimum KS statistic indicates the values of moraine age, initial moraine slope, and topographic diffusivity that are most consistent with each data set. We specified the initial

moraine heights for these model inversions because the distributions of cosmogenic exposure dates are only weakly sensitive to small changes in initial height (Chapter 2).

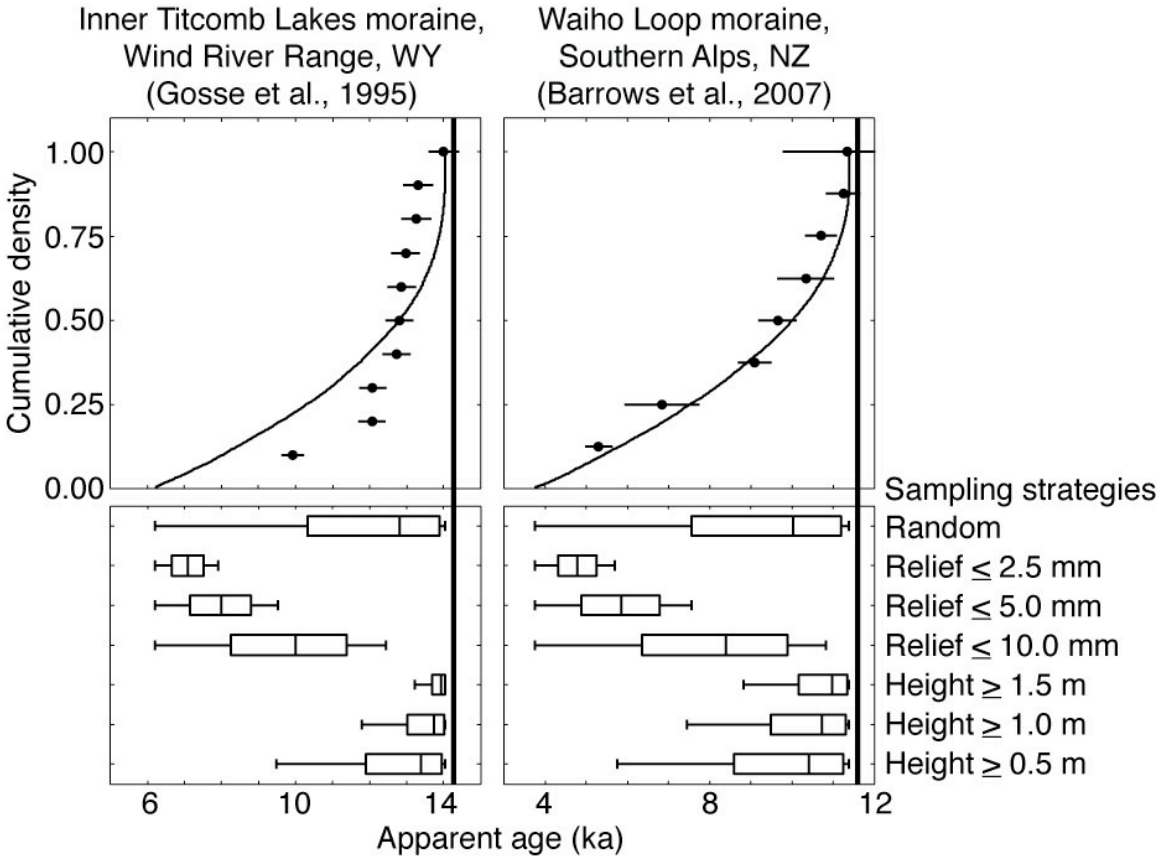

Figure 4.3: Top: Fits of the moraine degradation model to the beryllium-10 exposure dates from the inner Titcomb Lakes and Waiho Loop moraines (Gosse et al., 1995; Barrows et al., 2007). In each panel, the points with error bars represent the exposure dates with their 1σ measurement uncertainties; the curves are the best-fit modeled distributions for each data set. These fits presume an erosion rate for exposed boulders of 1.0 mm/ka. The initial height of the Titcomb Lakes moraine was prescribed at 25 m (cf. Gosse et al., 1995), and the initial height of the Waiho Loop moraine was prescribed to be 50 m (cf. Denton and Hendy, 1994). Bottom: Effects of different sampling strategies on the resulting distributions of cosmogenic exposure dates. The distributions are shown as boxplots (Chambers et al., 1983). Sampling very tall boulders (height $\geq$ 1.5 m) produces exposure dates that are within a few thousand years of the true age of the moraine (heavy line); sampling boulders with minimal surface relief (relief $\leq$ 2.5 mm) produces exposure dates that are thousands of years younger than the true age of the moraine.

Table 4.1: Best fits of the degradation model to the Waiho Loop and Titcomb Lakes data sets (Barrows et al., 2007; Gosse et al., 1995a).

Data set	Moraine age (ka)	Initial slope (°)	Diffusivity (m^2/yr)	KS statistic
Waiho Loop	11.59	32.77	$2.909 * 10^{-3}$	0.1400
Titcomb Lakes	14.27	36.80	$6.883 * 10^{-4}$	0.3113

KS, Kolmogorov-Smirnov (see Appendix D).
The parameter estimates here are probably good to two or three significant figures. Four figures are reported to allow checking of the model fits.

Implications for field sampling criteria

After identifying a moraine, the first step in cosmogenic exposure dating is deciding which boulders to sample. Depending on which boulders are sampled, the measured concentrations either will or will not be representative of the moraine's true age. Thus, imperfect boulder selection strategies could interfere with our ability to identify moraines associated with abrupt climate changes.

Field workers use a variety of criteria to select samples for cosmogenic nuclide measurements, but the two most common criteria are boulder height and surface freshness (e.g., Nishiizumi et al., 1989; Phillips et al., 1990; Cerling and Craig, 1994; Gosse et al., 1995b; Fabel and Harbor, 1999; Licciardi et al., 2001; Laabs et al., 2009). Most field geomorphologists avoid sampling boulders below some minimum height, often 1 m. This minimum height is often adjusted to take into account the distribution of boulder sizes available on particular moraines. Fresh boulders are those that retain polish or striations from subglacial transport. Few moraine boulders have polish or striations when they are sampled, so field geomorphologists estimate the thickness of material eroded from each boulder by measuring the relief on the boulders' upper surfaces (M. Kelly, personal communication). For a single boulder, relief is the distance between the lowest point and the highest point on the boulder's upper surface, measured at right angles to

the sampled surface. The style of weathering varies with lithology, but the low points on boulder surfaces are often weathering pits, and the high points are often veins of resistant mineralogies such as quartz (e.g., Barrows et al., 2007). Unless the high points retain polish, boulder surface relief is a minimum estimate of the thickness of material removed from the surfaces of the boulders.

Both these criteria are intended to minimize the chance that the samples have been shielded from cosmic rays during part of their postdepositional history. Tall boulders are less likely to have been covered by sediment or snow; boulders with polished or striated surfaces have not lost their nuclide-rich outer surfaces to erosion.

However, tall and fresh boulders sometimes yield exposure dates that are much younger than shorter and more weathered boulders from the same moraine. There is no correlation between boulder height and apparent exposure time for the samples from the inner Titcomb Lakes moraine (Fig. 4.4; boulder heights were not reported for the Waiho Loop data set). Briner (2009) took both pebble collections and boulder samples from moraines in Colorado, and found no relationship between the clast size from which each sample was taken and the apparent exposure time of the sample. Likewise, a literature review by K. Walsh (now at Ohio State University) found no consistent relationship between boulder size and apparent exposure time (unpublished compilation). We are unaware of any study that reports on the relationship between surface freshness and apparent exposure time. However, we believe that surface freshness is a poor predictor of the apparent exposure times yielded by individual boulders; that is, fresh boulders are not more likely than weathered boulders to yield exposure dates that are representative of the moraine's actual age.

Moraine degradation can explain the failure of these sampling criteria to indicate which boulders to sample on moraines (although other scenarios are also possible; see Discussion, below). If moraines lose meters of material from their crests over time, and boulders are

distributed throughout the removed soil column, then there will be no correlation between boulder height and apparent exposure time. If boulders do not erode while buried, but do erode at a constant rate after exhumation, then those boulders that are least eroded are also those that have spent the least amount of time at the surface.

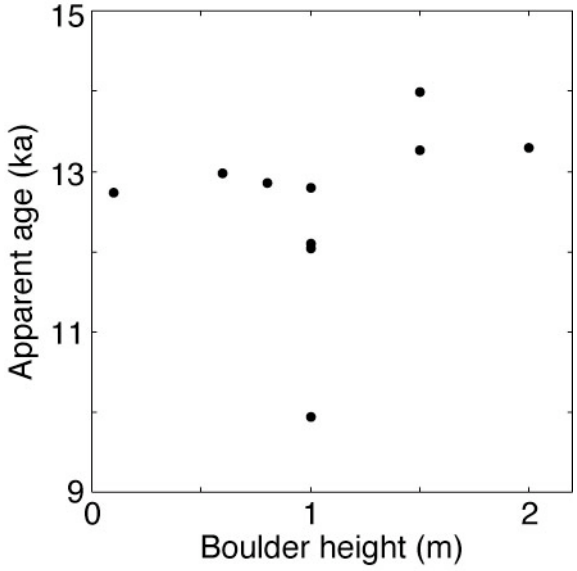

Figure 4.4: Apparent exposure time as a function of boulder height for the inner Titcomb Lakes moraine (Gosse et al., 1995). For this data set, there appears to be no relationship between boulder height and apparent exposure time. The exposure dates shown here have not been corrected for snow cover or boulder erosion.

Our model fits and limited field observations support these assumptions. The scatter among the beryllium-10 exposure dates from the Waiho Loop moraine are best explained by the progressive loss of ~4.2 m of material from the moraine's crest; similarly, the model fit suggests that the inner Titcomb Lakes moraine has lost ~2.6 m of material from its crest. It is more difficult to assess the correctness of our assumptions about boulder erosion from the model fits, because the shape of the modeled distributions is insensitive to the boulder erosion rate. However, some support for our statements about boulder erosion comes from the Huancané II moraines near the Quelccaya Ice Cap (Mercer and Palacios, 1977). On these moraines, clasts buried less than a meter below the surface are fresh and have striated surfaces, but surface

boulders adjacent to the soil pits are weathered. The weathered boulders have pits and pedestals on their upper surfaces that indicate several centimeters of lost material. Taken together, these observations suggest that boulders in this environment do not erode unless they are exposed at the surface.

Given our model fits (Fig. 4.3, top), we can evaluate the effects of different sampling strategies on the distributions of cosmogenic exposure dates (Fig. 4.3, bottom). The modeled boulders have heights, surface relief values, and exposure dates that are consequences of the model physics. Thus, we can identify the modeled boulders that are taller than a certain height or have less than a certain amount of surface relief. By comparing the exposure dates within each subsample to the "true" age of the moraine, we can determine which sampling strategies produce exposure dates that are closest to this true value.

Very tall boulders are most likely to yield exposure dates that are close to the true age of the moraine (Fig. 4.3, bottom). The median exposure date moves closer to the true moraine age as the minimum boulder height becomes greater. However, even fairly large boulders, standing at least 1.5 m above the moraine's crest, can yield exposure dates that are several thousand years younger than the moraine's true age.

Sampling boulders with minimal surface relief always yields exposure dates that are younger than the moraine's true age (Fig. 4.3, bottom). Moreover, as the criterion is made more stringent, the median exposure date moves away from the true age. Thus, the more strictly one adheres to the freshness criterion, the worse the resulting exposure dates become.

This result can be understood by comparing the thicknesses of material that can be eroded from a boulder's surface and from a moraine's crest over the same period of time (D. Pollard, personal communication). The changes in moraine heights implied by our model fits (Fig. 4.3, top) are much greater than the thickness of material that can be removed by erosion from boulder surfaces over an equivalent period. Even if we allow a very rapid boulder erosion rate of 100

mm/ka (cf. Gosse et al., 1995a, b), a boulder exposed to surface weathering for 12 ka would lose only 1.2 m of material from its surface. This thickness is much smaller than the 2-4 m of moraine height change implied by our model fits, even allowing for the difference in density between boulders and till. Thus, the effects of moraine degradation on cosmogenic exposure dates appear to dominate those of boulder erosion for late glacial and early Holocene moraines (Hallet and Putkonen, 1994).

Implications for determining nuclide production rates

Step 5 in determining the age of a moraine using cosmogenic exposure dating involves calculating the apparent exposure time of each sample, using the estimated local production rate of the nuclide (Balco et al., 2008). Thus, any error in determining the local production rate will translate into errors in the apparent exposure times, reducing our ability to identify moraines associated with short-lived climate events.

The production rates of cosmogenic nuclides are not known *a priori*. Instead, the concentrations of cosmogenic nuclides are measured in boulders from moraines whose ages are known independently from other chronologic methods, usually radiocarbon dating. Ideally, the nuclide concentration in a single boulder, divided by the independently determined moraine age, yields the local time-averaged production rate after correcting for nuclear decay. In practice, the nuclide concentrations in boulders at the calibration sites are highly scattered (Balco et al., 2008). Consequently, there is uncertainty about the representative nuclide concentration at each calibration site.

Recent efforts to determine a reference production rate from the calibration database (Balco et al., 2008) average the measured nuclide concentrations to determine a representative nuclide concentration for each site. This procedure is reasonable, but it ignores the effects of

geomorphic processes on the nuclide concentrations, as well as problems with the independent age constraints. These potential problems were fully acknowledged by Balco et al. (2008).

The measured beryllium-10 concentrations from the inner Titcomb Lakes moraine are part of the global nuclide production rate calibration database (Gosse and Klein, 1996; Balco et al., 2008). The degree of scatter in the exposure dates from the inner Titcomb Lakes moraine is probably larger than can be explained by measurement error, and the skewness of the data set suggests that the maximum exposure date is the best estimator of the moraine's age (Fig. 4.2; Chapter 3). Thus, the representative nuclide concentration at the Titcomb Lakes study site is probably the maximum measured concentration. Prior studies that used the Titcomb Lakes concentration measurements to estimate the production rate of beryllium-10 took the average of the nine largest observed concentrations as the representative nuclide concentration for this site, treating the smallest concentration as a statistical outlier (Gosse and Klein, 1996; Balco et al., 2008). The largest concentration is about 7% greater than the mean of the nine largest concentrations. In turn, the time-averaged production rate of beryllium-10 at the Titcomb Lakes site may be about 7% larger than previously believed.

A potential error of a few percent in estimating nuclide production rates has serious implications for our ability to identify moraines associated with abrupt, short-lived climate changes such as the Younger Dryas. Even a 5% error in estimating nuclide production rates translates into an error in apparent exposure time of ~600 yr (5% of 12 ka), about half the length of the Younger Dryas.

This example suggests that the calibration of beryllium-10 production rates should be reevaluated, taking the effects of geomorphology on the calibration measurements into account. This recalibration might help reduce the extreme mismatch between some of the calibration samples and the best fit of the scaling models to the calibration data set (Balco et al., 2008, their Fig. 4.5).

Discussion

In this chapter, we have identified two challenges in the use of cosmogenic exposure dating to date moraines associated with abrupt climate changes such as the Younger Dryas. First, pristine boulders will tend to yield exposure dates that are younger than the true age of the moraine. Second, geomorphic processes likely impart an additional uncertainty of at least several percent in our present estimates of reference cosmogenic nuclide production rates. For moraines of late glacial to early Holocene age, these effects bias exposure dates by hundreds to thousands of years. Thus, these challenges limit our confidence in the ability of cosmogenic exposure dating to identify moraines associated with abrupt climate changes, which have time scales of a few years to a few hundred years.

Moreover, our results confirm prior suggestions that preferentially sampling tall boulders is a good strategy (Phillips et al., 1990; Gosse et al., 1995). However, even exposure dates from tall boulders may underestimate the age of a moraine by thousands of years, depending on the maximum boulder height and the thickness of material lost from the moraine's crest.

Our conclusions do not hold where geomorphic processes other than moraine degradation and boulder erosion affect exposure dates. In particular, inheritance might cause the exposure dates from tall boulders to overestimate the ages of moraines; boulders that fall onto the glacier from oversteepened valley walls will not be eroded in transport, and thus may be larger than other clasts that have had most of their inherited nuclides stripped away by subglacial transport.

Moreover, we assume that the erosion rate for exposed boulders is the same for all the rocks on a moraine. However, we expect that boulders on real moraines will weather at different rates, depending on their lithology, position in the landscape, and size. Our models also assume slow, grain-by-grain erosion of moraine boulders, but the rapid loss of several centimeters of rock

is also possible (Zimmerman et al., 1995). In the future, we will update our models to represent this style of erosion, perhaps following Muzikar (2009).

Here, we explain the lack of correlation between boulder height and apparent exposure time (Fig. 4.4) with moraine degradation. Other explanations are also possible. In cases where inheritance dominates the scatter among exposure dates, there may be no relationship between boulder size and apparent exposure time. If all the boulders on a moraine are taller than the thickness of snow cover or the thickness of sediment that has been removed from the surface of a moraine, there will also be no correlation between boulder height and apparent exposure time. We believe that the geomorphic processes responsible for the scatter among exposure dates vary between moraines, and so the degree and sign of the correlation between boulder height and apparent exposure time probably also vary between moraines.

Our results imply that our ability to invert our models against collections of exposure dates depends on how the samples were chosen. The inverse methods can account for the heights of boulders from which samples were taken, as long as these heights are reported with the exposure dates. However, the inverse methods cannot account for use of the surface pristinity criterion. Preferentially sampling fresh boulders produces distributions of exposure dates that are all younger than the true age of the moraine and emphasize the tail of the modeled distribution at the expense of the mode (Fig. 4.3), if both moraine degradation and boulder erosion are active on a particular moraine. Given a data set collected in this way, our methods would likely be unable to determine whether the excess scatter in the data were caused by inheritance or moraine degradation. Any age estimates made using our methods from such a data set would be far too young.

For future field campaigns, and in evaluating past data sets, we recommend determining what overall precision would be necessary to answer the paleoclimate question at hand. For

example, confident determination of whether a moraine dates to the Younger Dryas probably requires an overall 1σ uncertainty of about 100 yr.

With that information, the minimum number of samples required to answer the question can be estimated from the expected measurement uncertainty of the exposure dates and Figure 4.1. Figure 4.1 represents the uncertainty of the weighted mean (Bevington and Robinson, 2003, their eqn. 4-19). This quantity is the uncertainty of repeated exposure dating on a single moraine in the very special case where geomorphology has no effect on the exposure dates. Note that repeated sampling will not reduce uncertainty associated with external factors such as production rate errors (Balco et al., 2008). In practice, the uncertainty of exposure dating will be larger than Figure 1 implies, so more samples will be required.

The number of samples required to achieve a desired precision will sometimes be unrealistically large. The curve in Figure 4.1 reaches a point of diminishing returns around 10-15 samples, where the uncertainty of the weighted mean is 25-30% of the uncertainty of one date. The number of samples required to achieve a precision better than 25-30% of the uncertainty of one date will often be larger than can be produced with available resources. Thus, some questions can be answered only approximately with cosmogenic exposure dating.

In choosing which boulders to sample, we recommend sampling all the tallest boulders on the moraine. If resources for further sampling are available, additional boulders should be chosen randomly. All the sampled boulders should be on the crest of the moraine. The samples from the tall boulders have a good chance of producing at least one exposure date that correctly estimates the moraine's age, assuming inheritance is not important. The randomly chosen samples will help identify the source of any geomorphic bias, if the exposure dates from the tall boulders are widely scattered. Moreover, the surface relief of sampled boulders should be recorded in the field and given in papers that report new exposure dates.

REFERENCES

Agassiz, L., trans. Carrozzi, A. V., 1967, Studies on glaciers, preceded by the discourse of Neuchatel: Haffner, 213 p.

Aitken, M. J., 1997, Luminescence dating: in Taylor, R. E., and Aitken, M. J. (eds.), Chronometric dating in archaeology: Plenum Press, p. 183-215.

Alley, R. B., 2000, The Younger Dryas cold interval as viewed from central Greenland: Quaternary Science Reviews, v. 19, p. 213-226.

Alley, R. B., 2000, The two-mile time machine: Princeton University Press, 229 p.

Alley, R. B., 2007, Wally was right: predictive ability of the North Atlantic "conveyor belt" hypothesis for abrupt climate change: Annual Reviews in Earth and Planetary Sciences, v. 35, p. 241-272.

Anderson, B., and Mackintosh, A., 2006, Temperature change is the major driver of late-glacial and Holocene glacier fluctuations in New Zealand: Geology, v. 34, p. 121-124.

Anderson, R. S., and Humphrey, N. F., 1989, Interaction of weathering and transport processes in the evolution of arid landscapes: in Cross, T. A. (ed.), Quantitative dynamic stratigraphy, Prentice-Hall, p. 349-361.

Antevs, E., 1922, The recession of the last ice sheet in New England: American Geological Society Research Series, v. 11, 120 p.

Applegate, P. J., 2005, Synchroneity of the last deglaciation in the western United States, with some observations on the glacial history of the San Juan Mountains, Colorado: unpublished thesis, Purdue University, 178 p.

Applegate, P. J., Lowell, T. V., and Alley, R. B., 2008, Comment on "Absence of cooling in New Zealand and the adjacent ocean during the Younger Dryas chronozone": Science, v. 320, p. 746d.

Atwood, W. W., 1909, Glaciation of the Uinta and Wasatch Mountains: U. S. Geological Survey Professional Paper 61, 96 p.

Balco, G., and Schaefer, J. M., 2006, Cosmogenic-nuclide and varve chronologies for the deglaciation of southern New England: Quaternary Geochronology, v. 1, p. 15-28.

Balco, G., Stone, J. O., Lifton, N. A., and Dunai, T. J., 2008, A complete and easily accessible means of calculating surface ages or erosion rates from 10Be and 26Al measurements: Quaternary Geochronology, v. 3, p. 174-195.

Barrows, T. T., Lehman, S. J., Fifield, L. K., and de Deckker, P., 2007, Absence of cooling in New Zealand and the adjacent ocean during the Younger Dryas chronozone: Science, v. 318, p. 86-89.

Barrows, T. T., Lehman, S. J., Fifield, L. K., and de Deckker, P., 2008, Response to comment on "Absence of cooling in New Zealand and the adjacent ocean during the Younger Dryas chronozone": Science, v. 320, p. 746e.

Benn, D. I., and Evans, D. J. A., 1998, Glaciers and glaciation: Hodder Arnold, 734 p.

Benson, L., Madole, R., Landis, G., and Gosse, J., 2005, New data for late Pleistocene Pinedale alpine glaciation from southwestern Colorado: Quaternary Science Reviews, v. 24, p. 49-65.

Berger, A. L., 1978, Long-term variations of daily insolation and Quaternary climatic changes: Journal of the Atmospheric Sciences, v. 35, p. 2362-2367.

Berger, A. L., and Loutre, M.-F., 1991, Insolation values for the climate of the last 10 millon years: Quaternary Science Reviews, v. 10, p. 297-317.

Bevington, P. R., and Robinson, D. K., 2003, Data reduction and error analysis for the physical sciences: McGraw-Hill, 336 p.

Beyer, W. H. (ed.), 1978, CRC standard mathematical tables: CRC Press, 613 p.

Bierman, P. R., 1994, Using in situ produced cosmogenic isotopes to estimate rates of landscape evolution: a review from the geomorphic perspective: Journal of Geophysical Research, v. 99, p. 13,885-13,896.

Bierman, P. R., Reuter, J. M., Pavich, M., and four others, 2005, Using cosmogenic nuclides to contrast rates of erosion and sediment yield in a semi-arid, arroyo-dominated landscape, Rio Puerco Basin, New Mexico: Earth Surface Processes and Landforms, v. 30, p. 935-953.

Borns, H. W., Doner, L. A., Dorion, C. C., and six others, 2004, The deglaciation of Maine, U. S. A.: in Ehlers, J., and Gibbard, P. L., Quaternary glaciations – extent and chronology: part II: North America: Elsevier, p. 89-110.

Boulton, G. S., Dongelmans, P., Punkari, M., and Broadgate, M., 2001, Paleoglaciology of an ice sheet through a glacial cycle: the European ice sheet through the Weichselian: Quaternary Science Reviews, v. 20, p. 591-625.

Box, G. E. P., and Draper, N., 1987, Empirical model building and response surfaces: Wiley, 688 p.

Briner, J. P., and Swanson, T. W., 1998, Using inherited cosmogenic 36Cl to constrain glacial erosion rates of the Cordilleran ice sheet: Geology, v. 26, p. 3-6.

Briner, J. P., Kaufman, D. S., Manley, W. F., Finkel, R. C., and Caffee, M. W., 2005, Cosmogenic exposure dating of late Pleistocene moraine stabilization in Alaska: Geological Society of America Bulletin, v. 117: p. 1108-1120.

Briner, J. P., 2009, Moraine pebbles and boulders yield indistinguishable 10Be ages: a case study from Colorado, USA: Quaternary Geochronology, v. 4, p. 299-305.

Broecker, W. S., Kennett, J. P., Flower, B. P., Teller, J. T., Trumbore, S., Bonani, G., and Wolfli, W., 1989, Routing of meltwater from the Laurentide ice sheet during the Younger Dryas cold episode: Nature, v. 341, p. 318-321.

Broecker, W. S., 2002, The glacial world according to Wally (3rd ed.): Eldigio Press, 76 p. Available online at http://cfellows.org/wally/ (accessed 17 September 2009).

Broecker, W. S., 2003, Does the trigger for abrupt climate change reside in the ocean or in the atmosphere?: Science, v. 300, p. 1519-1522.

Broecker, W. S., 2006, Abrupt climate change revisited: Global and Planetary Change, v. 54, p. 211-215.

Brown, E. T., Molnar, P., and Bourlés, D. L., 2005, Comment on "Slip-rate measurements on the Karakorum Fault may imply secular variations in fault motion": Science, v. 309, p. 1326b.

Cerling, T. E., and Craig, H., 1994, Geomorphology and in-situ cosmogenic isotopes: Annual Reviews in Earth and Planetary Science, v. 22, p. 273-317.

Chambers, J. M., Cleveland, W. S., Kleiner, B., and Tukey, J. W., 1983, Graphical methods for data analysis: Wadsworth, 395 p.

Chevalier, M.-L., Ryerson, F. J., Tapponier, P., and four others, 2005, Slip-rate measurements on the Karakorum Fault may imply secular variations in fault motion: Science, v. 307, p. 411-414.

Chiang, J. C. H., and Bitz, C. M., 2005, Influence of high latitude ice cover on the marine Intertropical Convergence Zone: Climate Dynamics, DOI 10.1007/s00382-005-0040-5.

Clark, C. D., Gibbard, P. L., and Rose, J., 2004, Pleistocene glacial limits in England, Scotland, and Wales: in Ehlers, J., and Gibbard, P. L., Quaternary glaciations – extent and chronology, part I: Europe: Elsevier, p. 47-82.

Clauset, A., Shalizi, C. R., and Newman, M. E. J., 2007, Power-law distributions in empirical data: arXiv.org physics, http://arxiv.org/abs/0706.1062v1, accessed 18 September 2009.

Croarkin, C., and Tobias, P., 2006, NIST/SEMATECH e-Handbook of Statistical Methods, http://www.itl.nist.gov/div898/handbook/, accessed 18 September 2009.

Cuffey, K. M., and Clow, G. D., 1997, Temperature, accumulation, and ice sheet elevation in central Greenland through the last deglacial transition: Journal of Geophysical Research, v. 102, p. 26,383-26,396.

Dansgaard, W., 1964, Isotope systematics in high latitude precipitation: Tellus, v. 16, p. 437-468.

Dyurgerov, M. B., and Meier, M. F., 2000, Twentieth century climate change: evidence from small glaciers: Proceedings of the National Academy of Sciences, v. 97, p. 1406-1411.

de Geer, G., 1912, A geochronology of the last 12,000 years: Compte rendu du XI Congrés Géologique International (Stockholm 1910), p. 241-253.

Denton, G. H., Alley, R. B., Comer, G. C., and Broecker, W. S., 2005, The role of seasonality in abrupt climate change: Quaternary Science Reviews, v. 24, p. 1159-1182.

Dreimanis, A., 1988, Tills: their genetic terminology and classification: in Goldthwait, R. P., and Matsch, C. L. (eds.), Genetic classification of glacigenic deposits: Balkema, p. 17-84.

Dunne, J., Elmore, D., and Muzikar, P., 1999, Scaling factors for the rates of production of cosmogenic nuclides for geometric shielding and attenuation at depth on sloped surfaces: Geomorphology, v. 27, p. 3-11.

Dyke, A. S., and Prest, V. K., 1987, Late Wisconsinan and Holocene history of the Laurentide ice sheet: Géographie physique et Quaternaire, v. XLI, p. 237-263.

Dyke, A. S., 2004, An outline of North American deglaciation with emphasis on central and northern Canada: in Ehlers, J., and Gibbard, P. L., Quaternary glaciations – extent and chronology, part II: North America: Elsevier, p. 373-424.

Fabel, D., and Harbor, J., 1999, The use of in-situ produced cosmogenic radionuclides in glaciology and glacial geomorphology: Annals of Glaciology, v. 28, p. 103-110.

Fabel, D., Harbor, J., Dahms, D., and six others, 2004, Spatial patterns of glacial erosion at a valley scale derived from terrestrial cosmogenic 10Be and 26Al concentrations in rock: Annals of the Association of American Geographers, v. 94, p. 241-255.

Fisher, T. G., and Lowell, T. V., 2006, Questioning the age of the Moorhead Phase in the glacial Lake Agassiz basin: Quaternary Science Reviews, v. 25, p. 2688-2691.

Fletcher, C. A. J., 1991, Computational techniques for fluid dynamics, volume 1 (2nd ed.): Springer, 401 p.

Funder, S., 1978, Holocene stratigraphy and vegetation history in the Scoresby Sund area, East Greenland. Grønlands Undersøgels Bulletin, v. 129, 66 p.

Gibbons, A. B., Megeath, J. D., and Pierce, K. L., 1984, Probability of moraine survival in a succession of glacial advances: Geology, v. 12, p. 327-330.

Gillespie, A., and Molnar, P., 1995, Asynchronous maximum advances of mountain and continental glaciers: Reviews of Geophysics, v. 33, p. 311-364.

Gosse, J. C., Evenson, E. B., Klein, J., Lawn, B., and Middleton, R., 1995a, Precise cosmogenic 10Be measurements in western North America: support for a global Younger Dryas cooling event: Geology, v. 23, p. 877-880.

Gosse, J. C., Klein, J., Evenson, E. B., Lawn, B., and Middleton, R., 1995b, Beryllium-10 dating of the duration and retreat of the last Pinedale glacial sequence: Science, v. 268, p. 1329-1333.

Gosse, J., and Klein, J., 1996, Production rate of in-situ cosmogenic 10Be in quartz at high altitude and mid latitude: Radiocarbon, v. 38, p. 154-155.

Gosse, J. C., and Phillips, F. M., 2001, Terrestrial in situ cosmogenic nuclides: theory and application: Quaternary Science Reviews, v. 20, p. 1475-1560.

Granger, D. E., and Muzikar, P. F., 2001, Dating sediment burial with in situ-produced cosmogenic nuclides: theory, techniques, and limitations: Earth and Planetary Science Letters, v. 188, p. 269-281.

Granger, D. E., Fabel, D., and Palmer, A. N., 2001, Pliocene-Pleistocene incision of the Green River, Kentucky, determined from radioactive decay of cosmogenic 26Al and 10Be in Mammoth Cave sediments: Geological Society of America Bulletin, v. 113, p. 825-836.

Håkansson, L., Briner, J., Alexanderson, H., Aldahan, A., and Possnert, G., 2007, 10Be ages from central east Greenland constrain the extent of the Greenland ice sheet during the Last Glacial Maximum: Quaternary Science Reviews, v. 26, p. 2316-2321.

Hallet, B., and Putkonen, J., 1994, Surface dating of dynamic landforms: young boulders on aging moraines: Science, v. 265, p. 937-940.

Hanks, 2000, The age of scarplike landforms from diffusion-equation analysis: in Noller, J. S., Sowers, J. M., and Lettis, W. R. (eds.), Quaternary geochronology: methods and applications: American Geophysical Union Reference Shelf, v. 4, American Geophysical Union, 582 p.

Hays, J. D., Imbrie, J., and Shackleton, N. J., 1976, Variations in the earth's orbit: pacemaker of the ice ages: Science, v. 194, p. 1121-1132.

Heisinger, B., Lal, D., Jull, A. J. T., and six others, 2002a, Production of selected cosmogenic radionuclides by muons 1. Fast muons: Earth and Planetary Science Letters, v. 200, p. 345-355.

Heisinger, B., Lal, D., Jull, A. J. T., and four others, 2002b, Production of selected cosmogenic radionuclides by muons 2. Capture of negative muons: Earth and Planetary Science Letters, v. 200, p. 357-369.

Hilborn, R., and Mangel, M., 1997, The ecological detective: confronting models with data: Monographs in Population Biology, v. 28, Princeton University Press, 315 p.

Huybers, P., and Wunsch, C., 2005, Obliquity pacing of the late Pleistocene glacial terminations: Nature, v. 434, p. 491-494.

Huybers, P., 2006, Early Pleistocene glacial cycles and the integrated summer insolation forcing: Science, v. 313, p. 508-511.

Ivy-Ochs, S., Schlüchter, C., Kubik, P. W., and Denton, G. H., Moraine exposure dates imply synchronous Younger Dryas glacier advances in the European Alps and in the Southern Alps of New Zealand: Geografiska Annaler, v. 81, p. 313-323.

Ivy-Ochs, S., Kerschner, H., Reuther, A., Maisch, M., Sailer, R., Schaefer, J., Kubik, P.W., Synal, H., and Schlüchter, C., 2006, The timing of glacier advances in the northern European Alps based on surface exposure dating with cosmogenic 10Be, 26Al, 36Cl, and 21Ne, in Siame, L.L., Bourlès, D.L., and Brown, E.T., eds., In situ–produced cosmogenic nuclides and quantification of geological processes: Geological Society of America Special Paper 415, p. 43–60.

Ivy-Ochs, S., Kerschner, H., and Schlüchter, C., 2007, Cosmogenic nuclides and the dating of Lateglacial and early Holocene glacier variations: the Alpine perspective: Quaternary International, v. 164-165, p. 53-63.

James, L. A., Harbor, J., and Fabel, D., Dahms, D., and Elmore, D., 2002, Late Pleistocene glaciations in the northwestern Sierra Nevada, California: Quaternary Research, v. 57, p. 409-419.

Jansen, E., Overpeck, J., Briffa, K. R., and 13 others, 2007, Paleoclimate: in Solomon, S., Qin, M., Manning, Z., and five others (eds.), Climate change 2007: the physical science basis: contribution of Working Group I to the Fourth Assessment Report of the Intergovernmental Panel on Climate Change: Cambridge University Press, p. 433-498.

Jones, P. D., and Mann, M. E., 2004, Climate over past millennia: Reviews of Geophysics, v. 42, RG2002.

Kaplan, M. R., Douglass, D. C., Singer, B. S., Ackert, R. P., and Caffee, M. W., 2005, Cosmogenic nuclide chronology of pre-last glacial maximum moraines at Lago Buenos Aires, 46°S, Argentina: Quaternary Research, v. 63, p. 301-315.

Kelly, M. A., Kubik, P. W., von Blanckenburg, F., and Schlüchter, C., 2004, Surface exposure dating of the Great Aletsch Glacier Egesen moraine system, western Swiss Alps, using the cosmogenic nuclide 10Be: Journal of Quaternary Science, v. 19, p. 431-441.

Kelly, M. A., Lowell, T. V., Hall, B. L., and five others, 2008: A 10Be chronology of lateglacial and Holocene mountain glaciation in the Scoresby Sund region, east Greenland: implications for seasonality during lateglacial time: Quaternary Science Reviews, v. 27, p. 2273-2282.

Kirkbride, M. P., and Brazier, V., 1998, A critical evaluation of the use of glacier chronologies in climatic reconstruction with reference to New Zealand: Quaternary Proceedings, v. 6, p. 55-64.

Kohl, C.P., and Nishiizumi, K., 1992, Chemical isolation of quartz for measurement of in situ-produced cosmogenic nuclides: Geochimica et Cosmochimica Acta, v. 56, 3583–3587.

Krüger, J., 1996, Moraine ridges formed from subglacial frozen-on sediment slabs and their differentiation from push moraines: Boreas, v. 25, p. 57-63.

Lal, D., 1991, Cosmic ray labeling of erosion surfaces: in situ nuclide production rates and erosion models: Earth and Planetary Science Letters, v. 104, p. 424-439.

Lal, D., and Chen, J., 2005, Cosmic ray labeling of erosion surfaces II: special cases of exposure histories of boulders, soils, and beach terraces: Earth and Planetary Science Letters, v. 236, p. 797-813.

Lawson, D. E., 1979, Sedimentological analysis of the western terminus region of the Matanuska Glacier, Alaska: U. S. Army Corps of Engineers, Cold Regions Research and Engineering Laboratory, 112 p.

Laabs, B. J. C., Plummer, M. A., and Mickelson, D. M., 2006, Climate during the last glacial maximum in the Wasatch and southern Uinta Mountains inferred from glacier modeling: Geomorphology, v. 75, p. 300-317.

Laabs, B. J. C., Refsnider, K. A., Munroe, J. S., and four others, 2009, Latest Pleistocene glacial chronology of the Uinta Mountains: support for moisture-driven asynchrony of the last deglaciation: Quaternary Science Reviews, v. 28, p. 1171-1187.

Lemke, P., Ren, J., Alley, R. B., and eight others, 2007, Observations: changes in snow, ice and frozen ground: in Solomon, S., Qin, M., Manning, Z., and five others (eds.), Climate change 2007: the physical science basis: contribution of Working Group I to the Fourth Assessment Report of the Intergovernmental Panel on Climate Change: Cambridge University Press, p. 337-384.

Licciardi, J. M., Clark, P. U., Brook, E. J., and four others, Cosmogenic 3He and 10Be chronologies of the late Pinedale northern Yellowstone ice cap, Montana, USA: Geology, v. 29, p. 1095-1098.

Licciardi, J. M., Clark, P. U., Brook, E. J., Elmore, D., and Sharma, P., 2004, Variable responses of western U. S. glaciers during the last deglaciation: Geology, v. 32, p. 81-84.

Lowell, T. V., Savage, K. M., Brockman, C. S., Stuckenrath, R., 1990, Radiocarbon analyses from Cincinnati, Ohio, and their implications for glacial stratigraphic interpretations: Quaternary Research, v. 34, p. 1-11.

Lowell, T. V., 1995a, The application of radiocarbon age estimates to the dating of glacial sequences: an example from the Miami sublobe, Ohio, U. S. A.: Quaternary Science Reviews, v. 14, p. 85-99.

Lowell, T. V., Heusser, C. J., Andersen, B. G., and six others, 1995b, Interhemispheric correlation of late Pleistocene glacial events: Science, v. 269, p. 1541-1549.

Lowell, T. V., Larson, G. J., Hughes, J. D., and Denton, G. H., 1999: Age verification of the Lake Gribben forest bed and the Younger Dryas advance of the Laurentide ice sheet: Canadian Journal of Earth Science, v. 36, p. 383-393.

Lowell, T. V., 2000, As climate changes, so do glaciers: Proceedings of the National Academy of Sciences, v. 97, p. 1351-1354.

Lowell, T. V., Fisher, T. G., Comer, G. C., Hajdas, I., Waterson, N., Glover, K., Loope, H. M., Schaefer, J. M., Rinterknecht, V., Broecker, W., Denton, G., and Teller, J. T., 2005, Testing the Lake Agassiz meltwater trigger for the Younger Dryas: Eos, Transactions, American Geophysical Union, p. 365, 372.

Luckman, B. H., 2000, The Little Ice Age in the Canadian Rockies: Geomorphology, v. 32, p. 357-384.

Mangerud, J., Anderson, D. T., Berglund, B. E., and Donner, J. J., 1974, Quaternary stratigraphy of Norden, a proposal for terminology and classification: Boreas, v. 3, p. 109-127.

Mangerud, J., 2004, Ice sheet limits in Norway and on the Norwegian continental shelf: in Quaternary glaciations – extent and chronology, part I: Europe: Elsevier, p. 271-294.

Masarik, J., and Wieler, R., 2003, Production rates of cosmogenic nuclides in boulders: Earth and Planetary Science Letters, v. 216, p. 201-208.

Mercer, J. H., and Palacios M., O., Radiocarbon dating of the last glaciation in Peru: Geology, v. 5, p. 600-604.

Munroe, J. S., Laabs, B. J. C., Shakun, J. D., and four others, 2006, Latest Pleistocene advance of alpine glaciers in the southwestern Uinta Mountains, Utah, USA: evidence for the influence of local moisture sources: Geology, v. 34, p. 841-844.

Murphy, E. A., 1964, One cause? Many causes? The argument from the bimodal distribution: Journal of Chronic Diseases, v. 17, p. 301-324.

Muzikar, P., Elmore, D., and Granger, D. E., 2003, Accelerator mass spectrometry in geological research: Geological Society of America Bulletin, v. 115, p. 643-654.

Muzikar, P., 2009, General models for episodic surface denudation and its measurement by cosmogenic nuclides: Quaternary Geochronology, v. 4, p. 50-55.

Nash, 1986, Morphologic dating and modeling degradation of fault scarps: in Geophysics Research Forum, Active tectonics: National Academy Press, 266 p.

Nishiizumi, K., Winterer, E. L., Kohl, C. P., and four others, 1989, Cosmic ray production rates of 10Be and 26Al in quartz from glacially polished rocks: Journal of Geophysical Research, v. 94, p. 17,907-17,915.

Oerlemans, J., 2005, Extracting a climate signal from 169 glacier records: Science, v. 308, p. 675-677.

Oldroyd, D., 1996, Thinking about the earth: a history of ideas in geology: Harvard University Press, 410 p.

O'Neal, M. A., 2006, The effects of slope degradation on lichenometric dating of Little Ice Age moraines: Quaternary Geochronology, v. 1, p. 121-128.

Owen, L. A., Finkel, R. C., Minnich, R. A., and Perez, A. E., 2003, Extreme southwestern margin of late Quaternary glaciation in North America: timing and controls: Geology, v. 31, p. 729-732.

Paillard, D., 1998, The timing of Pleistocene glaciations from a simple multiple-state climate model: Nature, v. 391, p. 378-381.

Pelletier, J. D., DeLong, S. B., al-Suwaidi, A. H., and four others, 2006, Evolution of the Bonneville shoreline scarp in west-central Utah: comparison of scarp-analysis methods and implications for the diffusion model of hillslope evolution: Geomorphology, v. 74, p. 257-270.

Pelletier, J. D., 2008, Quantitative modeling of earth surface processes: Cambridge University Press, 304 p.

Petterson, G., 1996, Varved sediments in Sweden: a brief review: in Kemp, A. E. S. (ed.), Paleoclimatology from laminated sediments: Geological Society Special Publication 116, p. 73-77.

Phillips, F. M., Zreda, M. G., Smith, S. S., and three others, 1990, Cosmogenic chlorine-36 chronology for glacial deposits at Bloody Canyon, eastern Sierra Nevada: Science, v. 248, p. 1529-1532.

Pierrehumbert, R.T., 1999, Huascaran d18O as an indicator of tropical climate during the Last Glacial Maximum: Geophysical Research Letters, v. 26, p. 1345–1348.

Paterson, W.S.B., 1994, The physics of glaciers (3rd ed.): Pergamon, Oxford, 496 p.

Plummer, M. A., and Phillips, F. M., 2003, A 2-D numerical model of snow/ice energy balance and ice flow for paleoclimatic interpretation of glacial geomorphic features: Quaternary Science Reviews, v. 22, p. 1389-1406.

Pollard, D., 1982, A simple ice sheet model yields realistic 100 kyr glacial cycles: Nature, v. 296, p. 334-338.

Porter, Stephen C., 2004, Glaciation of the Hawaiian islands: in Ehlers, J., and Gibbard, P. L., Quaternary glaciations – extent and chronology: part II: North America: Elsevier, p. 69-70.

Press, W. H., Teukolsky, S. A., Vetterling, W. T., and Flannery, B. P., 1992, Numerical recipes in Fortran 77 (2nd ed.): Cambridge, 927 p.

Price, K. V., Storn, R. M., and Lampinen, J. A., 2005, Differential evolution: a practical approach to global optimization: Springer, 538 p.

Putkonen, J., and Swanson, T., 2003, Accuracy of cosmogenic ages for moraines: Quaternary Research, v. 59, p. 255-261.

Putkonen, J., Connolly, J., and Orloff, T., 2007, Landscape evolution degrades the geologic signature of past glaciations: Geomorphology, v. 97, p. 208-217.

Raymo, M. E., and Nisancioglu, K., 2003, The 41 kyr world: Milankovitch's other unsolved mystery: Paleoceanography, v. 18, 1011.

Richmond, G. M., 1973, Geologic map of the Fremont Lake South quadrangle, Sublette County, Wyoming, 1:50,000: U. S. Geological Survey Geologic Quadrangle Map GQ-1138.

Roering, J. J., Kirchner, J. W., Sklar, L. S., and Dietrich, W. E., 2001, Hillslope evolution by nonlinear creep and landsliding: an experimental study: Geology, v. 29, p. 143-146.

Rupper, S., and Roe, G., 2008, Glacier changes and regional climate: a mass and energy balance approach: Journal of Climate, v. 21, p. 5384-5401.

Schaefer, J. M., Denton, G. H., Barrell, D. J. A., and six others, 2006, Near-synchronous interhemispheric termination of the Last Glacial Maximum in mid-latitudes: Science, v. 312, p. 1510-1513.

Schaefer, J. M., Oberholzer, P., Zhao, Z, and five others, 2008, Cosmogenic beryllium-10 and neon-21 dating of late Pleistocene glaciations in Nyalam, monsoonal Himalayas: Quaternary Science Reviews, v. 27, p. 295-311.

Seong, Y. B., Owen, L. A., Caffee, M. W., and five others, 2009, Rates of basin-wide rockwall retreat in the K2 region of the central Karakoram defined by terrestrial cosmogenic nuclide 10Be: Geomorphology, v. 107, p. 254-262.

Shackleton, N. J., 2000, The 100,000-year ice-age cycle identified and found to lag temperature, carbon dioxide, and orbital eccentricity: Science, v. 289, p. 1899-1902.

Severinghaus, J. P., Sowers, T., Brook, E. J., Alley, R. B., and Bender, M. L., 1998, Timing of abrupt climate change at the end of the Younger Dryas interval from therally fractionated gases in polar ice: Nature, v. 391, p. 141-146.

Sharp, W. D., Ludwig, K. R., Chadwick, O. A., Amundson, R., and Glaser, L. L., 2003, Dating fluvial terraces by 230Th/U on pedogenic carbonate, Wind River Basin, Wyoming: Quaternary Research, v. 59, p. 139-150.

Taylor, R. E., 2000, Fifty years of radiocarbon dating: American Scientist, v. 88, p. 60-67.

Turney, C. S. M., Roberts, R. G., de Jonge, N., and four others, 2007, Redating the advance of the New Zealand Franz Josef glacier during the last termination: evidence for asynchronous climate change: Quaternary Science Reviews, v. 26, p. 3037-3042.

Vacco, D. A., Alley, R. B., and Pollard, D., 2009, Modeling dependence of moraine deposition on climate history: the effect of seasonality: Quaternary Science Reviews, v. 28, p. 639-646.

Vellinga, M., and Wood, R. A., 2002, Global climatic impacts of a collapse of the Atlantic thermohaline circulation: Climatic Change, v. 54, p. 251-267.

Walker, M., Johnsen, S., Rasmussen, S. O., and 16 others, 2009, Formal definition and dating of the GSSP (Global Stratotype Section and Point) for the base of the Holocene using the Greenland NGRIP ice core, and selected auxiliary records: Journal of Quaternary Science, v. 24, p. 3-17.

Weertman, J., 1976, Milankovitch solar radiation variations and ice age ice sheet sizes: Nature, v. 261, p. 17-20.

Wolkowinsky, A. J., and Granger, D. E., 2004, Early Pleistocene incision of the San Juan River, Utah, dated with 26Al and 10Be: Geology, v. 32, p. 749-752.

Wratt, D. S., Revell, M. J., Sinclair, M. R., and three others, 2000, Relationships between air mass properties and mesoscale rainfall in New Zealand's Southern Alps: Atmospheric Research, v. 52, p. 261-281.

Zielinski, G. A., and Davis, P. T., 1987, Late Pleistocene age of the type Temple Lake moraine, Wind River Range, Wyoming, U. S. A.: Géographie physique et Quaternaire, v. 41, p. 397-401.

Zimmerman, S. G., Evenson, E. B., Gosse, J. C., and Erskine, C. P., 1995, Extensive boulder erosion resulting from a range fire on the type-Pinedale moraines, Fremont Lake, Wyoming: Quaternary Research, v. 42, p. 255-264.

Zreda, M. G., Phillips, F. M., and Elmore, D., 1994, Cosmogenic 36Cl accumulation in unstable landforms 2. Simulations and measurements on eroding moraines: Water Resources Research, v. 30, p. 3127-3136.

Appendix A

Comment on "Absence of cooling in New Zealand and the adjacent ocean during the Younger Dryas Chronozone"

Barrows et al. (2007) presented evidence, from cosmogenic exposure dating and an ocean sediment core, that "overturn[s]... glacier advance in New Zealand during the [Younger Dryas] chronozone." Here, we argue that their cosmogenic exposure dates are inconclusive, based on modeling of geomorphic processes that influence exposure dates.

[This appendix was originally published as a peer-reviewed, technical comment in *Science* (Applegate et al., 2008; see Barrows et al., 2008, for their response). Thomas V. Lowell (University of Cincinnati) and Richard B. Alley were listed as second and third authors, respectively, on this technical comment. Dr. Lowell pointed out the Barrows et al. (2007) paper to me, and edited several drafts of the technical comment. Dr. Alley also commented on the text of the comment before submission. However, the model code, model simulations, and most of the text are my work. Permission to reprint this technical comment was granted under AAAS license number 2273780278520 on 21 September 2009. This appendix differs slightly from the published version.]

Barrows et al. (2007) argued that the Waiho Loop moraine in New Zealand was deposited after the end of the Younger Dryas (~11,600 yr BP). They presented 24 new cosmogenic exposure dates, ranging from ~5,000 yr BP to ~12,800 yr BP, from ten boulders on the moraine.

Barrows et al. estimated the age of the moraine by taking the error-weighted mean of the ages of their nine oldest boulders. This procedure yielded an age of 10,480 +/- 240 yr BP (1σ). The age of the Waiho Loop moraine had previously been estimated to be ~12,800 yr BP by radiocarbon dating (Denton and Hendy, 1994; cf. Turney et al., 2007). Because their new age

estimate for the Waiho Loop moraine is much younger than this previous estimate, Barrows et al. concluded that "the Waiho Loop advance... was not a Younger Dryas event..."

Barrows et al. determined each boulder age by taking the weighted mean of the exposure dates from that boulder (Bevington and Robinson, 2003, their eqn. 4.17), weighting the exposure dates by the inverse squares of their measurement errors. They then estimated the age of the moraine using the weighted mean of the boulder ages from their nine oldest boulders, this time weighting each boulder age by the inverse square of the standard deviation of the cosmogenic exposure dates from that boulder. They determined the uncertainty of their moraine age estimate from these standard deviations (Bevington and Robinson, 2003, their eqn. 4.19). This uncertainty (240 yr) is quite small compared to the range of their dates (~7,800 yr).

We applaud Barrows et al. (2007) for their investigation of the age of this moraine. As they note, the age of the Waiho Loop moraine is a critical test of various hypotheses explaining the climatic changes at the end of the last glaciation. Their use of multiple cosmogenic nuclides and multiple samples from each boulder enables assessment of their analytical work.

However, the age assignment for the Waiho Loop moraine given by Barrows et al. (2007) is potentially biased. Barrows et al. noted that the scatter in their exposure dates is greater than can be explained by measurement error alone. This additional scatter is common in sets of exposure dates from moraines (Putkonen and Swanson, 2003; Balco and Schaefer, 2006); it is usually attributed to geomorphic processes (Putkonen and Swanson, 2003; Balco and Schaefer, 2006; Ivy-Ochs et al., 2007). To address this scatter, many authors remove a subset of the data and then take an average, as Barrows et al. did. However, application of the error-weighted mean assumes that the differences between the exposure dates and the true age of the moraine are normally distributed (Bevington and Robinson, 2003) and have a mean of zero. The known geomorphic processes that affect cosmogenic exposure dates change the mean of these differences, as well as their standard deviation (Ivy-Ochs et al., 2007). Consequently, the error-

weighted mean may return a misleading estimate of the moraine's age if the dates have been affected by geomorphic processes.

Barrows et al. (2007) acknowledged the effects that "former shielding... or earlier exposure" may have had on their dates; here, we consider these effects more explicitly.

If the boulders sampled by Barrows et al. (2007) were shielded from cosmic rays by a till cover, their exposure dates would tend to underestimate the moraine's age. Barrows et al. noted that one of their boulders had "...smaller blocks resting on top of it, perhaps indicating a former till cover." Moreover, the Waiho Loop receives over 2 m of precipitation yearly (Wratt et al., 2009). These observations suggest that till has been removed from the crest of the moraine, exposing fresh boulders to cosmic rays.

We present output from a simple numerical model that shows the impact of till shielding on the distribution of cosmogenic exposure dates. We updated the moraine degradation model of Putkonen and Swanson (2003) and Hallet and Putkonen (1994) to predict the distributions of beryllium-10 exposure dates on moraines, including production at depth by muons (Granger and Muzikar, 2001). This model predicts that the distribution of beryllium-10 exposure dates from a degrading moraine should have a peak close to the true age of the moraine, and a long, heavy tail toward the young side of the distribution (Fig. A.1). This result is robust over a range of initial moraine heights, initial moraine slopes, and topographic diffusivities. For this exercise, we consider only the beryllium-10 dates, because the relationship between chlorine-36 dates and the true age of an eroding surface is complex (Zreda et al., 1994). Although further modeling work may change the shape of this distribution somewhat, the conclusions we draw from this exercise are sound.

For an assumed moraine age of 11,600 yr BP, at the end of the Younger Dryas, the model produces a distribution that resembles the beryllium-10 exposure dates reported by Barrows et al. (Fig. A.1). If their beryllium-10 exposure dates are drawn from a parent distribution like that

produced by the model, their error-weighted mean underestimates the age of the moraine. Instead, we suggest that the age of the moraine lies somewhere close to their oldest beryllium-10 dates, possibly at the end of the Younger Dryas chronozone. Our preferred age assignment is thus ~1,100 years older than that favored by Barrows et al.

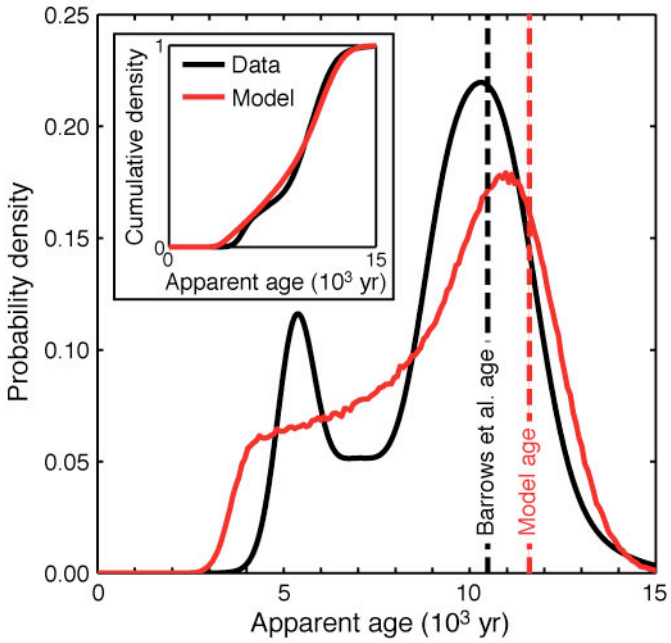

Figure A.1: Comparison of eight beryllium-10 exposure dates from the Waiho Loop moraine (black curves; Barows et al., 2007) to the distribution of 10^6 exposure dates predicted by the updated degradation model (red curves; Hallet and Putkonen, 1994; Putkonen and Swanson, 2003). The best fit between the model and the data occurs at a model age of 11,600 yr BP (dashed, red line), corresponding to the end of the Younger Dryas. Our preferred age assignment is thus ~1,100 years older than that given by Barrows et al. (2007; black, dashed line). This best fit was found by adjusting the modeled age of the moraine until both the sum of squared errors and the maximum vertical distance between the cumulative density curves (inset) were minimized. The probability density curve for the observed exposure dates was constructed by summing the Gaussian curves of the individual dates, and normalizing the total curve to 1. We assumed that the moraine's initial height and slope were 50 m and 34°, respectively; topographic diffusivities are from Putkonen and Swanson (2007). Although these diffusivities are probably too small for the wet West Coast of New Zealand (Wratt et al., 2000), multiplying the diffusivities by 10 does not change the fundamental resemblance of the model results to the beryllium-10 dates. [Compare this figure to Figure 4.3.]

We have also considered the possibility that the dates observed by Barrows et al. (2007) are biased by earlier exposure, rather than till shielding. Glaciers sometimes incorporate boulders

with preexisting concentrations of cosmogenic nuclides in their moraines (Ivy-Ochs et al, 2007). Dates from these preexposed boulders tend to overestimate the ages of the moraines they rest upon. Modeling of this process produces distributions with a peak near the true age of the moraine and a long, heavy tail toward the old side of the distribution. These distributions do not resemble the distribution of dates reported by Barrows et al. (2007). We conclude that earlier exposure is not primarily responsible for the spread in their dates, although their measured concentrations may include a small inherited component.

We do not intend to reinterpret the cosmogenic exposure dates presented by Barrows et al. (2007) as requiring a Younger Dryas age for the Waiho Loop moraine. Other geologic processes not treated by our modeling may have influenced the observed exposure dates, and further calibrations of nuclide production rates may require reassessment of these data. Instead, we use this example to argue that geomorphic processes must be carefully considered before making age assignments for moraines from cosmogenic exposure dates. In particular, discarding some observations and taking an average of the rest can lead to biased age estimates.

Acknowledgements

We thank M. Kelly (Lamont-Doherty Earth Observatory), G. Denton (U. of Maine), Aaron Putnam (U. of Maine), K. Keller (Pennsylvania State U.), and two anonymous reviewers for their comments on drafts of this paper. We also thank N. Urban (Pennsylvania State U.) for critical help with the statistical methods. Partial support for this research was provided by the US National Science Foundation under grant 0424589, and by the Gary Comer Science and Education Foundation.

Appendix B

Production of cosmogenic nuclides in spherical boulders

The production rates of cosmogenic nuclides vary as a function of position within solid bodies. In laterally extensive, planar surfaces, production rates decline exponentially with depth (Chapter 2; Lal, 1991; Dunne et al., 1999; Granger and Muzikar, 2001), where depth is measured normal to the surface. For solid bodies of other geometries, the production rate at a given point within the body must be determined from the total flux of cosmic rays that reaches the point of interest from the unobstructed part of the sky. In general, production rates are greatest at the apices of solid bodies (Masarik and Wieler, 2003).

This fact provides a potential means for identifying boulders that contain inherited nuclides (Schaefer et al., 2008), or have rotated. Exposure dating assumes that boulders are delivered to moraines with no inventories of cosmogenic nuclides, and that they remain in the same orientation during their post-depositional history. If these conditions are fulfilled for any individual boulder, then nuclide concentrations in the sides and bottom of the boulder will be less than the concentrations in the boulder's top. If nuclide concentrations in the sides or bottom of a boulder are greater than or equal to the concentrations in the boulder's top, then the exposure date from that boulder is suspect.

This point is well understood in the exposure dating community (Benson et al., 2005), but studies that take advantage of this potential method are rare (e.g., Schaefer et al., 2008). This rarity stems in part from the added time and expense required to measure nuclide concentrations in shielded portions of a boulder.

In addition, a theoretical basis is lacking in the literature for calculating the expected concentrations at different points within boulders. Masarik and Wieler (2003) and Lal and Chen

(2005) provide some guidance, but the results of these studies are difficult to transfer to situations not treated by their analyses. Masarik and Wieler (2003) use Monte Carlo-based particle transport codes that require a supercomputer. Lal and Chen (2005, their eqns. 3 and 4) provide a solution for the final concentration of a cosmogenic nuclide at any point within a body after a given exposure time, but this solution depends on knowledge of the path length of cosmic rays through the body for various azimuth and inclination angles. They give expressions for the path length for points lying on the axes of spheres and rectangular prisms, but more general solutions are needed.

Here, I generalize Equations 5 and 6 of Lal and Chen (2005) to allow determination of cosmic ray fluxes through any point within a sphere. This solution is potentially useful because 1) it provides a template for nuclide production rate estimates in bodies with more complex shapes, and 2) it provides an analytical solution against which more complex models of nuclide production in solid bodies can be tested.

The solution presented here only gives the path length d as a function of the sphere's radius R, the point's position within the sphere θ, ϕ, r, and the cosmic ray's orientation θ_{ray}, ϕ_{ray}. Determination of nuclide production rates at the chosen point also requires knowledge of the angular dependence of the cosmic ray flux over the unobstructed sky, the attenuation length of cosmic rays in matter, and the distribution of nuclide production over the earth's surface (Lal and Chen, 2005). These topics are beyond the scope of this appendix; see Nishiizumi et al. (1989), Dunne (1999), Gosse and Phillips (2001) and Balco et al. (2008) for more information.

Here, we take θ and θ_{ray} to be the azimuth as measured from the y-axis, and ϕ and ϕ_{ray} to be the inclination measured from the vertical. This convention is similar to that used by Beyer (1978); it is not the same as that used by Lal and Chen (2005), but their conventions appear to differ within their paper (cf. their Fig. 1 with their Appendix A).

The variables that describe the position of the point of interest and the orientation of the cosmic ray are shown schematically in Figure B.1.

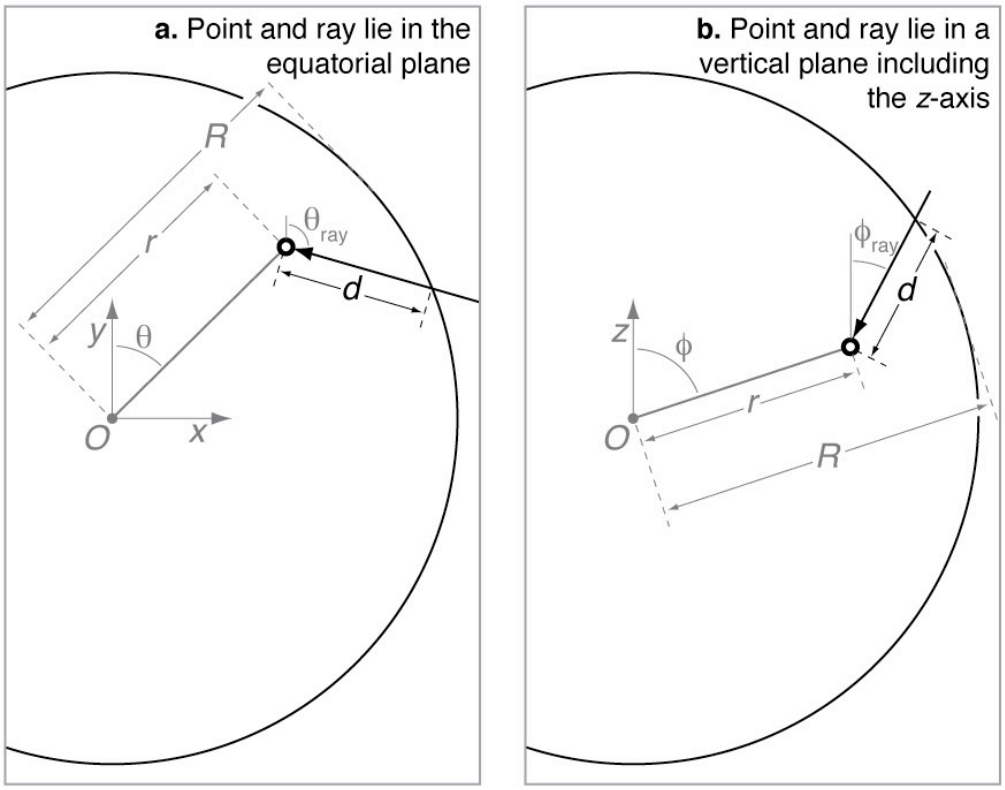

Figure B.1: Illustration of variables used in this appendix for two simplified cases. In both cases, the origin *O* is at the center of the spherical boulder; the *z*-axis is vertical, and the *x*- and *y*-axes are orthogonal to the *z*-axis and to each other. θ_{ray} is measured clockwise from a line drawn parallel to the *y*-axis, and ϕ_{ray} is measured clockwise from the vertical. The point of interest is shown by open circles; the cosmic ray path is represented by heavy, black arrows. The desired quantity is *d*, the distance between the point where the cosmic ray enters the sphere and the point of interest.

For a sphere with the center at the origin and a radius *R*,

$$x^2 + y^2 + z^2 = R^2 \qquad \text{(eqn. B.1)}$$

Our choice of a point θ, ϕ, r within the spherical boulder is limited by

$$0 \le \theta \le 360$$
$$0 \le \phi \le 180$$
$$0 \le r \le R$$

Likewise, the orientation of any single cosmic ray θ_{ray}, ϕ_{ray} passing through the point must satisfy

$$0 \le \theta_{ray} \le 360$$
$$0 \le \phi_{ray} \le 90$$

Given this point of interest and this cosmic ray orientation, our goal is to find the length d of the line segment that connects the point to the surface of the sphere along the path of the cosmic ray.

Converting the point of interest into Cartesian coordinates x_0, y_0, z_0, we have

$$x_0 = r \sin\theta \sin\phi$$
$$y_0 = r \cos\theta \sin\phi$$
$$z_0 = r \cos\phi$$

and, converting the line segment to Cartesian coordinates,

$$x = x_0 + ad$$
$$y = y_0 + bd \qquad \text{(eqns. B.2a-c)}$$
$$z = z_0 + cd$$

where

$$a = \sin\theta_{ray} \sin\phi_{ray}$$
$$b = \cos\theta_{ray} \sin\phi_{ray}$$
$$c = \cos\phi_{ray}$$

Thus, we have four equations and four unknowns (B1, B2a-c; x, y, z, d). We know the location of the point of interest in Cartesian coordinates x_0, y_0, z_0, because we can calculate those values from the specified spherical coordinates of the point θ, ϕ, r. We also know the values of the unit vector parallel to the cosmic ray a, b, c, because those values are uniquely determined from the orientation of the cosmic ray θ_{ray}, ϕ_{ray}. The unknowns are just the location x, y, z of a point common to the surface of the sphere and the line segment, and the length of the line segment d.

Substituting B.2 into B.1, we have

$$(x_0 + ad)^2 + (y_0 + bd)^2 + (z_0 + cd)^2 = R^2$$

Solving for *d*,

$$x_0^2 + 2adx_0 + a^2d^2 + y_0^2 + 2bdy_0 + b^2d^2 + z_0^2 + 2cdz_0 + c^2d^2 = R^2$$

$$(x_0^2 + y_0^2 + z_0^2 - R^2) + 2d(ax_0 + by_0 + cz_0) + d^2(a^2 + b^2 + c^2) = 0$$

$$d^2(a^2 + b^2 + c^2) + 2d(ax_0 + by_0 + cz_0) + (x_0^2 + y_0^2 + z_0^2 - R^2) = 0$$

This expression has the form of the quadratic equation,

$$Ad^2 + Bd + C = 0$$

which is solved

$$d = \frac{-B \pm \sqrt{B^2 - 4AC}}{2A}$$

$$A = (a^2 + b^2 + c^2)$$
$$B = 2(ax_0 + by_0 + cz_0)$$
$$C = (x_0^2 + y_0^2 + z_0^2 - R^2)$$

Although this derivation could be carried forward to yield a full solution for the path length *d*, in practice this equation will be solved by a computer program as part of a numerical integration. Because longer equations are more difficult to code and debug, we leave the expression for *d* in this shorter form.

As usual, the quadratic equation will generally have more than one root. For a point actually within the spherical boulder ($r < R$), there will always be two roots, one positive, and one negative. The positive root is the one to use as the path length. Points on the surface of the sphere ($r = R$) will have either one or two roots, depending on the orientation of the cosmic ray.

The determination of nuclide production rates at a single point is then found by integrating production over all cosmic ray orientations, following Lal and Chen (2005). The contribution of each cosmic ray orientation to the integrated production rate is weighted by the

angular separation between adjacent cosmic ray orientations (that is, the coarseness of the angle step in the numerical integration), and the distribution of cosmic ray fluxes over the open sky.

A simplified example application of this work is shown in Figure B.2.

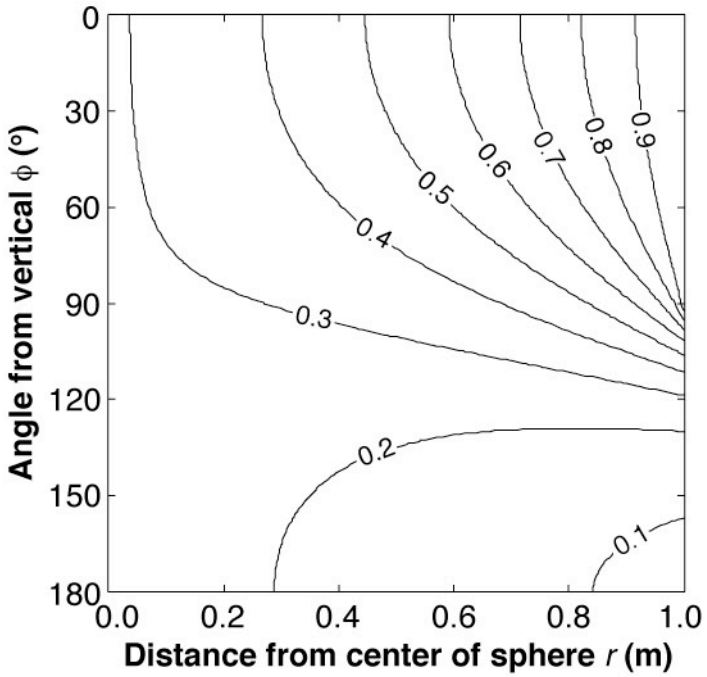

Figure B.2: Distribution of cosmogenic nuclide production within a spherical boulder with a radius of 1 m, assuming that the cosmic ray flux is exclusively vertical. Contours show nuclide production rates in atoms per gram of rock per year. Because a sphere has rotational symmetry about the vertical axis, the distribution of production is independent of the azimuth θ. This figure assumes that the production rate on an unobstructed surface is 1 atom/ g/ yr at this site, and that the attenuation length of nuclide production along a single ray path is 80 cm, consistent with a rock density of 2.6 g/ cm^3 (Dunne, 1999; Gosse and Phillips, 2001; eqn. 2.3). Compare this figure with Figure 2 of Masarik and Wieler (2003).

Appendix C

Model code for Chapter 2, with documentation

The codes given in this appendix (Table C.1) are numerical models that describe the influence of moraine degradation and inheritance on the statistical distributions of cosmogenic exposure dates from glacial landforms, especially moraines. These two processes are treated in separate models, so the degradation model and the inheritance model reside in distinct files.

These codes were written in MATLAB version R2008a, and were run on an Intel-based Macintosh MacBook.

These codes were written carefully, and they have been checked for obvious errors. However, no warranty of any kind is implied. The output from these codes should not be trusted without testing.

Please give proper credit if using these codes in research and teaching. Derivative works based on this code should include a reference to this dissertation.

Table C.1: List of files given in Appendix C.

File name	Description
degradation_model.m	Main file for degradation model; calls the function m_diffusion.m
m_diffusion.m	Contains the part of the code that describes how moraine profiles change over time; based on a derivation prepared by Dr. Nathan Urban
inheritance_model.m	Main file for inheritance model

The moraine degradation model

Input variables

The user-adjustable input parameters (Table C.2) are contained in the same file as the model code, degradation_model.m. The values of these parameters are defined in lines 31-87.

Table C.2: Input parameters for the degradation model.

Name	Line	Default value	Symbol in Chapter 2	Description
moraine_age	32	20 ka		Age of moraine (ka)
initial_height	33	50 m	h_0	Initial height of moraine (m)
initial_slope	34	34°	$\tan^{-1}(S_0)$	Initial slope of moraine flanks; note that the variable initial_slope is the slope angle, whereas S_0 in the text is the slope (rise over run). Few measurements of this parameter exist in the literature; see Hallet and Putkonen (1994), Putkonen and Swanson (2003), and Putkonen and O'Neal (2006).
k	39	10^{-2} m^2/yr (range: 10^{-4} to 10^{-1})	k	Topographic diffusivity (m^2/yr). See Hallet and Putkonen (1994), Hanks (2000), Putkonen and Swanson (2003), and Putkonen et al. (2007).
erosion_rate	42	0 mm/ka		Erosion rate of boulders when exposed at the moraine's surface (mm/ka)
boulder_height	43	1 m	h_b	Minimum sampled boulder height (m). The minimum boulder height that a field geomorphologist would sample.
rho_rock	44	2.6 g/cm^3		Density of the boulders (g/cm^3); controls the *e*-folding length of cosmic rays into the boulders.
rho_till	45	2.0 g/cm^3		Density of the unconsolidated sediment surrounding the boulders; controls the *e*-folding length of cosmic rays into the till.

Table C.2 (continued): Input parameters for the degradation model.

Name	Line	Default value	Symbol in Chapter 2	Description
P_spall	48	4.97 atoms ^{10}Be/g/yr	$P_{i=1}$	Production rate of cosmogenic nuclide by spallation at the earth's surface at the latitude and elevation of the study site. Get this from Balco et al. (2008), using the St scaling model.
P_mu	53	0.133 atoms ^{10}Be/g/yr	$\Sigma(P_{i=2, 3, 4})$	Production rate of cosmogenic nuclide by muons at the earth's surface at the latitude and elevation of the study site. Get this from Balco et al. (2008).
decay_const	56	4.67* 10^{-7} yr^{-1} (?) for ^{10}Be	λ	Decay constant of the cosmogenic nuclide. For ^{10}Be, this value is in dispute (Balco et al., 2008, and refs therein), but this parameter has little effect on ^{10}Be exposure dating over the time scales of interest (10^2-10^5 yr).
P_slhl	59	[5, 0.09, 0.02, 0.02] atoms ^{10}Be/g/yr	$P_{i=1, 2, 3, 4}$	Surface production rates of nuclide at sea level and high latitude for various production pathways; see Granger and Muzikar (2001).
att_length	64	[160, 738, 2688, 4360] g/cm^2	material density* $\Lambda_{i=1, 2, 3, 4}$	Attenuation lengths of components of the cosmic ray flux; see Granger and Muzikar (2001). In the text, $\Lambda_{i=1, 2, 3, 4}$ are these values, divided by the density (in g/cm^3) of the material the cosmic rays are passing through.
num_boulders	71	10^5 boulders		Number of boulders to simulate; more boulders produce a more robust distribution of exposure dates, but also cause the model to run more slowly.
time_step	75	25-100 yr		Controls fineness of model discretization in time; smaller values produce more accurate results, but also cause the model to run more slowly.
plots	82	0 or 1		If 0, the code produces no plots; if 1, the plots described below are generated.
bin_width	87	1-5 ka		If plots = 1, this variable controls the widths of the bins into which the calculated exposure dates are sorted to create the histogram (see below).

Output variables

The degradation model places its output into the following variables (Table C.3).

Table C.3: Output variables for the degradation model.

Name	Line	Symbol in Chapter 2	Description
initial_profile	109	$z(x, t = 0)$	Initial height of the moraine above its base as a function of distance from the crest (m).
final_profile	109	$z(x, t)$	Final height of the moraine above its base as a function of distance from the crest (m).
crest_height	109	$z(x = 0, t)$	Height of the moraine's crest above its base as a function of time.
distances	109	x	A plotting variable that contains evenly spaced values of distance from the moraine crest (m).
times	109	t	A plotting variable that contains evenly spaced values of time from the beginning of the simulation (yr or ka).
initial_depth	116	d_0	Initial burial depth of each boulder in the moraine (m).
naive_age	171	t_{app}	Apparent exposure time yielded by each boulder (yr or ka).

If the variable plots is set to 1, the degradation model also produces plots of these variables. The plots show the initial and final profile of the moraine (initial_profile and final_profile vs. distances), the height of the moraine crest as a function of time (crest_height vs. times), and a histogram of the exposure dates simulated by the model (naive_age).

The inheritance model

Input variables

Many of the inheritance model's parameters are the same as those used in the degradation model (Table C.4).

Table C.4: Input parameters for the inheritance model.

Name	Line	Default value	Symbol in Chapter 2	Description
moraine_age	27	20 ka		Age of moraine (ka).
max_pre_time	28	100 ka	$\max(t_{pre})$	Maximum predepositional exposure time for the boulders (ka).
max_pre_depth	30	2.0 m	$\max(d_{pre})$	Maximum predepositional burial depth for the boulders (m).
pre_slope	32	0°		Slope of surface from which preexposed boulders were derived (°).
erosion_rate		0 mm/ka		Erosion rate of boulders after being deposited on the moraine (mm/ka)
rho_rock	36	2.6 g/cm^3		Density of the boulders (g/cm^3); controls the *e*-folding length of cosmic rays into the boulders.
rho_over	37	2.6 g/cm^3		Density of material overlying the boulders during the predepositional exposure period (g/cm^3); controls the *e*-folding length of cosmic rays into the boulders during that time.
P_spall	42	4.97 atoms ^{10}Be/g/yr	$P_{i=1}$	Production rate of cosmogenic nuclide by spallation at the earth's surface at the latitude and elevation of the study site. Get this from Balco et al. (2008), using the St scaling model.
P_mu	47	0.133 atoms ^{10}Be/g/yr	$\Sigma(P_{i=2, 3, 4})$	Production rate of cosmogenic nuclide by muons at the earth's surface at the latitude and elevation of the study site. Get this from Balco et al. (2008).
decay_const	50	4.67* 10^{-7} yr^{-1} (?) for ^{10}Be	λ	Decay constant of the cosmogenic nuclide. For ^{10}Be, this value is in dispute (Balco et al., 2008, and refs therein), but this parameter has little effect on 10Be exposure dating over the time scales of interest (10^2-10^5 yr).
P_slhl	53	[5, 0.09, 0.02, 0.02] atoms ^{10}Be/g/yr	$P_{i=1, 2, 3, 4}$	Surface production rates of nuclide at sea level and high latitude for various production pathways; see Granger and Muzikar (2001).

Table C.4 (continued): Input parameters for the inheritance model.

Name	Line	Default value	Symbol in Chapter 2	Description
att_length	58	[160, 738, 2688, 4360] g/cm^2	material density* $\Lambda_{i=1, 2, 3, 4}$	Attenuation lengths of components of the cosmic ray flux; see Granger and Muzikar (2001). In the text, $\Lambda_{i=1, 2, 3, 4}$ are these values, divided by the density (in g/cm^3) of the material the cosmic rays are passing through.
num_boulders	65	10^5 boulders		Number of boulders to simulate; more boulders produce a more robust distribution of exposure dates, but also cause the model to run more slowly.
plots	71	0 or 1		If 0, the code produces no plots; if 1, the plots described below are generated.
bin_width	76	2-10 ka		If plots = 1, this variable controls the widths of the bins into which the calculated exposure dates are sorted to create the histogram (see below).

Output variables

The inheritance model places its output into these variables (Table C.5).

Table C.5: Output parameters for the inheritance model.

Name	Line	Symbol in Chapter 2	Description
pre_time	99	t_{pre}	Predepositional exposure time of each boulder (yr).
pre_depth	100	d_{pre}	Predepositional burial depth of each boulder (m).
naive_age	118	t_{app}	Apparent exposure time yielded by each boulder (yr or ka).

If the variable plots is set to 1, the model produces a histogram of the apparent exposure times.

Model codes

The files listed in Table C.1 follow.

```
% degradation_model.m
%
% Evaluates probability distributions of cosmogenic exposure dates on a
% degrading moraine.  Based on a conceptual model first described by
% Hallet and Putkonen (1994) and Putkonen and Swanson (2003), but the
% code presented here is entirely original.  Uses an analytical solution
% for moraine degradation developed by Dr. Nathan Urban, Penn State.  Code
% written by Patrick Applegate, Penn State (papplegate@psu.edu).
%
% Code written to run under MATLAB R2008a on an Intel-based Macintosh
% MacBook.
%
% Calls the function m_diffusion.m, which is provided in a separate file.
%
% This code was written carefully and has been checked for obvious errors.
% However, no warranty of any kind is implied.  The code may not even run
% on your system.  The output from the code should not be trusted without
% testing.
%
% Please give proper credit if using this code in research and teaching.
% Derivative works based on this code should include a reference to the
% original paper.

% Clear all variables, commands, and figures.  Set figures to dock
% automatically.
clear all
close all
clc
set(0,'DefaultFigureWindowStyle','docked')

% Define parameters that will be tuned during model inversion.
moraine_age = 20.0;         % ka (10^ 3 yr); true age of moraine
initial_height = 50.0;      % m; initial height of moraine
initial_slope = 34;         % degrees; initial moraine slope angle (Hallet
                            % and Putkonen (1994) assume 31 degrees;
                            % Putkonen and Swanson (2003) use 34 degrees;
                            % 25 degrees may be more reasonable, given
                            % Putkonen and O'Neal (2006))
k = 10^ -2;                 % sq. m/ yr; topographic diffusion coefficient

% Define other geomorphic parameters that are not part of the inversion.
erosion_rate = 0.0;         % mm/ ka; erosion rate of exposed boulders
boulder_height = 1.0;       % m; observed height of boulders when sampled
rho_rock = 2.6;             % g/ cm^ 3; density of boulders
rho_till = 2.0;             % g/ cm^ 3; density of till matrix

% Define nuclide production parameters.
P_spall = 4.97;             % atoms/ g/ yr; surface production rate due to
                            % spallation (get this from the CRONUS online
                            % calculator described in Balco et al., 2008;
                            % assumed to be constant over the lifetime of
                            % the moraine)
```

```
P_mu = 0.133;               % atoms/ g/ yr; surface production rate due to
                            % muons (also get this from the CRONUS
                            % calculator)
decay_const = 4.62* 10^ -7; % yr^ -1; nuclear decay constant of nuclide of
                            % interest (4.62* 10^ -7 for 10Be, following
                            % Balco et al., 2008, and refs therein)
P_slhl = [5 0.09 ...        % atoms/ g/ yr; sea level, high-latitude
    0.02 0.02];             % production rates of different cosmic ray
                            % flux components, following Granger and
                            % Muzikar (2001); for 10Be, about
                            % [5 0.09 0.02 0.02]
att_length = [160 738 ...   % g/ sq. cm; effective attenuation lengths of
    2688 4360];             % exponential components of Granger and Muzikar
                            % (2001) production-as-a-function-of-depth
                            % parameterization; for 10Be and 26Al, about
                            % [160 738 2688 4360]

% Define model parameters.
num_boulders = 1* 10^ 3;    % number of randomly generated synthetic
                            % boulders (at least 10^ 4; bigger numbers
                            % yield more consistent results, but the model
                            % will take more time to run)
time_step = 25;             % yr; time step during post-depositional
                            % period (25 yr works well; small values
                            % increase the accuracy of the calculation,
                            % but also cause the code to run more
                            % slowly)

% Turn plotting on and off.
plots = 1;                  % If 1, plots the moraine profile, height of
                            % the moraine's crest as a function of time,
                            % and a histogram of the modeled exposure
                            % dates.  If 0, none of these plots are
                            % produced.
bin_width = 1;              % ka; width of bins in naive age histogram

% Convert all quantities to consistent units.  All lengths should be in
% meters, slopes should be dimensionless, times should be in years, and
% masses should be in grams.
moraine_age = moraine_age* 10^ 3;               % yr
initial_slope = tand(initial_slope);            % d'less
erosion_rate = erosion_rate* 10^ -6;            % m/ yr
rho_till = rho_till* 100^ 3;                    % g/ cu. m
rho_rock = rho_rock* 100^ 3;                    % g/ cu. m
att_length = att_length* 100^ 2;                % g/ sq. m

% Scale production rates to site.
P_surf(1) = P_spall; % atoms/ g/ yr
P_surf(2: 4) = P_slhl(2: 4)* P_mu/ sum(P_slhl(2: 4));

% Determine length scales for nuclide production.
L_till = att_length/ rho_till; % m
```

```
L_rock = att_length/ rho_rock; % m

% Determine height of moraine crest as a function of time and initial
% and final moraine profiles.
[times, crest_height, distances, initial_profile, ...
    final_profile] = m_diffusion(initial_height, initial_slope, k, ...
    moraine_age, time_step);

% Establish the initial depth for each boulder.
final_height = min(crest_height); % m
max_depth = initial_height- final_height- boulder_height; % m
initial_depth = max_depth* rand(1, num_boulders); % m
% initial_depth = 0: max_depth/ (num_boulders- 1): max_depth;

% Determine the thickness of the erodible shell on each boulder.  This
% thickness depends on the time that each boulder's upper surface is
% higher than the crest of the moraine, and on the erosion rate.
shell_thick = zeros(1, num_boulders); % m
if erosion_rate > 0; % don't do these steps if erosion is nil
    for count1 = 1: 1: num_boulders;
        boulder_top = initial_height- initial_depth(count1); % m
        yn = 0;
        count2 = 1;
        while yn == 0;
            if crest_height(count2) <= boulder_top;
                exposure_time = moraine_age- times(count2); % yr
                shell_thick(count1) = exposure_time* erosion_rate;
                yn = 1;
            end
            count2 = count2+ 1;
        end
    end
    initial_shell_thick = shell_thick; % m
end

% Step through time, tracking the nuclide concentration in each boulder.
boulder_conc = zeros(1, num_boulders); % atoms/ g
% num_exposed = zeros(1, numel(times));
for count1 = 2: 1: numel(times);
    disp(['Calculating time step #', num2str(count1- 1), ' of ',...
        num2str(numel(times)- 1), '... '])
    % Increment concentrations for nuclear decay.
    boulder_conc = boulder_conc.* exp(-decay_const* time_step);
    % Step through the list of boulders.
    for count2 = 1: 1: num_boulders;
        depth = crest_height(count1)- ...
            (initial_height- initial_depth(count2)); % m
        % If the boulder is at the surface,
        if depth <= 0;
            P_sample = P_surf.* exp(-shell_thick(count2)./ L_rock);
            shell_thick(count2) = shell_thick(count2)- ...
                erosion_rate* time_step;
```

```
            % num_exposed(count1) = num_exposed(count1)+ 1;
        % Otherwise,
        else
            P_till = P_surf.* exp(-depth./ L_till);
            P_sample = P_till.* exp(-shell_thick(count2)./ L_rock);
        end
        % Increment the concentration in the boulder by the production rate
        % during this time step.
        boulder_conc(count2) = boulder_conc(count2)+ ...
            sum(P_sample)* time_step;
    end
end

% Calculate the apparent exposure time for each boulder.
naive_age = -decay_const^ -1* ...
    log(1- ((boulder_conc.* decay_const)./ (P_spall+ P_mu))); % yr

% For ease of plotting, convert variables with a time dimension to ka
% (10^3 yr).
times = times/ 10^ 3;
naive_age = naive_age/ 10^ 3;
moraine_age = moraine_age/ 10^ 3;

if plots == 1;
    % Plot the initial (dotted) and final (solid) moraine profiles.
    figure
    plot(distances, initial_profile, 'k--', 'LineWidth', 1.5)
    axis square
    hold on
    plot(distances, final_profile, 'k', 'LineWidth', 1.5)
    xlabel('Distance from moraine crest (m)', 'FontSize', 16, ...
        'FontWeight', 'bold')
    ylabel('Height (m)', 'FontSize', 16, ...
        'FontWeight', 'bold')
    h_leg = legend('Initial profile', 'Final profile');
    legend('boxoff')
    set(h_leg, 'FontSize', 14)
    set(gca, 'FontSize', 14)
    set(gca, 'LineWidth', 1)
%    set(gca, 'Box', 'off')

    % Plot moraine height as a function of time.
    figure
    plot(times, crest_height, 'k', 'LineWidth', 1.5)
    axis square
    xlabel('Elapsed time (ka)', 'FontSize', 16, 'FontWeight', 'bold')
    ylabel('Crest height (m)', 'FontSize', 16, ...
        'FontWeight', 'bold')
    set(gca, 'FontSize', 14)
    set(gca, 'LineWidth', 1)
%    set(gca, 'Box', 'off')
```

```
    % Histogram the apparent ages given by the modeled boulders.
    figure
    nbins = ceil((max(naive_age)- min(naive_age))/ bin_width);
    hist(naive_age, nbins)
    axis square
    hold on
    xlabel('Apparent age (ka)', 'FontSize', 16, 'FontWeight', 'bold')
    ylabel('Number of boulders', 'FontSize', 16, 'FontWeight', 'bold')
    set(gca, 'FontSize', 14)
    set(gca, 'LineWidth', 1)
    set(gca, 'XTickMode', 'auto')
%    set(gca, 'Box', 'off')
    h = findobj(gca, 'Type', 'patch');
    set(h, 'FaceColor', 'b', 'EdgeColor', 'k')
    ylimits = get(gca, 'YLim');
    plot([moraine_age moraine_age], ylimits, 'k--', 'LineWidth', 1.5)
end

beep
```

```
function [times, crest_height, distances, initial_profile, ...
    final_profile] = m_diffusion(initial_height, initial_slope, k, ...
    moraine_age, time_step)

% m_diffusion.m
%
% Calculates the height of a moraine's crest as a function of time, plus
% the final topographic profile of the moraine.  Assumes a "sawtooth"
% initial profile.  Based on an analytical solution developed by Dr. Nathan
% Urban, Penn State.
%
% Syntax: [times, crest_height, distances, initial_profile, ...
%    final_profile] = m_diffusion(initial_height, initial_slope, k, ...
%    moraine_age, time_step)
% times, vector of elapsed time values (yr)
% crest_height, height of moraine crest as a function of the values in the
%   vector times (m)
% distances, vector of distance from the moraine crest (m)
% initial_profile, height of moraine as a function of the values in the
%   vector distances (m)
% final_profile, height of moraine as a function of the values in the
%   vector distances (m)
% initial_height, initial height of the moraine (m)
% initial_slope, initial slope of the moraine sides (d'less)
% k, topographic diffusion coefficient (sq. m/ yr)
% moraine_age, assumed age of moraine (yr)
% time_step, interval between calculations of moraine height (yr)

% Set model variables.
length_step = 2;            % m; space step (1-2 m is best)
length_factor = 1.5;        % profile length factor (at least 1.5; not
                            % important, except for large, old moraines)

% Establish plotting variables times and distances.
L = initial_height/ initial_slope; % m; half-width of the moraine's base
times = 0: time_step: moraine_age; % yr
distances = 0: length_step: (length_factor* L); % m

% Calculate height of moraine as a function of time.
crest_height = zeros(1, numel(times)); % m
h0 = initial_height; % m
for count1 = 1: 1: numel(times);
    t = times(count1);
    crest_height(count1) = (h0/ L)* ((2* sqrt(k* t)/ sqrt(pi))* ...
        (exp(-L^ 2/ (4* k* t))- 1)+ ...
        L* erf(L/ (2* sqrt(k* t))));
end

% Calculate initial moraine profile as a function of distance from the
% moraine's crest.
initial_profile = zeros(1, numel(distances)); % m
for count1 = 1: 1: numel(distances);
```

```
    initial_profile(count1) = initial_height- (count1- 1)* ...
        length_step* initial_slope;
    if initial_profile(count1) < 0;
        initial_profile(count1) = 0;
    end
end

% Calculate final moraine profile as a function of distance from the
% moraine's crest.
final_profile = zeros(1, numel(distances)); % m
h0 = initial_height; % m
t = moraine_age; % yr
for count1 = 1: 1: numel(distances);
    x = distances(count1); % m
    z1 = exp(-(L+ x)^ 2/ (4* k* t))- ...
        2* exp(-x^ 2/ (4* k* t))+ ...
        exp(-(L- x)^ 2/ (4* k* t));
    z2 = (L+ x)* erf((L+ x)/ (2* sqrt(k* t)))- ...
        2* x* erf(x/ (2* sqrt(k* t)))+ ...
        (L- x)* erf((L- x)/ (2* sqrt(k* t)));
    final_profile(count1) = (h0/ (2* L))* ...
        ((2* sqrt(k* t)/ sqrt(pi))* z1+ z2);
end
```

```
% inheritance_model.m
%
% Evaluates probability distributions of cosmogenic exposure dates for
% boulders that contain inherited nuclides.  Code written by Patrick
% Applegate, Penn State (papplegate@psu.edu).
%
% Code written to run under MATLAB R2008a on an Intel-based Macintosh
% MacBook.
%
% This code was written carefully and has been checked for obvious errors.
% However, no warranty of any kind is implied.  The code may not even run
% on your system.  The output from the code should not be trusted without
% testing.
%
% Please give proper credit if using this code in research and teaching.
% Derivative works based on this code should include a reference to the
% original paper.

% Clear all variables, commands, and figures.  Set figures to dock
% automatically.
clear all
close all
clc
set(0,'DefaultFigureWindowStyle','docked')

% Define parameters that will be tuned during model inversion.
moraine_age = 20.0;         % ka (10^ 3 yr); true age of moraine
max_pre_time = 100.0;       % ka; maximum time that any individual boulder
                            % had to acquire inherited nuclides
max_pre_depth = 2.0;        % m; maximum depth of sample point on any
                            % boulder during predepositional exposure time
pre_slope = 0;              % degrees; slope of surface from which boulders
                            % are derived

% Define other geomorphic parameters that are not part of the inversion.
erosion_rate = 0.0;         % mm/ ka; erosion rate of boulders on moraine
rho_rock = 2.6;             % g/ cm^ 3; density of boulders
rho_over = 2.0;             % g/ cm^ 3; density of material overlying
                            % boulders during predepositional exposure time

% Define nuclide production parameters.
P_spall = 4.97;             % atoms/ g/ yr; surface production rate due to
                            % spallation (get this from the CRONUS online
                            % calculator described in Balco et al., 2008;
                            % assumed to be constant over the lifetime of
                            % the moraine)
P_mu = 0.133;               % atoms/ g/ yr; surface production rate due to
                            % muons (also get this from the CRONUS
                            % calculator)
decay_const = 4.62* 10^ -7; % yr^ -1; nuclear decay constant of nuclide of
                            % interest (4.62* 10^ -7 for 10Be, following
                            % Balco et al., 2008, and refs therein)
```

```
P_slhl = [4.97 0.09 ...     % atoms/ g/ yr; sea level, high-latitude
    0.02 0.02];             % production rates of different cosmic ray
                            % flux components, following Granger and
                            % Muzikar (2001); for 10Be, about
                            % [4.97 0.09 0.02 0.02]
att_length = [160 738 ...   % g/ sq. cm; effective attenuation lengths of
    2688 4360];             % exponential components of Granger and Muzikar
                            % (2001) production-as-a-function-of-depth
                            % parameterization; for 10Be and 26Al, about
                            % [160 738 2688 4360]

% Define model parameters.
num_boulders = 1* 10^ 5;    % number of randomly generated synthetic
                            % boulders (at least 10^ 3; bigger numbers
                            % yield more consistent results, but the model
                            % will take more time to run)

% Turn plotting on and off.
plots = 1;                  % If 1, plots the moraine profile, height of
                            % the moraine's crest as a function of time,
                            % and a histogram of the modeled exposure
                            % dates.  If 0, none of these plots are
                            % produced.
bin_width = 10;             % ka; width of bins in naive age histogram

% Convert all quantities to consistent units.  All lengths should be in
% meters, times should be in years, and masses should be in grams.  Note
% that pre_slope should remain in degrees -- do not reduce this angle to
% its slope equivalent.
moraine_age = moraine_age* 10^ 3;               % yr
max_pre_time = max_pre_time* 10^ 3;             % yr
erosion_rate = erosion_rate* 10^ -6;            % m/ yr
rho_over = rho_over* 100^ 3;                    % g/ cu. m
rho_rock = rho_rock* 100^ 3;                    % g/ cu. m
att_length = att_length* 100^ 2;                % g/ sq. m

% Scale production rates to site.
P_surf(1) = P_spall; % atoms/ g/ yr
P_surf(2: 4) = P_slhl(2: 4)* P_mu/ sum(P_slhl(2: 4));

% Determine length scales for nuclide production.
L_over = att_length/ rho_over; % m
L_rock = att_length/ rho_rock; % m

% Determine predepositional exposure time for each boulder, and the depth
% of the sample point on each boulder during that time.
pre_time = max_pre_time* rand(1, num_boulders); % yr
pre_depth = max_pre_depth* rand(1, num_boulders); % m

% Calculate the final nuclide concentration in each boulder.  The
% production rate parameterization here follows Dunne et al. (1999), using
% the four-component production rate scheme described by Granger and
```

```
% Muzikar (2001).
boulder_conc = zeros(1, num_boulders);
for count1 = 1: 1: num_boulders;
    P_pre = sum(P_surf.* (1- 3.6* 10^ -6* pre_slope^ 2.64).* ...
        exp((-pre_depth(count1)./ L_over).* (1+ pre_slope^ 2/ 5000)));
    C_pre = (P_pre/ decay_const)* ...
        (1- exp(-decay_const* pre_time(count1)));
    boulder_conc(count1) = C_pre* exp(-decay_const* moraine_age)+ ...
        (P_spall+ P_mu)/ (decay_const+ erosion_rate* L_over(1))* ...
        (1- exp(-decay_const* moraine_age));
end

% Calculate the apparent exposure time for each boulder.
naive_age = -decay_const^ -1* ...
    log(1- ((boulder_conc.* decay_const)./ (P_spall+ P_mu))); % yr

% For ease of plotting, convert variables with a time dimension to ka
% (10^3 yr).
naive_age = naive_age/ 10^ 3;
moraine_age = moraine_age/ 10^ 3;
pre_time = pre_time/ 10^ 3;

if plots == 1;
    % Histogram the apparent ages given by the modeled boulders.
    figure
%     bins = floor(min(naive_age)): bin_width: ceil(max(naive_age));
%     bar(bins, histc(naive_age, bins), 'histc')
    nbins = ceil((max(naive_age)- min(naive_age))/ bin_width);
    hist(naive_age, nbins)
    axis square
    xlabel('Apparent age (ka)', 'FontSize', 16, 'FontWeight', 'bold')
    ylabel('Number of boulders', 'FontSize', 16, 'FontWeight', 'bold')
    set(gca, 'FontSize', 14)
    set(gca, 'LineWidth', 1)
    set(gca, 'XTickMode', 'auto')
%    set(gca, 'Box', 'off')
    h = findobj(gca, 'Type', 'patch');
    set(h, 'FaceColor', 'b', 'EdgeColor', 'k')
    hold on
    ylimits = get(gca, 'YLim');
    plot([moraine_age moraine_age], ylimits, 'k--', 'LineWidth', 1.5)
end

beep
```

Appendix D

Additional methods and data table for Chapter 3

In this appendix, we provide descriptions of the methods that we used to generate the results described in Chapter 3.

Model descriptions

Chapter 2 includes a full description of our numerical models, including tests of the models' sensitivity to changes in their input parameters and the assumptions involved in constructing the models. We provide brief descriptions of these models here to preserve the continuity of this chapter.

The model of moraine degradation couples an analytical solution for the evolution of moraine slopes over time to a parameterization of nuclide production at depth (Granger and Muzikar, 2001). The slope evolution equation describes the height of the moraine crest as a function of time. With this curve, we can determine the depth as a function of time for any boulder with a specified initial depth. The final nuclide concentration in the boulder is then the integral of production within the boulder over time, correcting for nuclear decay.

Our inheritance model tracks nuclide concentrations in boulders that had significant exposure to cosmic rays in the landscape before being deposited on the moraine, where they are eventually sampled. The model formulation is identical for boulders that were derived from subglacial material and boulders that fell onto the glacier from the adjacent valley walls. In both cases, the final concentration in each boulder is the sum of production during the predepositional and postdepositional exposure periods, after accounting for nuclear decay. The model calculates

the concentration acquired during the predepositional exposure period for each boulder, given the length of that boulder's predepositional exposure time and the depth to which the boulder was buried during that time. This calculation is performed using the same parameterization of production as a function of depth used in the moraine degradation model (Granger and Muzikar, 2001), with a correction for the slope of the surface during the predepositional exposure time (Dunne et al., 1999).

Latin hypercube sampling

To produce probability distributions of exposure dates using the models, we run the models repeatedly for different values of the free parameters. In the moraine degradation model, the only free parameter is the initial depth of each boulder. In the inheritance model, the free parameters are the predepositional exposure time and the predepositional burial depth of each boulder. In effect, this procedure indicates the statistical distribution of exposure dates that we would expect to obtain if we could collect an arbitrarily large number of samples from a single moraine.

We select the free parameter values using Latin hypercube sampling (Urban and Fricker, in review, *Computers and Geosciences*) instead of the more-common and simpler Monte Carlo methods (Chapter 2; Bevington and Robinson, 2003). Latin hypercube methods select model free parameter values such that no two points within free parameter space share the same value for any parameter. In a two-dimensional parameter space divided into equal-width rows and columns, this rule requires that each row and column contains one and only one point. Thus, Latin hypercube methods provide a more even sampling of parameter space than do Monte Carlo methods, ensuring that the distributions produced by our models are consistent between different

runs of the models for the same parameter values. We found that $3* 10^3$ Latin hypercube samples produced acceptably consistent statistical distributions for the applications discussed here.

The Kolmogorov-Smirnov test statistic

There are several fitting statistics that we could use to compare a modeled distribution to a data set, but the simplest is probably the Kolmogorov-Smirnov test statistic (KS statistic; Press et al., 1992; Croarkin and Tobias, 2006; Clauset et al., 2007). The KS statistic D_{KS} is the maximum distance between the two cumulative density functions, measured parallel to the *y*-axis. That is,

$$D_{KS} = \max_{x \geq x_{\min}} \left| F_{\mathrm{model}}(x) - F_{\mathrm{data}}(x) \right|,$$

where F_{model} and F_{data} are the cumulative density functions of the modeled and observed exposure dates, respectively.

The Differential Evolution genetic algorithm

To search for the model parameter values that minimize the KS statistic for each data set, we use the Differential Evolution genetic algorithm (Price et al., 2005). Differential Evolution is a fast, widely used method for minimizing functions that avoids local minima, unlike gradient descent techniques.

Differential Evolution requires the user to specify ranges in which to search for the best-fit model parameters. In fitting the degradation model to the Uinta Mountains data sets, we assumed that the moraines' ages must lie in the range of 15-25 ka, their initial slopes must have been between 30° and 40°, and their topographic diffusivities must be between $0.5* 10^{-2}$ m^2/ yr and $0.5* 10^{-4}$ m^2/ yr. These parameter ranges are in line with the chronology of glaciation in the

western United States (Richmond, 1986; Pierce, 2004; Applegate, 2005; Licciardi and Pierce, 2008), recent topographic profiles measured on these moraines (P. Applegate and B. J. C. Laabs, unpublished data), and prior estimates of topographic diffusivity from unconsolidated landforms in arid environments (Hanks, 2000; Putkonen et al., 2007).

In fitting the inheritance model to the Gurreholm Dal data sets, we assumed that the maximum predepositional burial depth ranged between 1 and 5 m, consistent with prior estimates of the depth of glacial erosion (Briner and Swanson, 1998; Fabel and Harbor, 1999; James et al., 2002; Fabel et al., 2004). We found it necessary to adjust the ranges of moraine age and maximum predepositional exposure time for each data set, but in general we searched between 5-25 ka and 10-120 ka for these parameters, respectively. The moraine age range is based on the likely ages of the moraine groups, given their stratigraphic positions upvalley from the LGM-age Kap Brewster moraine (Funder, 1978; Kelly et al., 2008; cf. Hakansson et al., 2007). The maximum end of the predepositional exposure time range is based on the lengths of glacial-interglacial cycles (Hays et al., 1976; Shackleton, 2000).

Tests of the inverse method

As a test of our inverse method, we attempted perfect model experiments. In these experiments, we created two synthetic data sets, one from each of our models, using specified values of the model input parameters. We then attempted to recover these parameter values using the inverse methods described above.

We created our test data sets by sampling the percentiles of two modeled distributions, one from the moraine degradation model and one from the inheritance model. This procedure yielded data sets containing 100 observations each, and these observations were guaranteed to be representative of the underlying statistical distribution. For real moraines, we never have so many

observations, and we have no assurances that the few observations we do have are really representative of the underlying statistical distribution. However, our purpose in making this test is to check the reasonableness of the algorithm; whether we can reliably reconstruct moraine age from a few randomly chosen observations is a separate issue. The input parameters for the degradation model were moraine age, 20 ka; initial moraine height, 50 m; initial moraine slope, 34°; and topographic diffusivity, 10^(-2) m^2/yr. The input parameters for the inheritance model were moraine age, 20 ka; maximum predepositional exposure time, 100 ka; maximum burial depth, 2.0 m.

The inverse method successfully recovered the appropriate parameter values for these test data sets. The best fit of the degradation model to the test data set was achieved for the parameter values moraine age, 20.064 ka; initial slope, 36.0139°; topographic diffusivity, 10^(-2.10845) m^2/yr. We do not invert for the initial moraine height because the distributions produced by the degradation model are insensitive to changes in the initial height above ~35 m (Chapter 2). The best fit of the inheritance model to the test data set was found for moraine age 19.9875 ka; maximum predepositional exposure time, 104.389 ka; and maximum predepositional burial depth, 2.06155 m.

The recovered values all lie within 6% of the correct values, except for the topographic diffusivity, which is about 22% different from the correct value. Still, the estimated topographic diffusivity is only about a tenth of a log unit from the correct value. Given that the topographic diffusivity can range over four orders of magnitude (Putkonen et al., 2007), we consider this degree of accuracy to be acceptable.

The influence of scaling model choice on the scatter among exposure dates

We have recalculated the exposure dates from eastern Greenland and the southern Uinta Mountains using the Lal/ Stone scaling model (Lal, 1991; Stone, 2000; Balco et al., 2008) and the CRONUS online calculator (Balco et al., 2008; main production code, v. 2.1; constants file, v. 2.1; muon production code, v. 1.1). We use the Lal/ Stone scaling model because it produces time-averaged estimates of nuclide production rates, as required by our geomorphic models (Chapter 2). The exposure dates from the eastern Greenland sites have been corrected for isostatic uplift (B. Goehring, personal communication; Kelly et al., 2008), using uplift curves derived from radiocarbon dating of raised marine terraces (Hall et al., 2008).

To ensure that our results are not strongly dependent on the scaling model we used to calculate the exposure dates, we calculated the exposure dates using a variety of presently accepted scaling models (Balco et al., 2008).

Figure D.1 shows the effect of scaling model choice on the distributions of exposure dates from our chosen data sets (also see Table D.1, at the end of this appendix). For the Greenland data sets, the scaling models that account for magnetic field variations (Lm, De, Du, and Li; Balco et al., 2008) produce exposure dates that are somewhat older than exposure dates calculated from the same samples using the St scaling model. The more sophisticated scaling models also increase the range of the exposure dates from these moraines relative to the St scaling model. In the Uinta Mountains, the effects of scaling model choice are larger and have the opposite sign. That is, the scaling models that account for magnetic field variation indicate that the Uinta Mountains samples are somewhat younger and more narrowly distributed than the St scaling model suggests.

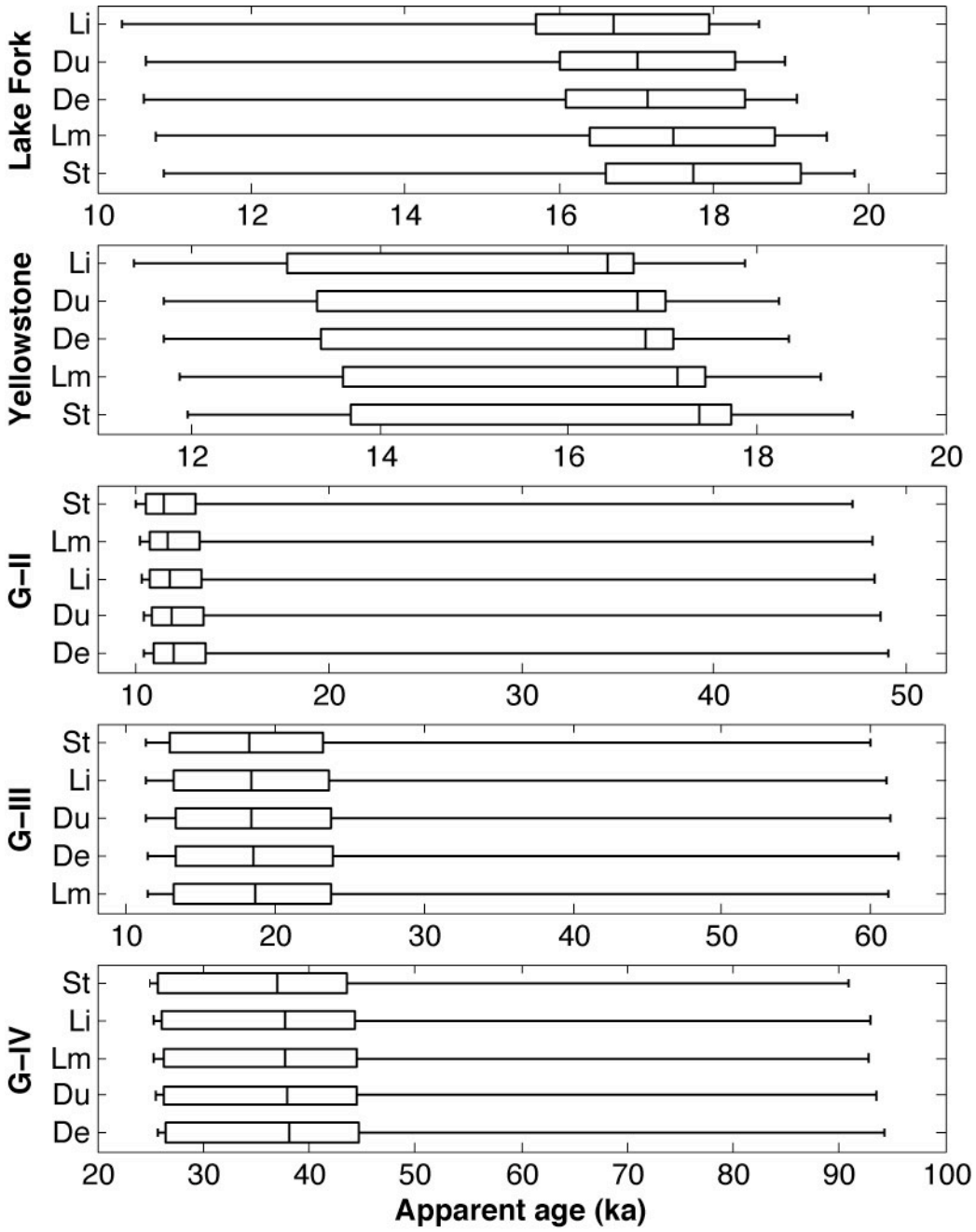

Figure D.1: Effects of scaling model choice on the distributions of exposure dates within our chosen data sets. Each set of box plots (Chambers et al., 1983) represents the influence of scaling method on the statistical distribution of exposure dates for one data set treated in this paper. The scaling model abbreviations on the *y*-axis follow those used by Balco et al. (2008). In each line, the box represents the middle 50% of the observations, the line in the box shows the position of the median, and the ends of the whiskers indicate where the maximum and minimum of the distribution lie.

In general, the choice of scaling model has the greatest influence on the oldest values in a collection of exposure dates. This result is a consequence of how the exposure dates are calculated; a change in the production rate will affect the apparent ages of high-concentration samples more than the apparent ages of low-concentration samples.

Overall, the effect of scaling model choice on the spread of exposure dates within each data set is small compared to the likely effects of geomorphic processes on this spread. That is, the scatter among exposure dates is always the same (to within 10%) for these data sets, regardless of the scaling model used in calculating the exposure dates. For each data set and scaling model, we compared the range of the exposure dates to the range of exposure dates calculated using the St scaling model for the same moraine by calculating a quantity R,

$$R = \left| \frac{r_{i,M} - r_{i,St}}{r_{i,St}} \right|,$$

where $r_{i,M}$ is the range of exposure dates from the ith moraine or moraine group, calculated using scaling model M. The maximum value of R for the data sets treated here is less than 8%. If the range of exposure dates is a proxy for the effects of geomorphic processes on these exposure dates, this result suggests that the geomorphic processes responsible for the scatter in our chosen data sets have a larger influence on the spread of the exposure dates than our choice of scaling model.

Normal probability plots

Normal probability plots provide a graphical test for normality. If a set of observations fall in a line when displayed on a normal probability plot, then the observations are likely to be drawn from a normal distribution. This statement remains true regardless of the mean and standard deviation of the normal distribution. Like most tests for normality, we have low

confidence in conclusions drawn from normal probability plots of small data sets (n < ~20). Chambers et al. (1983) give procedures for the construction of normal probability plots.

The reduced chi-squared statistic

The degree of scatter in a data set relative to the scatter expected from the measurement error can be expressed using the reduced chi-squared statistic χ_R^2 (Bevington and Robinson, 2003; Balco and Schaefer, 2006). The reduced chi-squared statistic is sometimes called the mean square of weighted deviates in the exposure dating literature (e.g., Kaplan and Miller, 2003; Douglass et al., 2006). For well-behaved data sets, the reduced chi-squared value approaches 1.0; more scattered data sets have larger reduced chi-squared values.

We calculate the reduced chi-squared statistic for each group of exposure dates as

$$\chi_R^2 = (n-1)^{-1} \sum_{i=1}^{n} \left[\frac{\left(\mu_i - \mu_{\text{avg}}\right)^2}{\sigma_i^2} \right]$$

(Bevington and Robinson, 2003). Here, n is the number of exposure dates from different boulders, and μ_i and σ_i are the central estimate and 1σ measurement uncertainty of the ith exposure date. μ_{avg} is the arithmetic mean of the exposure dates, following Kaplan et al. (2005); it is not the mean weighted by the inverse variance.

In calculating the reduced chi-squared statistic for each data set, we use only the mass spectrometric measurement uncertainties of the exposure dates (the "internal uncertainties" of Balco et al., 2008; see also Gosse et al., 1995; Gosse and Phillips, 2001). The total uncertainties of these exposure dates are somewhat larger than these internal uncertainties (Gosse and Phillips, 2001, their section 6), because the nuclide production rates and half-life values that we use to calculate the dates are not exact. However, these additional sources of uncertainty are highly

correlated between samples from the same moraine (Balco et al., 2008); they may bias the exposure dates from a moraine toward too-young or too-old values, but they should not increase the variance among exposure dates from a single moraine. Using the total uncertainties of the exposure dates would produce a too-small value for the reduced chi-squared statistic, effectively underestimating the real spread of the exposure dates.

Recalculated exposure dates

The following table (Table D.1) lists the exposure dates referred to in Chapter 3 and this appendix, as recalculated using various presently accepted scaling models (Balco et al., 2008).

Table D.1: Beryllium-10 exposure dates recalculated according to Balco et al. (2008).

Sample ID	Nucleon ^{10}Be prod'n rate[a] (atoms/g/yr)	Muon ^{10}Be prod'n rate (atoms/g/yr)	Lal/Stone (St) Apparent age (yr)	Lal/Stone (St) 1-sigma uncertainty[b] (yr)	Lal time-variant (Lm) Apparent age (yr)	Lal time-variant (Lm) 1-sigma uncertainty[b] (yr)
G-II moraines, Gurreholm Dal., eastern Greenland (Kelly et al., 2008)[c]						
MKG-32	10.070	0.257	10440	265	10667	271
MKG-33	9.760	0.254	12109	281	12376	287
MKG-35	8.980	0.248	13690	294	13993	301
MKG-36	9.240	0.249	11307	379	11555	388
MKG-89	7.340	0.228	10651	311	10883	318
MKG-90	7.310	0.227	13400	337	13698	345
MKG-91	7.220	0.226	17175	417	17556	426
MKG-92	7.060	0.224	10994	298	11234	304
MKG-98	8.300	0.238	11623	389	11879	398
MKG-99	8.310	0.239	47203	827	48209	845
MKG-100	9.700	0.258	11450	506	11701	517
MKG-101	10.130	0.257	10107	414	10327	423
MKG-102	10.400	0.260	11637	281	11894	287
MKG-103	10.590	0.261	10327	256	10552	261
MKG-104	9.050	0.247	10027	246	10244	252
G-III moraines, Gurreholm Dal., eastern Greenland (Kelly et al., 2008)[c]						
MKG-11	6.910	0.225	12690	433	12970	442
MKG-12	7.010	0.226	37083	862	37877	880
MKG-13	5.630	0.208	17675	529	18066	541
MKG-14	5.710	0.208	18854	438	19270	448
MKG-15	5.600	0.208	11221	262	11467	268
MKG-20	6.180	0.215	12547	323	12824	331
MKG-21	6.230	0.215	22957	965	23458	986
MKG-22	6.870	0.223	13092	304	13382	311
MKG-24	7.110	0.227	20811	715	21267	731
MKG-25	7.300	0.228	59930	1433	61201	1464
MKG-26	7.240	0.228	23539	455	24053	465
MKG-30	5.580	0.207	14740	344	15068	352

Table D.1 (continued): Beryllium-10 exposure dates recalculated according to Balco et al. (2008).

Sample ID	Desilets (De)		Dunai (Du)		Lifton (Li)	
	Apparent age (yr)	1-sigma uncertainty[b] (yr)	Apparent age (yr)	1-sigma uncertainty[b] (yr)	Apparent age (yr)	1-sigma uncertainty[b] (yr)
G-II moraines, Gurreholm Dal., eastern Greenland (Kelly et al., 2008)[c]						
MKG-32	10906	277	10820	275	10710	272
MKG-33	12655	293	12552	291	12451	289
MKG-35	14297	307	14184	305	14081	302
MKG-36	11809	396	11718	393	11632	390
MKG-89	11046	322	10975	320	10920	319
MKG-90	13886	349	13792	347	13733	345
MKG-91	17758	431	17636	428	17562	427
MKG-92	11374	308	11302	306	11254	305
MKG-98	12112	405	12025	402	11955	400
MKG-99	49024	859	48646	853	48347	847
MKG-100	11966	529	11868	525	11768	520
MKG-101	10558	433	10475	430	10361	425
MKG-102	12164	294	12063	291	11958	289
MKG-103	10789	267	10702	265	10585	262
MKG-104	10465	257	10388	255	10287	253
G-III moraines, Gurreholm Dal., eastern Greenland (Kelly et al., 2008)[c]						
MKG-11	13137	448	13050	445	12997	443
MKG-12	38226	889	37957	882	37792	878
MKG-13	17867	535	17761	532	17733	531
MKG-14	19059	443	18945	440	18913	439
MKG-15	11405	266	11342	265	11323	264
MKG-20	12860	331	12783	329	12751	329
MKG-21	23452	986	23302	979	23236	977
MKG-22	13528	314	13440	312	13390	311
MKG-24	21525	740	21374	735	21278	731
MKG-25	61809	1478	61362	1467	61080	1461
MKG-26	24351	470	24178	467	24065	465
MKG-30	14921	349	14834	347	14813	346

Table D.1 (continued): Beryllium-10 exposure dates recalculated according to Balco et al. (2008).

Sample ID	Nucleon ^{10}Be prod'n rate[a] (atoms/g/yr)	Muon ^{10}Be prod'n rate (atoms/g/yr)	Lal/Stone (St) Apparent age (yr)	Lal/Stone (St) 1-sigma uncertainty[b] (yr)	Lal time-variant (Lm) Apparent age (yr)	Lal time-variant (Lm) 1-sigma uncertainty[b] (yr)
G-IV moraines, Gurreholm Dal., eastern Greenland (Kelly et al., 2008)[c]						
MKG-07	7.180	0.226	25654	594	26211	607
MKG-08	7.210	0.226	38681	917	39509	937
MKG-09	7.330	0.228	24899	838	25441	856
MKG-16	8.050	0.236	90920	1996	92849	2040
MKG-19	6.910	0.224	45125	761	46085	777
MKG-27	7.290	0.227	25646	943	26203	964
MKG-28	7.020	0.224	37040	858	37833	876
Outer Smiths Fork lateral moraine, Lake Fork drainage, Uinta Mountains (Laabs et al., 2009)						
LF-RK-5	31.200	0.443	19123	1200	18792	1200
LF04-1	30.770	0.441	16604	758	16399	758
LF04-2	30.500	0.439	17428	734	17179	734
LF04-3	30.910	0.441	10863	548	10770	548
LF04-4	30.150	0.437	19835	1010	19467	1010
LF04-5A	29.910	0.436	18332	796	18038	796
LF04-5B	30.900	0.441	17747	806	17483	806
Wtd mean[d]			18043	566	17764	566
Outer Smiths Fork lateral moraine, Yellowstone drainage, Uinta Mountains (Laabs et al., 2009)						
YS-3	31.410	0.445	17419	797	17171	797
YS-6	29.870	0.435	13230	547	13144	547
YS-7	30.190	0.437	15095	627	14965	627
YS-8	30.530	0.439	19013	734	18690	734
YS-9	30.470	0.439	17399	747	17156	747
YS-10	31.210	0.444	17826	756	17558	756
YS-11	28.860	0.430	11970	497	11887	497

Table D.1 (continued): Beryllium-10 exposure dates recalculated according to Balco et al. (2008).

Sample ID	Desilets (De)		Dunai (Du)		Lifton (Li)	
	Apparent age (yr)	1-sigma uncertainty[b] (yr)	Apparent age (yr)	1-sigma uncertainty[b] (yr)	Apparent age (yr)	1-sigma uncertainty[b] (yr)
G-IV moraines, Gurreholm Dal., eastern Greenland (Kelly et al., 2008)[c]						
MKG-07	26485	614	26301	609	26186	607
MKG-08	39868	946	39589	939	39416	935
MKG-09	25743	867	25561	860	25443	856
MKG-16	94222	2071	93501	2054	92965	2042
MKG-19	46392	782	46073	777	45885	774
MKG-27	26503	975	26316	968	26196	963
MKG-28	38120	883	37856	877	37701	873
Outer Smiths Fork lateral moraine, Lake Fork drainage, Uinta Mountains (Laabs et al., 2009)						
LF-RK-5	18414	1200	18287	1200	17945	1200
LF04-1	16083	758	16000	758	15684	758
LF04-2	16841	734	16744	734	16421	734
LF04-3	10609	548	10622	548	10311	548
LF04-4	19067	1010	18928	1010	18578	1010
LF04-5A	17679	796	17566	17566	17234	17566
LF04-5B	17140	806	17038	17038	16712	17038
Wtd mean[d]	17413	566	17294	12230	16965	12230
Outer Smiths Fork lateral moraine, Yellowstone drainage, Uinta Mountains (Laabs et al., 2009)						
YS-3	16830	797	16733	797	16410	797
YS-6	12924	547	12899	547	12588	547
YS-7	14709	627	14652	627	14345	627
YS-8	18351	734	18226	734	17887	734
YS-9	16863	747	16766	747	16446	747
YS-10	17213	756	17109	756	16782	756
YS-11	11714	497	11709	497	11398	497

Dates recalculated using the CRONUS online calculator (Balco et al., 2008), v. 2.1, with v. 2.1 of the constants file and v. 1.1 of the muon production code.

a, Nucleon production rates from the St scaling model (Balco et al., 2008).

b, 1-sigma uncertainties reflect measurement uncertainties only, that is, the internal uncertainties of Balco et al. (2008).

c, Exposure dates from Gurreholm Dal recalculated by Brent Goehring (Lamont-Doherty Earth Observatory, Columbia University) with a correction for uplift over the exposure times of the samples (Kelly et al., 2008).

d, Weighted mean of samples LF04-5A and -5B, which come from the same boulder.

Appendix E

Data table for Chapter 4

The following table (Table E.1) gives the recalculated exposure dates described in Chapter 4.

Table E.1: Beryllium-10 exposure dates recalculated following Barrows et al. (2007).

Sample ID	Boulder height (m)	Nucleon ^{10}Be prod'n rate (atoms/g/yr)	Muon ^{10}Be prod'n rate (atoms/g/yr)	Apparent age (yr)	1-sigma uncertainty (yr)
Waiho Loop moraine, western New Zealand (Barrows et al., 2007)					
WH-01B		5.554	0.157	11.24	0.42
WH-02		5.580	0.157	10.33	0.70
WH-03		5.576	0.157	10.70	0.38
WH-04B		5.575	0.157	9.65	0.47
WH-05		5.472	0.156	9.10	0.41
WH-08A		5.473	0.156	6.85	0.91
WH-09		5.473	0.156	5.30	0.33
WH-10		5.475	0.156	11.33	1.55
Inner Titcomb Lakes moraine, Wind River Range (Gosse et al., 1995a)					
WY-92-138	1.0	51.892	0.568	12.80	0.38
WY-92-139	1.0	51.892	0.568	12.06	0.36
WY-92-140	1.0	51.892	0.568	9.93	0.30
WY-93-333	1.0	51.892	0.568	12.08	0.36
WY-93-334	1.5	51.892	0.568	14.00	0.42
WY-93-335	0.6	51.892	0.568	12.97	0.39
WY-93-336	2.0	51.892	0.568	13.30	0.40
WY-93-337	1.5	51.892	0.568	13.26	0.40
WY-93-338	0.8	51.892	0.568	12.86	0.39
WY-93-339	0.1	51.892	0.568	12.73	0.38
WY-92-138	1.0	51.892	0.568	12.80	0.38
WY-92-139	1.0	51.892	0.568	12.06	0.36
WY-92-140[b]	1.0	51.892	0.568	9.93	0.30

prod'n, production.
Production rates and exposure dates recalculated following Barrows et al. (2007), using the scaling model of Stone (2000) for both nucleon and muon production.
1-sigma uncertainties reflect measurement uncertainty only.

VITA

Patrick J. Applegate

Education

Ph. D. in Geosciences, anticipated December 2009
Pennsylvania State University, University Park, Pennsylvania
Advisor: Richard B. Alley

MS in Geology, December 2005
Purdue University, West Lafayette, Indiana
Advisor: Darryl E. Granger

BS in Geology, June 2003
University of Cincinnati, Cincinnati, Ohio

Awards

Outstanding Poster, PAGES Young Scientists' Meeting (2009)
Ohmoto Graduate Fellowship (2008)
Geological Society of America Student Grant ($3,010; 2008)
Parizek Graduate Fellowship (2007)
Earth and Environmental Science Institute Assistantship (2007)
University Graduate Fellowship (2005-2006)
Anne C. Wilson Graduate Research Award (2005)
Graduate Student Award for Outstanding Teaching (2005)

Experience

Adjunct Lecturer, State University of New York-Geneseo, Fall 2008
Course: Our Geologic Environment

Reviewed Papers

Applegate, P. J., Lowell, T. V., Alley, R. B., 2008, Comment on "Absence of Cooling in New Zealand during the Younger Dryas Chronozone:" *Science*, v. 320, p. 746d.

Applegate, P., 2003, Detection of sinkholes developed on shaly Ordovician limestones, Hamilton County, Ohio, using digital topographic data; dependence of topographic expression of sinkholes on scale, contour interval, and slope: *Journal of Cave and Karst Studies*, v. 65, p. 126-129.

Selected Abstracts

Applegate, P. J., Kelly, M. A., Urban, N. M., Lowell, T. V., Alley, R. B., 2009, Inferring moraine age and depth of glacial erosion from cosmogenic exposure dates using geomorphic process modeling: European Geosciences Union Annual Meeting, Vienna, Austria.

Applegate, P. J., Kelly, M. A., Lowell, T. V., Alley, R. B., 2008, Boulder recycling, moraine degradation, and their effects on cosmogenic exposure dating of moraines: American Geophysical Union Fall Meeting, San Francisco, California.